Drag reduction using additives in a Taylor-Couette Flow

by

Pallavi Bhambri

A thesis submitted in partial fulfillment of the requirements for the degree of

Master of Science

Department of Mechanical Engineering
University of Alberta

ABSTRACT

The current study investigates the drag reduction (DR) using high molecular weight polymers such as commercial polyacrylamide, polysaccharides and thermo-responsive polymers. A Taylor-Couette (TC) setup was designed and fabricated to examine the abovementioned polymers for drag reduction, and to demonstrate that turbulent Taylor-Couette testing is a convenient and cost effective analogue for pipe flow drag reduction. Initial experiments were conducted with water as a working fluid and the dimensionless torque was used to scale the torque which compared well with the previous TC studies. Further, the results obtained were found to scale well with the turbulent drag in wall bounded shear flows (such as pipe/channel flow).

Using TC flow, commercial polyacrylamide along with polysaccharides such as aloe vera, pineapple fibers, tamarind powder and cellulose nano crystals (CNC) were studied for DR. The effect of Reynolds number (*Re*) and concentration of these high molecular weight polymers was observed. Polysaccharides are environmentally friendly and offer a huge advantage over commercial polymers due to their biodegradable nature.

Furthermore, the high molecular weight polymers are also used extensively in oil recovery during hydraulic fracturing for DR. However, due to their long chain length, these polymers get adsorbed on the surface of reservoir, diminishing the effectiveness of fracking. Hence, this study was then extended to Poly-(N-isopropylacrylamide) (PNIPAM), a thermoresponsive polymer. PNIPAM collapses reversibly beyond 33°C known as Lower Critical Solution Temperature (LCST), thereby preventing it from getting adsorbed beyond this temperature. In the current study, PNIPAM was synthesized using free radical polymerization and then

examined for DR. The effect of concentration of this thermo-responsive polymer, Reynolds number (*Re*) and temperature on DR was studied.

In summary, the current study exploits several polymers such as a commercial drag reducing agent (Polyacrylamide), biodegradable polymers such as polysaccharides, and smart polymers like thermo-responsive polymer for drag reduction. Taylor-Couette flow is utilized as a tool for testing these polymers for DR.

PREFACE

The work done in this thesis is an original work carried out by Pallavi Bhambri under the supervision of Prof. Brian Fleck from Department of Mechanical Engineering, University of Alberta; and co-supervision of Prof. Ravin Narain from Department of Chemical & Material Engineering, University of Alberta. The technical apparatus discussed in Chapter 4 is designed by me with the assistance of Prof. Brian Fleck, Bernie Faulkner and Roger Marchand.

Magnafloc 5250 utilized in Chapter 5 was purchased from BASF. Polysaccharides (Aloe Vera, Pineapple fibers and Tamarind powder) and Cellulose Nano Crystals used in Chapter 6 were kindly supplied by Dr. Phanphen Wattanarsakit from Chulalongkorn University, Thailand and Alberta Innovates Technology Futures, respectively. Thermo-responsive polymer used in Chapter 7 was synthesized in Prof. Narain's lab. All the drag reduction testing in Chapter 5, 6 & 7 was conducted in Prof. Fleck's Lab in Department of Mechanical Engineering.

Chapter 5 of this thesis has been published in International Journal of Mechanical and Production Engineering Research and Development in as Bhambri, P., Fleck, B., "*Drag reduction using high molecular weight polymers in Taylor-Couette Flow*" , 6(1), 59–72. I was responsible for the conducting the experiments, data analysis and the manuscript composition. Prof. Fleck was the supervisory author and contributed to concept analysis along with editing of manuscript.

Chapter 6 of this thesis has been submitted to Journal of Rheology as Bhambri, P., Narain, R., Fleck, B., "*Drag reduction using polysaccharides in Taylor-Couette Flow*". Responsibilities such as experiments, data analysis and composition of manuscript, were carried out by me. Prof. Narain assisted in analyzing the experiments as well as manuscript editing. Prof. Fleck was the supervisory author and contributed to data analysis along with editing of manuscript.

Chapter 7 of this thesis has been submitted to Journal of Applied Polymer Science as Bhambri, P., Narain, R., Fleck, B., "*Thermo-responsive polymers for drag reduction in Taylor-Couette Flow*". I was responsible for the polymer synthesis, conducting the

experiments, data analysis and the manuscript composition. Prof. Narain assisted in examining the synthesis experiments as well as manuscript editing. Prof. Fleck was the supervisory author and contributed to data analysis along with editing of manuscript.

DEDICATION

I dedicate this work to my family for their enormous love and support

ACKNOWLEDGEMENT

First of all, I would like to express my sincere gratitude towards my supervisor Prof. Brian Fleck for his continuous support during my graduate studies, his patience and immense knowledge in every walk of life. I am thankful to him for always motivating me and giving me an insight to solve research problems. He has been a wonderful mentor, I will always be indebted for his kindness and further, his academic experience has been invaluable for my project. I am confident that working under him, not only made me a better scientist but a better & stronger individual as well.

I would like to thank my co-supervisor, Prof. Ravin Narain, whose tremendous knowledge in the area of polymers, guided me to carry most of my work related to polymer synthesis. I am grateful to him for removing my fear from synthesis reactions and making me skillful in the area of polymer chemistry. I am also grateful to Roger Marchand, Dave Waege, Bernie Faulkner, Rick Conrad and Rick Bubenko from MECE Machine Shop, for helping me while designing the setup and fabricating it.

I am thankful to my colleague Dr. Yinan Wang from Dr. Narain's lab for training me in the synthesis reactions. I owe my sincere respect to him for his views, suggestions and helping me to think in a different direction for any research problem.

My sincere thanks to Kevin Zhu and Jianfeng Hou, my colleagues and friends from Dr. Fleck's lab, for their enormous support throughout the project and for making my research lab an enjoyable work space. I would like to wish them all the very best for their future endeavors.

In the end, I would like to thank my loving and caring family for always standing beside me and trusting me in my decisions. Without you all, this work would never have been possible.

Pallavi

TABLE OF CONTENTS

LIST OF TABLES

LIST OF FIGURES

NOMENCLATURE AND ABBREVIATIONS

c_f	Skin friction coefficient
U_∞	Free stream velocity (m/s)
Re	Reynolds number
ρ	Fluid density (kg/m^3)
r_o	Outer cylinder radius (m)
r_i	Inner cylinder radius (m)
d	Annular gap (r_o-r_i)
μ	Dynamic viscosity (Pa.s)
L	Inner Cylinder length (m)
Re_i *or* Re	Inner cylinder Reynolds number
Re_o	Outer cylinder Reynolds number
Γ	Aspect ratio (m)
τ_w	Wall shear stress (N/m^2)
v	Kinematic viscosity (m^2/s)
η	Radius ratio
Ω_i	Inner cylinder angular velocity (1/s)
Ω_o	Outer cylinder angular velocity (1/s)
u'	Fluctuating component of stream wise velocity
v'	Fluctuating component of span wise velocity
G	Dimensionless Torque
T	Torque acting on inner cylinder (N.m)

μ_{inf}	Constant viscosity based on Carreau Model
$c_{f,w}$	Skin friction coefficient of water
$c_{f,s}$	Skin friction coefficient of DRA solution
MDR	Maximum Drag Reduction
OD	Outer Diameter
ID	Inner Diameter
DRA	Drag Reducing Agent/Additives
DR	Drag Reduction
TC	Taylor Couette
RO	Rated Output
PPM	Weight parts per million
CNC	Cellulose Nano Crystals
RPM	Revolutions per minute
hp	Horse power
NIPAM	N-isopropylacrylamide
PNIPAM	Poly-n-isopropylacrylamide
APS	Ammonium per sulfate
TEMED	Tetramethylethylenediamine
CTAB	Cetyltrimethylammonium bromide

1. BACKGROUND AND OBJECTIVES

1.1 Brief Introduction

Drag reduction (DR) in turbulent pipe flow has been a well-documented field or research over the past 70 years. It has been a field of intensive research due to potential cost and energy savings to a variety of potential applications (Lumley 1973). The substantial benefits include reduction in pumping costs due to lower pressure drop, decrease in capital cost due to smaller diameter pipe and significant increase in flow rate in pipes due to reduction in turbulence. As a result of the abovementioned benefits, it has gained utmost importance in oil production and fluid transportation systems (Hoyt 1972).

Pipe or channel flow is the most commonly used setup to quantify the drag reduction using pressure drop. However, the flow requires a significant amount of additives to conduct a lab scale test and the polymer degradation is difficult to monitor. On the other hand, Taylor-Couette (TC) flow retains similar characteristics to a turbulent boundary layer and has been identified as a suitable alternative for this purpose (Lathrop et al. 1992). TC flow is a fluid flow in between two differentially rotating concentric cylinders and has an advantage of closed geometry, thus continuously employing a fixed small fluid sample and avoiding exposure of the test section to pumps which accelerates degradation.

High molecular weight polyacrylamide, polyethylene oxide, polyisobutylene etc. are the well-known drag reducing agents in the industry (Hou et al. 2008; Hoyt 1972; Ptasinski et al. 2001). However, due to environmental impact caused by slower degradation of these high molecular weight polymers, attention has been switched to biopolymers. Plant polysaccharides such as xylan, guar gum etc. have been recognized as a natural and biodegradable alternative to synthetic polymers (Hong et al. 2010). Following the similar path, the current study also utilizes some plant derivatives such as aloe vera, pineapple fibers, tamarind powder and cellulose nano crystals (CNC) as drag reducing agents. Further, as a next step, the surface of CNC is modified with surfactants to employ them as drag reducing agents.

Drag reduction is also employed extensively in hydraulic fracturing as an enhanced oil recovery technique. However, these high molecular weight polymers have a disadvantage of getting adsorbed on the reservoirs surfaces. Hence, there is potential demand for responsive polymers which can reversibly collapse with the application of some trigger, thereby preventing them from getting adsorbed. In general, development of DR additives which can be automatically controlled, provides potential innovation in flow control. Keeping this in mind, high molecular weight thermo-responsive polymers were developed and tested for drag reduction in this study. Further, the cost of synthesizing the polymer at lab scale was considerably reduced due to utilization of Taylor-Couette setup as a drag reduction testing equipment, and the small geometry allowed for an exhaustive range of tests on most additives.

1.2 Objectives

There are three main objectives of this study:

- To design a Taylor-Couette setup and verify it as a platform for assessing the drag reduction of commercial polymers in pipe flow
- To explore the high molecular weight biodegradable polysaccharides for drag reduction in Taylor-Couette system
- To develop the high molecular weight thermoresponsive polymers and examine them for drag reduction

1.3 Outline

This thesis is divided into eight chapters.

Chapter 2 provides an overview about two major types of turbulent flow: Pipe/Channel flow and Taylor Couette Flow. It briefly discusses the turbulent flow in pipe /channel flow and provides an insight about Taylor-Couette flow with a brief review about the previous studies done using this setup.

Chapter 3 provides a brief literature review regarding drag reduction in both pipelines and Taylor-Couette flow. It provides an insight about different kind of additives such as polymers,

surfactants and fibers, which have been used as drag reducing agents in the past. It discusses some background information about Taylor-Couette flow, as a tool for drag reduction.

Chapter 4 summarizes the design considerations for Taylor-Couette setup. It provides details and design schematics used while fabricating the instrument.

Chapter 5 reports the experimental work on water and drag reducing solution (using commercial polymer) as working fluids. It compares the results with water as an operating fluid, with the previous literature. Effect of concentration (of commercial polymer and Reynolds number on drag reduction is analyzed. Further, it verifies the TC system as a tool for evaluating drag reduction.

Chapter 6 exploits the use of high molecular weight polysaccharides for drag reduction in TC system. Aloe vera, pineapple fibers, tamarind powder, cellulose nano crystals (CNC) and bonded structures of CNC-surfactant are examined as drag reducing additives at various Reynolds number.

Chapter 7 describes the experimental work on thermo-responsive polymers for drag reduction. Poly-(N-isopropylacryalmide), a thermoresponsive polymer is synthesized using free radical polymerization. This is tested as a DR additive, with the effect of concentration, Reynolds number and temperature studied.

Chapter 8 summarize the key findings of the whole study and provide some suggestions for the future work.

2. FLUID FLOW

Fluid flow phenomena are often characterized into two broad categories: laminar and turbulent flow. Laminar flow is characterized by fluid traveling in smooth and steady streamlines whereas turbulent flow consists of unsteady three dimensional eddies, irregularities and fluctuations in fluid motion. In the current study, turbulent flow in a Taylor Couette system is investigated. The following section presents an overview about Taylor Couette flow.

2.1 Turbulent flow in Pipe

Turbulent flow is the most commonly encountered fluid flow in everyday practices. Unlike laminar flow, in which fluid follows a smooth path in absence of irregularities, turbulent flow is characterized by tremendous unsteady, three dimensional, multiscale stochastic fluctuations. Turbulent flow in pipe has been an object of huge attention in research because of its design simplicity. Several topics such as transition in turbulent flow in pipe, effect of roughness on turbulence have been investigated in the past (Benson et al.2005; Hamilton et al. 1995; Hof 2004).

Whenever a fluid flows (laminar or turbulent) in a pipe there is a pressure drop created, due to which a considerable amount of energy is spent in pumping the fluid. This pressure drop comes from the drag force or fluid resistance acting on the fluid. Two types of drag force acting on a fluid are: Skin friction, which is caused by the friction of fluid against the surface of object and form drag which comes from the shape of object. For flows in pipe, skin friction is the significant drag force. The skin friction coefficient (c_f) is calculated with the help of wall shear stress (τ_w) using the Equation 2.1:

$$\boldsymbol{c_f = \frac{\tau_w}{\frac{1}{2}\rho U_\infty^2}} \qquad (2.1)$$

where U_∞ is the free stream velocity and ρ is the density of fluid (Cengel and Cimbala, 2006).

Turbulent wall shear stress comprises of two components (Figure 2-1): laminar component, which represents the friction between fluid layers ($-\mu\frac{\partial u}{\partial r}$), and turbulent component, which represents the mean transport of fluctuating momentum by turbulent velocity fluctuations known as the Reynold Stress ($-\rho\overline{u'v'}$).

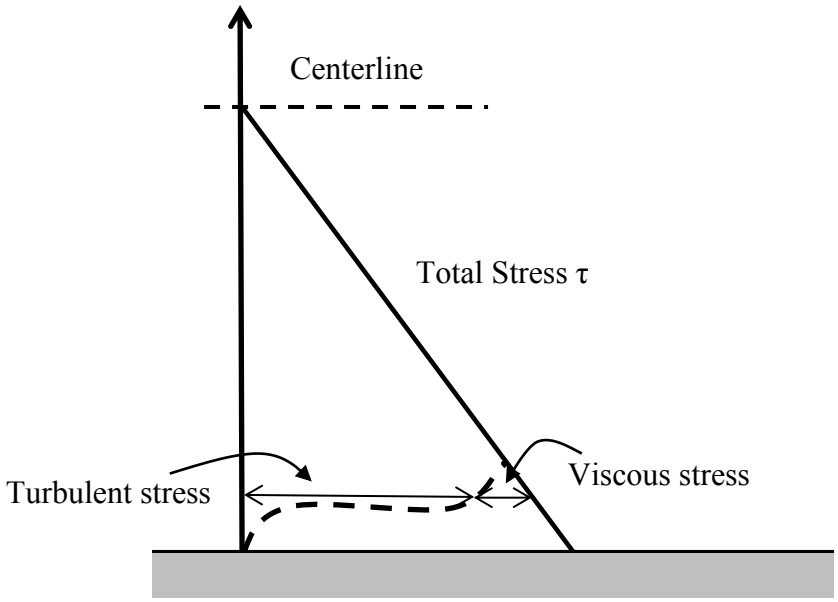

Figure 2-1: Two components of turbulent shear stress across turbulent channel flow (Adapted from Kundu et al. 2012).

Wall shear stress for both laminar and turbulent pipe flow can be inferred from pressure drop as shown in Figure 2-2 and Equation 2.2 (Cengel and Cimbala, 2006). Here, τ is the wall shear stress acting on the pipe, r is the radius of the pipe and l is the test section of pipe where pressure drop is calculated. P_1 is the pressure at section 1 of the pipe and ΔP is the pressure drop across the section 1 & 2.

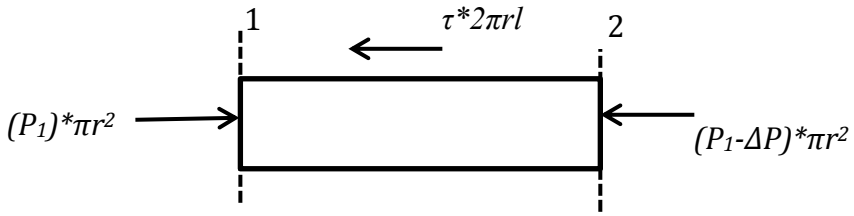

Figure 2-2: Wall shear stress and pressure drop in a pipe flow.

$$P_1\pi r^2 - (P_1 - \Delta P)\pi r^2 - \tau(2\pi rl) = 0 \qquad (2.2)$$

$$\tau = \frac{\Delta P r}{2l} \tag{2.3}$$

Hence, drag force can be indirectly inferred from the pressure drop occurring in pipe (Cengel and Cimbala, 2006).

2.2 Taylor-Couette Flow

Fluid flow arising in between two differentially rotating concentric cylinders is known as Taylor-Couette flow. It has widely been used to study the instability and pattern formulation in transition and turbulence at a lab scale. Figure 2-3 shows the basic geometry required in order to obtain TC flow. It is a closed system and possesses a simple geometry permitting a well-defined energy balance. Viscous energy dissipation can be easily calculated by simply measuring the torque on cylinders.

Several different flow regimes can be evaluated in TC flow by simply varying the angular velocity of inner or outer cylinder, thereby providing complete insight about the transition and turbulent structures. Section 2.2.1 discusses the mathematical background for the Taylor Couette flow.

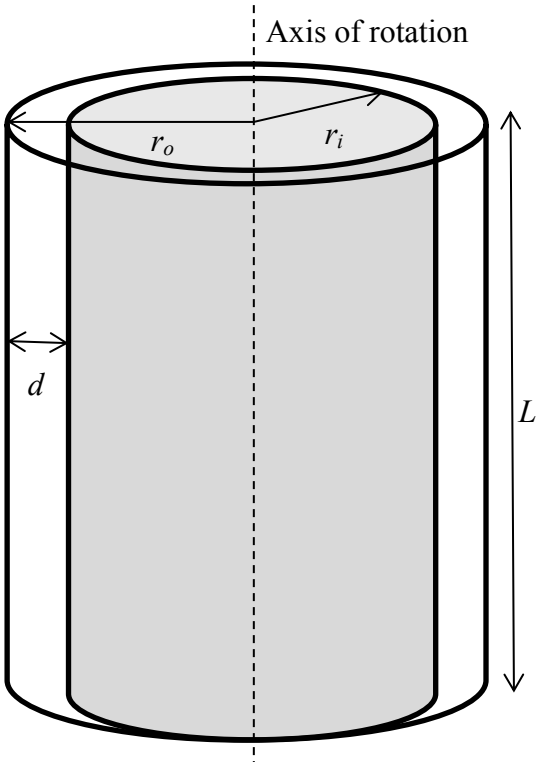

Figure 2-3: Basic schematic of Taylor-Couette Flow.

2.2.1 Navier Stoke equation for Taylor Couette Flow

The following parameters describe a Taylor Couette System: r_i is inner radius, r_0 is the outer radius, Ω_i is inner cylinder angular velocity, Ω_o is outer cylinder angular velocity, L is the length of inner cylinder, ν is fluid kinematic viscosity and ρ is the fluid density

η= radius ratio= r_i/r_o (2.4)

Re_i= Inner Cylinder Reynolds Number= $\frac{\Omega_i r_i(r_0-r_i)}{\nu}$ (2.5)

Re_o= Outer Cylinder Reynolds Number=$\frac{\Omega_o r_0(r_0-r_i)}{\nu}$ (2.6)

$d= r_0- r_i$ (2.7)

Γ= aspect ratio= L/d (2.8)

r, θ and z are cylindrical coordinates, p is the pressure and v_r, v_θ and v_z are velocity components. The boundary conditions for this system are:

$v_\theta(at\ r= r_i)= r_i\Omega_I$ (2.9)

$v_\theta(at\ r= r_o)= r_o\Omega_o$ (2.10)

$v_r= v_z=0$ (2.11)

The Navier stoke equations for cylindrical coordinates are:

$$\rho\left(\frac{\partial v_r}{\partial t}+v_r\frac{\partial v_r}{\partial r}+\frac{v_\theta}{r}\frac{\partial v_r}{\partial \theta}-\frac{v_\theta^2}{r}+v_z\frac{\partial v_r}{\partial z}\right)$$

$$=-\frac{\partial p}{\partial r}+\rho g_r+\mu\left[\frac{1}{r}\frac{\partial}{\partial r}\left(r\frac{\partial v_r}{\partial r}\right)-\frac{v_r}{r^2}+\frac{1}{r^2}\frac{\partial^2 v_r}{\partial \theta^2}-\frac{2}{r^2}\frac{\partial v_\theta}{\partial \theta}+\frac{\partial^2 v_r}{\partial z^2}\right] \quad (2.12)$$

$$\rho\left(\frac{\partial v_\theta}{\partial t}+v_r\frac{\partial v_\theta}{\partial r}+\frac{v_\theta}{r}\frac{\partial v_\theta}{\partial \theta}+\frac{v_r v_\theta}{r}+v_z\frac{\partial v_\theta}{\partial z}\right)$$

$$=-\frac{\partial p}{\partial \theta}+\rho g_\theta+\mu\left[\frac{1}{r}\frac{\partial}{\partial r}\left(r\frac{\partial v_\theta}{\partial r}\right)-\frac{v_\theta}{r^2}+\frac{1}{r^2}\frac{\partial^2 v_\theta}{\partial \theta^2}+\frac{2}{r^2}\frac{\partial v_r}{\partial \theta}+\frac{\partial^2 v_\theta}{\partial z^2}\right] \quad (2.13)$$

$$\rho\left(\frac{\partial v_z}{\partial t}+v_r\frac{\partial z}{\partial r}+\frac{v_\theta}{r}\frac{\partial v_z}{\partial \theta}+v_z\frac{\partial v_z}{\partial z}\right)$$

$$=-\frac{\partial p}{\partial z}+\rho g_z+\mu\left[\frac{1}{r}\frac{\partial}{\partial r}\left(r\frac{\partial v_z}{\partial r}\right)+\frac{1}{r^2}\frac{\partial^2 v_z}{\partial \theta^2}+\frac{\partial^2 v_z}{\partial z^2}\right] \quad (2.14)$$

A solution obtained after solving the abovementioned equations using these boundary conditions are:

$$v_\theta = Ar + \frac{B}{r} \tag{2.15}$$

$$\frac{\partial p}{\partial r} = \frac{\rho v_\theta^2}{r} \tag{2.16}$$

$$\text{Where } A = \frac{r_o^2\,\Omega_0 - r_i^2\,\Omega_i}{r_o^2 - r_i^2},\ B = -\frac{r_o^2\,r_i^2(\Omega_0 - \Omega_i)}{r_o^2 - r_i^2} \tag{2.17}$$

This simple solution is instable at increasing Reynolds number. Centrifugal instability is the reason for the development of well-known Taylor vortices in this setup at the first transition. In steady state, the centrifugal force ($\frac{\rho v_\theta^2}{r}$) is balanced by the pressure gradient ($\frac{\partial p}{\partial r}$) as shown in above solution (Equation 2.16). Since the angular momentum is conserved, if a fluid particle is moved slightly outwards, it will get a new velocity ($v=r_1v_1/r_2$). Since in the case of the inner cylinder moving, the pressure gradient decreases with increasing radius (due to decrease in velocity with increasing radius); damping/viscous force is less than the centrifugal force due to which particle may continue moving outward, giving rise to instability. A critical value of Reynolds number is required to observe this instability because at low Re instability is subjugated by fluid viscosity. However, with outer cylinder rotating, the pressure gradient increases with increasing radius (due to increase in velocity with increasing radius) which balances the change in centrifugal forces, thereby not creating the instability (Di Prima and Swinney, 1985). With increasing *Re*, a classical regime is obtained in which boundary layers are of laminar type, however, turbulence is developed in the bulk at length scales between the Kolmogorov and the integral scale. Further increasing the *Re*, leads to development of the fully turbulent regime in the system which consists of turbulent boundary layers with structures and drag mechanisms similar to that of a flat plate boundary layer (Huisman et al. 2013).

2.2.2 Literature Review

Taylor Couette flow was first studied by Taylor (1923) who observed and calculated a critical Reynolds number required to obtain the instability in the one dimensional solution in this

system. These instabilities are cellular toroidal vortices which spread out consistently along the cylinder axis and were originally visualized with the help of dye. However, these early experiments simply focused on primary instabilities which were far below the highly turbulent regime. Wendt (1933) for the first time provided an extra dimension to this setup by studying TC flow with two independently rotating cylinders, which easily enables the set up to reach a highly turbulent regime. Davey (1962) accurately predicted the torque acting on the cylinders through numerical calculation for the Taylor Vortex flow. Cole (1976) for the first time observed a second critical Reynolds number and demonstrated using flow visualization that with further increase in angular velocity (beyond first critical Reynolds number), a wavy vortex flow is observed. Using torque measurements, it was proven that Taylor vortex flow becomes unstable beyond this critical point and these experiments were conducted in a range of radius ratio and aspect ratio. Furthermore, an increase in the value of the second critical Reynolds number was exhibited with increasing annular gap and values were in well agreement with theoretical predictions for aspect ratio greater than 40.

Donnelly & Simon (1959) developed a mathematical relation (Equation 2.18) for the torque (G) imparted by fluid friction to the outer cylinder (static), as a function of inner cylinder angular velocity (Ω_i) and verified it with the experimental data.

$$G = a\Omega_i^{-1} + b\Omega_i^{1.36} \tag{2.18}$$

However, the relation required constant a and b to be experimentally determined from data and didn't consider radius ratio as the variable.

Wendt (1933) used non dimensional torque (G) (Equation 2.19) to scale the torque and to develop an empirical relation for TC system.

$$G = T/(L\rho\nu^2) \tag{2.19}$$

Here L is the length of inner cylinder, ρ is the fluid density and ν is the fluid kinematic viscosity. Wendt (1933) then proposed a correlation for dimensionless torque (G) as a function of radius ratio (η) and Reynolds number (Re) and validated it with experimental data.

$$G = 1.45\frac{\eta^{3/2}}{(1-\eta)^{7/4}}Re^{1.5} \qquad (400 < \mathrm{Re} < 10^4) \tag{2.20}$$

$$G = 0.23\frac{\eta^{3/2}}{(1-\eta)^{7/4}}Re^{1.7} \qquad (10^4 < \mathrm{Re} < 10^5) \tag{2.21}$$

Lathrop et al. (1992) used a power law model to fit the dimensionless torque (G) with the expression $G \propto Re^{\alpha}$, where α varies from 1.66 to 1.87 beyond Re of 1.3 X 10^4; which was validated later by Lewis & Swinney (1998) through experimental work at radius ratio (η) of 0.724.

Smith & Townsend (1982) observed boundary layers in high Re Taylor –Couette flow using hot-wire probe in air. Later, Lathrop et al. (1992) confirmed through experimental work, that after a well-defined transition at Re = 1.3 X 10^4, the TC system behaves like a wall-bounded shear flow. Lewis & Swinney (1998) observed change in the coherent structures of core flow beyond this critical Re of 1.3 X 10^4. So in the past two decades it has become evident that for Re >1.3x10^4, TC flow is a convenient analogue for wall bounded shear flow and drag reduction studies.

Several efforts have been made in the past to model the fully turbulent Taylor-Couette flow and contributions by Lathrop et al. (1992) and Panton (1992) are worth mentioning. Lathrop et al. (1992) considered the core region as an extension of turbulent boundary layers and assumed a logarithmic boundary layer at the wall. They demonstrated that the behavior of TC flow above critical Re is analogous to that of wall-bounded shear flows characterized by turbulent boundary layer in pipe. On the other hand, in an independent work, Panton (1992) assumed constant angular momentum in the core and modeled turbulent TC flow. Both the authors, independently arrived at a similar analytical solution using G and Re. Lathrop et al. (1992) equated Prandtl expression for turbulent shear stress with $T/(rA)$ where T is the Torque and A is the area of cylindrical fluid element at radius r. The final expression obtained was

$$\frac{Re}{\sqrt{G}} = N\log_{10}\sqrt{G} + M \tag{2.22}$$

$$\text{Where } N = \frac{(1-\eta^2)ln10}{\eta\kappa\sqrt{2\pi}} \tag{2.23}$$

$$M = N\left|ln\left\{\left(\frac{1-\eta}{1+\eta}\right)\frac{1}{y_0^+\sqrt{2\pi}}\right\} + \kappa y_0^+\right| \tag{2.24}$$

Here κ is the *von- Kármán constant* and $y_0^+$is the dimensionless distance from the wall stated in Law of the wall. The skin friction coefficient (c_f) is given by Equation 2.25, where τ_w is wall shear stress.

$$c_f = \frac{G}{Re^2} = \frac{2\pi r_o^2 \tau_w}{\rho \nu^2 Re^2} \quad (2.25)$$

The final expression was obtained as

$$\frac{1}{\sqrt{c_f}} = N\log_{10}(Re\sqrt{c_f}) + M \quad (2.26)$$

In the case of smaller aspect ratios (< 10), significant end effects can be observed due to Ekman circulation (Burin et al., 2006). It arises due to the no slip boundary condition at the ends, because of which pressure forces are not centrifugally balanced, leading to fluid movement in the radial direction. Some setups utilize intermediary rotating end rings in order to overcome this limitation (Hollerbach & Fournier 2005; Altmeyer et al. 2010). Kageyama et al. (2004) studied the TC flow in a small aspect ratio of 0.45. Due to the active role of vertical boundaries on the secondary flow at a small aspect ratio, a different approach to achieve a control over the velocity profile by increasing the number of endcap boundary conditions was proposed by the authors. A setup with multiple independent endcap rings (up to 5) rotating at different speeds was designed to achieve such boundary conditions. These rings have been observed to be suitable in reducing Ekman circulation.

In summary, intensive work has been carried out on Taylor-Couette Flow in the past and it has been proven to retain the similar characteristics as turbulent boundary layer. Further, due to its closed geometry, it offers an advantage over pipe flow.

3. DRAG REDUCTION

In countless applications, significant amount of power is depleted in pumping fluids to overcome the pressure drop in pipelines due to drag. Great deal of research has been carried out to decrease this pressure loss by either modifying the pipe inner surface or with some additives to the fluid. Reductions in pressure drop or "drag reduction" using high molecular weight polymers (known as Drag Reducing Agents (DRA)) is well recognized, because simply by the addition of a few ppm of these DRA, drag can be significantly reduced (up to 70%) leading to substantial energy savings (Ptasinski et al. 2001). After it was revealed by Toms (1949), this phenomenon has gathered enormous attention because of its application in oil pipe lines. Similarly, surfactants and fibers are also been studied as DRA; though, the mechanism for drag reduction with these is different from that of polymers. In the current chapter, drag reduction using polymers, surfactants and fibers is discussed. The section also provides a brief review on drag reduction testing conducted in both pipe flow and Taylor-Couette flow.

3.1 Types of Drag Reducing Agents

Three extensively studied Drag Reducing Additives (DRA) i.e. polymers, surfactants and fibers are discussed separately in this section.

3.1.1 Polymers

Currently, high molecular weight polymers are the most commonly used DRA's in industry and extensive research has been carried out on these polymers to find the mechanism behind the drag reduction. Surprisingly, just by using a little amount of these polymers, drag can be remarkably reduced.

In spite of several attempts made by the researchers, the phenomenon of drag reduction has not been entirely understood even today. After the discovery of drag reduction, Toms suggested that shear thinning near the wall region leads to viscosity drops which decreases the fluid resistance and reduces the drag. However later experiments conducted by Walsh (1967)

demonstrated drag reduction in shear thickening fluids too, thereby priving the previous theory to be incorrect.

Virk et al.(1967) made the first attempt to study the onset of drag reduction and characterized it in two categories; Type A and Type B (Virk, 1975)**.** For Type A, the drag reduction occurs only in turbulent regime indicating that there is a minimum value of Reynolds number required. Polymers were found to start reducing drag only beyond a particular value of wall shear stress (which is equal to 7 Pa for Polyethylene oxide) known as the onset of drag reduction. Virk et al. (1969) mentioned that the onset wall shear stress was related to the randomly coiled effective diameter of the polymer. Further, degree of drag reduction was observed to be dependent on either molecular weight or chain length of the polymer. On the other hand for Type B, comparatively high concentration of polymer is required and drag reduction occurs during transition from laminar to turbulent regime (Virk and Wagger, 1989). The existence of Virk or Maximum Drag reduction (MDR) asymptote was also demonstrated in their study, beyond which there is no increase in drag reduction. MDR was found to be independent of polymer concentration or type of polymer used. Increase in center line velocity of the fluid after injection of polymers was reported in this investigation.

Lumley (1969) postulated a time criterion hypothesis to understand the mechanism of drag reduction which suggested that matching the elongation relaxation time of polymer chains compared to the time scale of the turbulent eddy is the requirement for the drag reduction. de Gennes (1971) proposed reptation theory which proposes that chain relaxation time is proportional to cube of molecular mass, confirming that increase in molecular weight enhances the drag reduction. Min et al. (2003) verified this by conducting a theoretical study and noticed that drag reduction indeed increases with greater Weissenberg number, which is the ratio of viscous and elastic forces. So, when the chain relaxation time is high enough and this condition is fulfilled, the polymer chains become significantly stretched, known as the coil-stretch transition. The elongational viscosity rises by a magnitude of ten thousand in this state. Since the elongational strain rates are more prominent near the wall region, this coil stretch transition occurs predominantly near wall and the enhanced elongational viscosity dampens turbulent fluctuations, thereby decreasing the drag (Lumley 1973, Sreenivasan and White 2000).

However, a dissimilar theory was suggested by de Gennes (1986) which stated that coil stretch transition cannot be achieved due to high oscillations of strain rates and such a slight increase in elongational viscosity can't lead to substantial turbulence suppression. He proposed that the drag reduction is observed significantly when the elastic energy stored by the elongated polymer becomes comparable to the turbulent energy. The main idea of this model was that coils in the dilute regime behave elastically at high frequencies due to which elastic energy enhances with diminishing length scale of turbulence. On the contrary, the turbulent energy decreases with the scale size. When these two energies become equivalent, the elastic energy intervenes with the turbulent cascade mechanism hindering it to progress towards the Kolmogorov scale. Hence, the mechanism of generation of small scale turbulence is stopped at a scale greater than the Kolmogorov scale. These leads to enhancement in buffer layer thickness and subsequently, drag reduction (Sreenivasan and White 2000).

The first polymer studied for drag reduction in turbulent pipe flow was Polymethyl methacrylate with monochlorobenzene as a solvent, and significant pressure drop was reported (Toms 1949). Sodium carboxymethyl cellulose demonstrated similar behavior in water which was studied by Dodge and Metzner (1959). Table 3-1 summarizes the various polymers which have been investigated extensively for drag reduction.

Table 3-1: Various high molecular weight polymers used for drag reduction.

Polymer	**Solvent**	**Reference**
Polyacrylamide	Water	Hoyt (1972), Ptasinski et al. (2001) Graham (2004)
Polymethyl methacrylate	Methylchlorobenzene	Toms (1949), Hershey and Zakin (1967)
Polyethylene oxide	Benzene	Hou et al. (2008), Cadot et al. (1998)
Polyisobutylene	Toluene, Benzene	Hoyt (1972), Hershey and Zakin (1967)
GuarGum	Water	Pazwash (1984), Hoyt (1972)
Sodium Carboxymethyl Cellulose	Water	Deshmukh et al. (1991),Abdulbari et al. (2013)
Hydroxethyl Cellulose	Water	Hoyt (1972)

All the above-mentioned polymers had an ultra-high molecular weight of about 1 Million Da (Patterson et al. (1969)). Polyacrylamide is the most commonly used Drag reducing agent in

industry as well as for research purposes because of its high efficiency, low cost and less degradation as compared to other polymers.

Polymer solutions can be used either as homogeneous systems or as heterogeneous systems for reducing the pressure drop. Injection technique in case of heterogeneous systems has a huge effect on the effectiveness of drag reduction. Well and Spangler (1967) examined the effect of polymers on turbulent flow by injecting the solution at the center of pipeline. It was revealed that polymer solution does not reduce drag until it reached the near wall region. Similar results were reported by McComb and Rabie (1982) who demonstrated increase in drag reduction with increasing distance from injection point (known as core injection) which was attributed to diffusion of Polyethylene oxide solution towards the wall. Further drag reduction was observed to be better when polymer was injected near the wall region (known as wall region injection). Experiments conducted by Bewersdorff (1982) indicated that heterogeneous injection could reduce higher drag as compared to homogeneous injection.

3.1.1.1 Effect of Parameters

There are several factors that affect the drag reduction: Pipe Diameter, Polymer Concentration, Polymer Molecular weight etc. These will be discussed subsequently in this section.

- Pipe Diameter: With an increase in pipe diameter, higher concentration of polymer is required for the onset of drag reduction. (Virk 1971).
- Molecular Weight: For higher molecular weight polymers, there is a decrease in Reynolds number for onset of drag reduction (Virk, 1971). Moreover, lower polymer concentration is needed for accomplishing equivalent drag reduction. On the contrast, Morgan and McCormick (1990) suggested that coil volume attained by a polymer in the solution has more effect on drag reduction rather than the polymer molecular weight.
- Molecular Associations: McCormick et al. (1990) and Mumick et al. (1994) extensively studied the effect of molecular structure, molecular associations and solvation on drag reduction. Presence of higher molecular association increases the

stability of the polymer or reduces the degradation at higher shear rate because of the breakage of these weaker associations instead of covalent bond at higher stress rate.

- Molecular Structure: Hoyt and Fabula (1964) demonstrated that linear polymers with high molecular weight provide improved drag reduction in comparison to branched polymers. Further, chain flexibility has a profound effect on drag reduction. Flexible polymers exhibit enhanced diminution in drag when compared with rigid rod polymers.
- Polymer Concentration: With an increase in polymer concentration, there is an increase in Drag reduction until MDR asymptote is reached, beyond which drag reduction attains a constant value (Virk 1971).
- Reynolds Number: Drag reduction increases with increasing Reynolds number because of the higher stretching of the polymer chains which dampens the turbulence more effectively (Hof 2004).

3.1.1.2 Polymer Degradation

Polymers used as drag reducing agents are susceptible to mechanical as well as thermal degradation. There can be a significant chain breakage at high strain rate resulting in sharp decline in effectiveness of DRA after passage through pumps, valves and sharp turns (Abdel et al. 1973). It has been reported that 10ppm solution of PEO in water loses 10% of its drag reduction performance after a single pass through a centrifugal pump (Sellin et al. 1982). On the other hand, a subsequent study conducted by Moussa et al. (1994) using polyacrylamide as DRA has shown that degradation mostly occurs at the pipe entrance due to the presence of the higher shear stress present in that region. Temperature further increases the degradation of polymer. Choi and Kasza (1981) conducted an investigation on polyacrylamide solution degradation at various temperatures and concluded that the polymer chains break much faster at high temperature. In addition to degradation through temperature, polymeric DRA solutions have been observed to be aged and lose their effectiveness with time (Shin 1965).

3.1.2 Surfactants

Surfactants have a strong potential for reducing the drag, however these are not widely studied as compared to high molecular weight polymers for this application. Unlike polymers, surfactants have an advantage of endurance to shear degradation in pumps and other high stress zones which would be elucidated in detail, later in this section. The mechanism of drag reduction in case of surfactants is little different from polymers. Micelles formation (microscopic units assembled from the molecules of surfactants) of the surfactants above critical micelle concentration plays an important role in reducing the drag. These micelle structures have been reported to exhibit viscoelastic properties similar to polymers which reduce the drag. The micelles are less disrupted by high-shear stress zones in pumps or valves and although the structure might be broken up, it can automatically reorganize once the shear stress zone is no more, thereby restoring the drag reduction effect. Hence, these surfactants have an ability to self-repair which gives them an advantage over polymers (Hoyt 1989).

Micelles don't display viscoelastic behavior in static solution. Similar to polymers, these require a minimum Reynolds number beyond which they start demonstrating the phenomenon of drag reduction. Beyond this minimum *Re*, DR increases with increasing *Re*, but then decreases with increasing flow rate (or shear rate) because of the breakage of micelle at higher shear rate (Zhang et al 2005). Moreover, DR obtained in case of surfactants can be higher than of polymers and this maximum limit is known as Zakin Limit (Zakin et al. 1996).

Anionic, non-ionic and cationic surfactants have been known to display this effect. However, use of cationic surfactants has been limited because of environmental regulations and more research is currently being carried out to investigate the effect of zwitterionic surfactants (possess both negative and positive charge) on drag reduction. Sodium oleate is a widely studied anionic surfactant which showed 82% DR (with potassium chloride as an additive) in an experiment conducted by Savins (1967). Cetyltrimethylammonium bromide commonly known as CTAB (Fig. 3-1a) is a cationic surfactant which showed DR at very low concentrations (Sellin et al. 1982). Fatty acid amide ethoxylates in case of nonionic surfactant have been observed to show DR (Zakin and Chiang 1972). Hexa decyl dimethyl ammonio propane sulfonate (Fig. 3-1b) in category of zwitterionic surfactants was inspected by Saul et al. (1974) and was found to show viscoelastic behavior. Cationic surfactants have been found

to be toxic for marine life due to which more focus has been shifted towards the use of zwitterionic or amphoteric surfactants.

(a) (b)

Figure 3-1: Chemical structure of (a) CTAB and (b) Hexa decyl dimethyl ammonio propane sulfonate.

3.1.3 Fibers

Drag reduction using fibers comes in the category of solid suspension drag reduction which has not been extensively studied yet. Spherical particles have also been reported to show similar properties however this section will cover only fibers for drag reduction. Researchers have reported that dampening of turbulent structures by solid particles is the mechanism behind this kind of drag reduction. This turbulence suppression weakens the transverse momentum transport which subsequently reduces the turbulence dissipation (Patterson et al. 1969). Furthermore, there is an optimum concentration of fiber required in order to observe any change. If n is the number density, v is the fiber volume fraction, l is the fiber length, d is the fiber diameter and a is the aspect ratio (l/d); then three different concentrations can be explained by (Delfos et al. 2011):

- Dilute:

$nl^3=(nld^2)\ (l/d)^2=va^2<<1$

No drag reduction observed

- Semi Dilute:

$va^2>1;\ ca<<1$

Optimum condition for drag reduction

- Dense:

$va>1$

Leads to pipe clogging

Nylon, wood pulp and asbestos with high aspect ratio are found to reduce the drag. A study conducted by Forrest and Grierson (1931) validated the drag reducing using wood in a cast iron pipe. Similarly, Bobkowicz and Gauvin (1965) reported nylon as a DRA using few weight percent of these fibers. Amongst fibers, Asbestos fibers exhibit the best characteristics of drag reduction and their efficiency has been observed to be equivalent of drag reducing polymers (Ellis 1970). However, due to clogging of pipe from fibers and the health hazards due to asbestos, these have not been commercially tested yet.

3.2 Drag Reduction in pipe or channel flow

Most of the research in the area of drag reduction has been done using pipe or channel flow setup. Turbulent channel/pipe flow is the most commonly studied flow in fluid dynamics and drag reduction in such a setup can be easily inferred from pressure drop at constant flow rate. Drag reducing agents were first used commercially in Trans-Alaskan Pipe in 1979. Merely with 1 ppm of polymer solution, 30% of the drag was observed. Since then, this phenomenon has been utilized for several applications including hydraulic fracturing, slurry transportation, water jets in firefighting equipment etc (Wang et al. 2011).

Hershey and Zakin (1967) demonstrated two types of drag reduction occurring by different mechanisms and utilized polyisobutylene in cyclohexane and benzene. The first one, commonly encountered in turbulent flows, required a minimum value of Reynolds number in order to create the effect. The second occurred in the extended laminar region, which delayed the transition of laminar to turbulent regime by providing more stability to the liquid flow. Barnes and Walter (1968) studied drag reduction in curved pipe and observed that curvature enhanced the drag reduction in the extended laminar/ transition region however had a negative effect at high Reynolds number. Similarly, micellar additives in a suspension flow were observed to reduce the drag in extended laminar region (Myška and Vocel, 1977).

Vleggar and Tels (1973) investigated drag reduction using polymer threads which were injected axially in the pipe and visualized by utilizing colored polymer. These were observed to show drag reduction at even low Reynolds number. Lee and Duffy (1978) studied friction loss using wood pulp fibers and observed a significant decrease. Study on oscillating drag

reducing fluid showed improved flow rate in a circular tube which was found useful for various mass transfer applications (Sundstrom and Kaufman, 1977). A review based on drag reduction by Sellin et al. (1982) provides an insight about industrial scale application of DR, preparing polymeric solutions at large scale and prospects of DR in future. A vast literature (including reviews) has been published till then focusing on turbulence measurement techniques in drag reducing solutions (Lumley 1969; Lumley 1973; Campolo et al. 2015; Wang et al. 2011; Dezhong et al. 2005).

Since pressure drop measurements doesn't provide the complete picture of the mechanism of drag reduction; several turbulence measurements techniques such as Laser Doppler Velocimetry (LDV) and Particle Image Velocimetry (PIV) have been adopted by researchers to obtain greater insight into the effect of polymer chains on turbulent flow structures. The most recent contribution on DR was made by Warholic et al. (2001) and White et al. (2004). Warholic et al. (2001) investigated the effect of drag reducing polymers on turbulent structures using Particle Image Velocimetry (PIV) at Reynolds number $2x10^4$. A substantial decrease in wall normal Reynolds stress and skewness with increase in polymer concentration was observed. The considerable change in Reynolds stress was detected, which implied a large modification in turbulent structure after the addition of polymer. Similarly, White et al. (2004) examined the turbulent structure of Drag Reducing boundary layer flows using PIV in a zero pressure gradient boundary layer. It was observed that the polymers do not merely suppress the turbulence, but the stream-wise turbulence intensity is also enhanced. Further, the turbulence intensity normal to the wall (span wise) is diminished. In other words, polymers orient the stress tensor, reducing viscous transport to the wall where drag is felt.

3.3 Drag Reduction in Taylor-Couette Flow

The TC system has advantages of having a closed geometry along with requirement of low fluid volume. Energy is added to the fluid without subjecting the fluid to the higher strain field of the pump. Further, turbulent TC flow demonstrates the identical features of a turbulent boundary layer (Lathrop et al. 1992). TC system has been widely studied in the past for drag

reduction using, additives as well as surface modification (Dutcher & Muller, 2009; Greidanus et al. 2011; Srinivasan et al. 2015).

The system with a rotating inner cylinder was utilized by Jones & Marshall (1969) to study the polyacrylamide solution of water at very low concentration. The goal was to study the relaxation effects using polymers in a Taylor-Couette flow. Although, reduction in drag was reported, there was no effect on stabilization or destabilization of Taylor vortices. The observations were in agreement with the previous study conducted by Lee (1966) during his doctoral thesis. The system has also been utilized to theoretically quantify the drag reduction using fibers as additive (Nsom, 1994).

Groisman & Steinberg (1996) studied a dilute polymeric solution in TC flow and made different observations in comparison to Jones & Marshall (1969). A significant effect of these polymers on the pattern and stability in TC flow was observed. Two novel oscillatory patterns were visualized which were attributed to fluid elasticity. Yi & Kim (1997) investigated the effect of polymeric solution on the critical Taylor number in TC flow. Concentration of the polymer was high (0.5 wt. %) compared to the previous studies and the decrease in critical Taylor number with increase in polymeric concentration was observed. It validated the results by Groisman & Steinberg (1996) indicating that polymeric solutions have a profound effect on the stability in TC flow, which leads to drag reduction in turbulent pipe flow.

From then, several studies have been conducted on drag reduction in TC flow using polymers, surfactants, bubbles etc. (Sugiyama et al. 2008; Koeltzsch et al. 2003; Ashrafi 2011). Kalashnikov (1998) investigated drag reduction using high molecular weight polyethylene oxide as a DRA in rotating outer cylinder geometry and dimensionless representation of friction coefficient was achieved. DR was correlated with rheological properties of the solution such as shear thinning viscosity.

Koeltzsch et al. (2003) studied drag reduction using surfactants in a TC setup with a rotating outer cylinder and for the first time the effect of changing viscosity with varying shear stress was taken into account. Dutcher & Muller (2009) explored the effect of drag reducing agents on hydrodynamic transitions in TC flow at a wide range of Re_0 and Re_i. Eskin (2014) has

numerically verified the applicability of the TC setup for drag reduction characterization and recommended a radius ratio to be less than 0.5 for this purpose.

In summary, although the literature on drag reduction in TC flow is not as vast as in pipe/channel flow, still tremendous results have been observed for drag reduction in this system.

4. DESIGN OF TAYLOR-COUETTE SETUP

The current study investigates commercial polyacrylamide, polysaccharides and thermo-responsive polymers for drag reduction. Pipe flow requires large amount of polymer/additives to test for drag reduction and it becomes a challenge to synthesize large amount of drag reducing agents at lab scale. As a solution, the current investigation develops a platform to test these additives for drag reduction requiring significantly small quantity for investigation purposes. A Taylor-Couette setup was designed with a stationary outer cylinder and rotating inner cylinder, in which drag (skin friction coefficient) can be inferred from torque acting on inner cylinder. This chapter summarizes the design considerations looked at while fabricating this setup.

A Taylor-Couette setup with a rotating inner cylinder and static outer cylinder was designed in this study. The schematic of the setup is shown in Figure 4-1. The radius of the inner cylinder (r_i) is 6.03 cm and the radius of the outer cylinder (r_o) is 7.94 cm; providing a radius ratio (η) of 0.76. The height of inner cylinder is 20.08 cm and annular gap between two cylinders (d) is 1.9 cm; which leads to an aspect ratio of 10.57. The maximum angular velocity of the inner cylinder achieved in this study is 35 Hz. A Reynolds number of up to 2.9×10^5 can be attained with water as a working fluid. Further, a reaction torque sensor was installed beneath the motor to measure the torque acting on inner cylinder. Thermocouple installed at the top of the outer cylinder's plate monitors the temperature of the fluid inside the system and there is a tachometer installed at the shaft to measure the angular velocity of inner system.

The three major components of the system: Taylor-Couette chamber, a motor for rotating the inner cylinder and a torque sensor, are described in detail in the following sections.

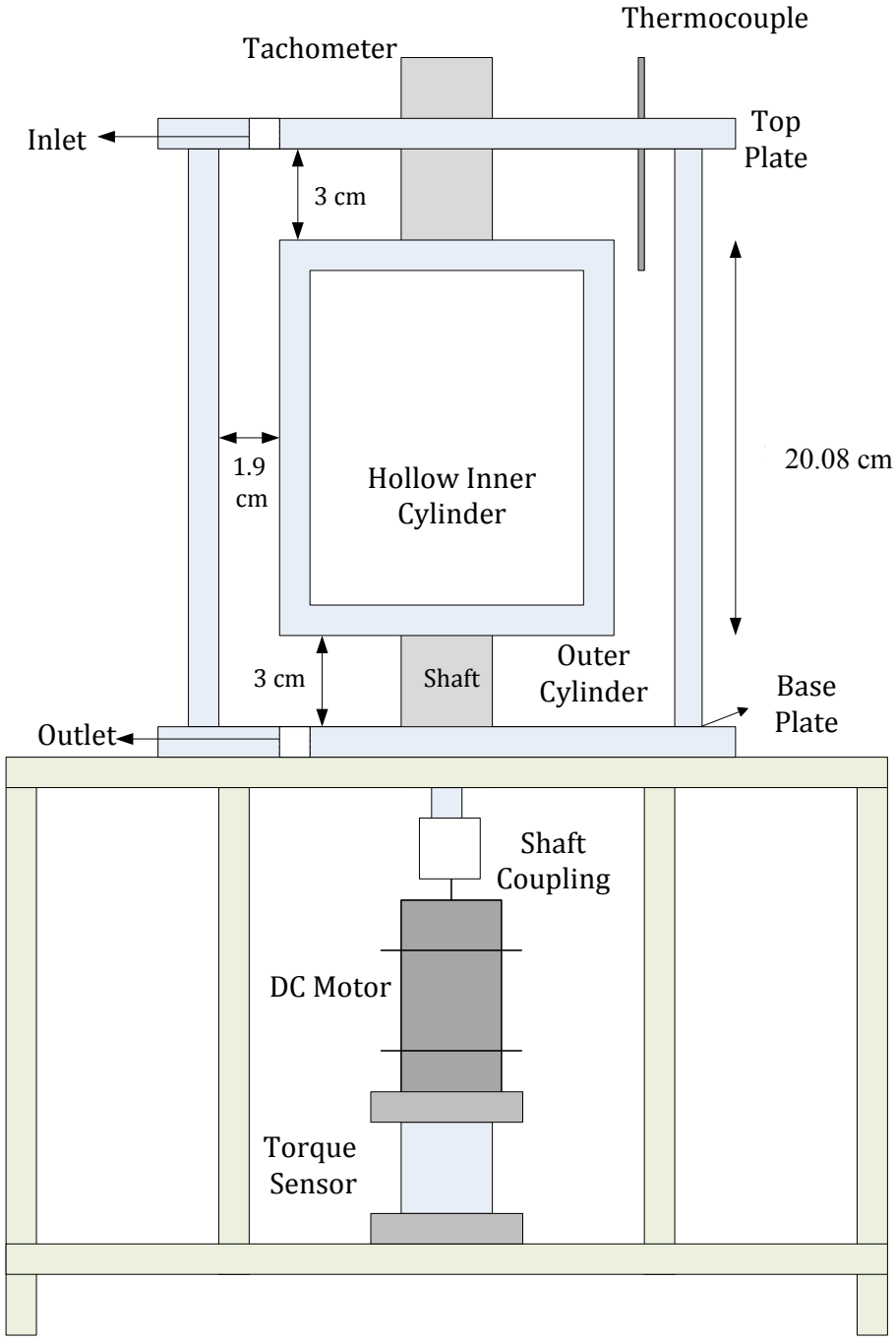

Figure 4-1: Schematic of Taylor-Couette setup.

4.1 Taylor-Couette Chamber

The Taylor-Couette (TC) chamber majorly consists of an outer cylinder, a hollow inner cylinder, a top plate, a base plate and a shaft.

The outer cylinder (Figure A-1) was made from an optically clear cast acrylic tube with an inner diameter (ID) of 15.875 cm and outer diameter (OD) of 17.78 cm. Due to the light weight, high tensile strength (5.5×10^7-7.75×10^7 N/m^2) and optical clarity, cast acrylic was chosen as a material for both the cylinders. The height of outer cylinder is 28.08 cm. A hollow inner cylinder was selected in order to minimize the inertial torque required to rotate the cylinder. The inner cylinder consisted of a cast acrylic tube and, two acrylic plates to cover the cylinder as well as to hold the shaft. An acrylic tube for the inner cylinder had an ID of 10.16 cm, an OD of 12.06 cm and a length of 15 cm. A ceramic coated shaft (1 inch) was chosen, where the ceramic coating provides a surface hardness of Rockwell C70 and is useful in withstanding the friction against the seal. A 2.54 cm thick acrylic plate (Figure A-2) with an outer radius of 12.06 cm was chosen to cover the inner cylinder, which had a clearance of 1 inch in the middle for the shaft. An adhesive seal was used to fix the cover plate to the inner cylinder, whereas a Buna N o-ring (Dash no. 215) and a stainless steel shaft collar were used to fix and seal the cover plate to the shaft. The shaft diameter was reduced to 1.27 cm at the end to connect it with the motor shaft using a coupling. The total assembly of inner cylinder is shown in Figure A-3.

The outer cylinder was covered with a top and a base acrylic plate. The top plate (Figure A-4) had a provision to hold the thermocouple probe and a clearance for the inlet opening; whereas the base plate had a clearance for outlet. A grooving was provided on both the plates to hold the bearing and seal. A double sealed stainless steel bearing (*BocoBearing*) with a ceramic ball material was used, whereas a graphite reinforced PTFE seal (*McMaster Carr*) was selected due to lower coefficient of friction and good wear resistance. An o-ring was placed in the grooving of both the top and base plates to tightly seal the TC chamber. Six threaded tie rods were used to firmly hold the assembly of chamber and the base plate (Figure A-5) was connected to a machine table using bolts and nuts. The complete assembly of the TC chamber is shown in Figure 4-2.

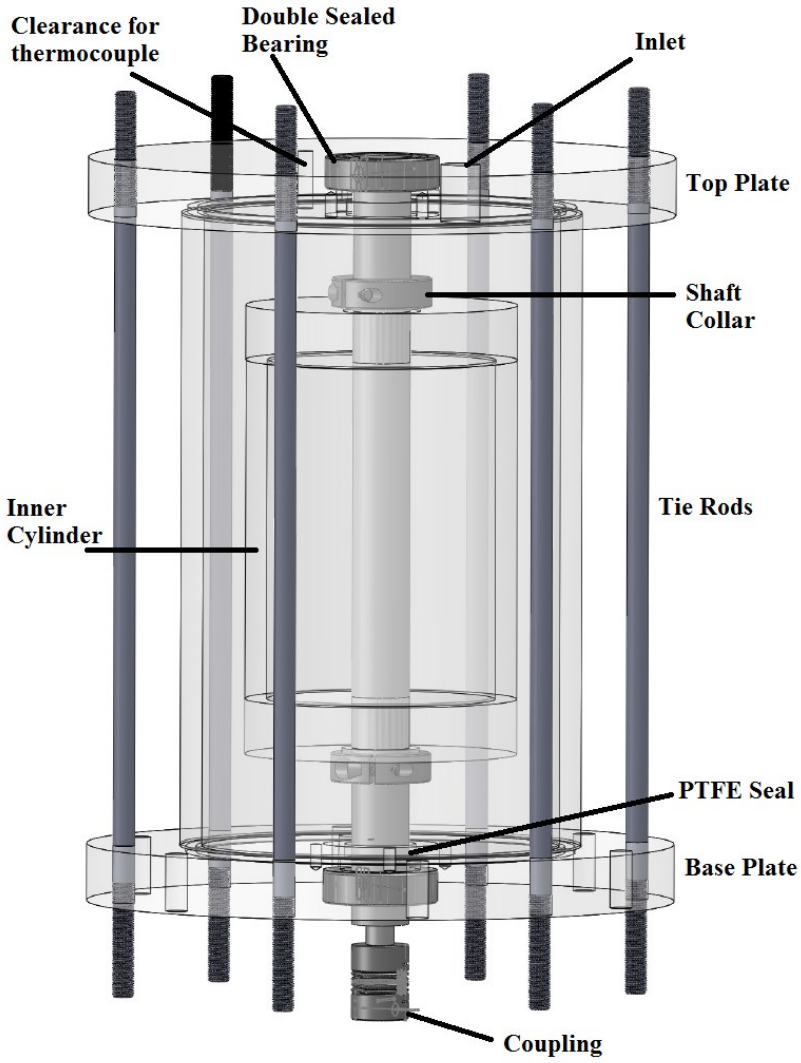

Figure 4-2: Complete assembly of TC Chamber.

4.2 Motor

A NEMA 34, 1/3 hp speed control DC Motor (*Amatek Inc*.) with the speed range of 300-3450 RPM was utilized in the current study. A frame was designed to connect the motor with torque sensor (Figure A-6). The specifications of Motor are listed in Table 4-1.

Table 4-1: Specification table of Motor.

hp	1/3
Maximum RPM	3450
Starting Torque	0.7344 N-m
Torque at Max. RPM	0.7344 N-m
Frame Size	NEMA 34
Shaft Diameter	1.27 cm

A high speed bellows flexible shaft coupling was used to connect the motor shaft to the inner cylinder shaft. The motor utilized in this study consists of a speed control with a feedback sensor that adjusts power to maintain the set speed. It combines the speed control characteristics of permanent magnet brushless DC motors with the convenience of AC power.

4.3 Torque Sensor

A reaction torque sensor (FSH02811; TFF425, *Futek Advanced Sensor Technology, Inc.*) was installed beneath the motor to measure the torque acting on inner cylinder. This torque sensor utilizes a bonded foil strain gauge to measure the reaction torque.

The strain gauge (approx. 8mm in size) is installed on an object and measures the strain acting on it. It works on a principle that electrical resistance or conductance is dependent on the geometry (or strain) of the conductor. A typical gauge consists of an alloy foil and has a backing material of polyamide (Futek A.S.T., 2013), which is then bonded or cemented on the object/shaft. When the object is deformed or the torsion is applied, the strain gauge is also deformed, resulting in a change in the electrical resistance. Four strain gauges are connected in a Wheatstone configuration; with potential difference across the bridge, a resulting change in electrical output is produced which is proportional to strain (this is used to calculate the torque). There are predominantly two kinds of torque sensors: Reaction and Rotary torque sensor. Rotary torque sensors are in alignment with the shaft and motor; and contain bearings and slip rings. Reaction torque sensors do not require any alignment, bearing or slip ring. Because reaction torque sensors are low maintenance, they were selected in this study. These are typically installed beneath the motor.

The complete assembly of the setup is shown in Figure 4-3.

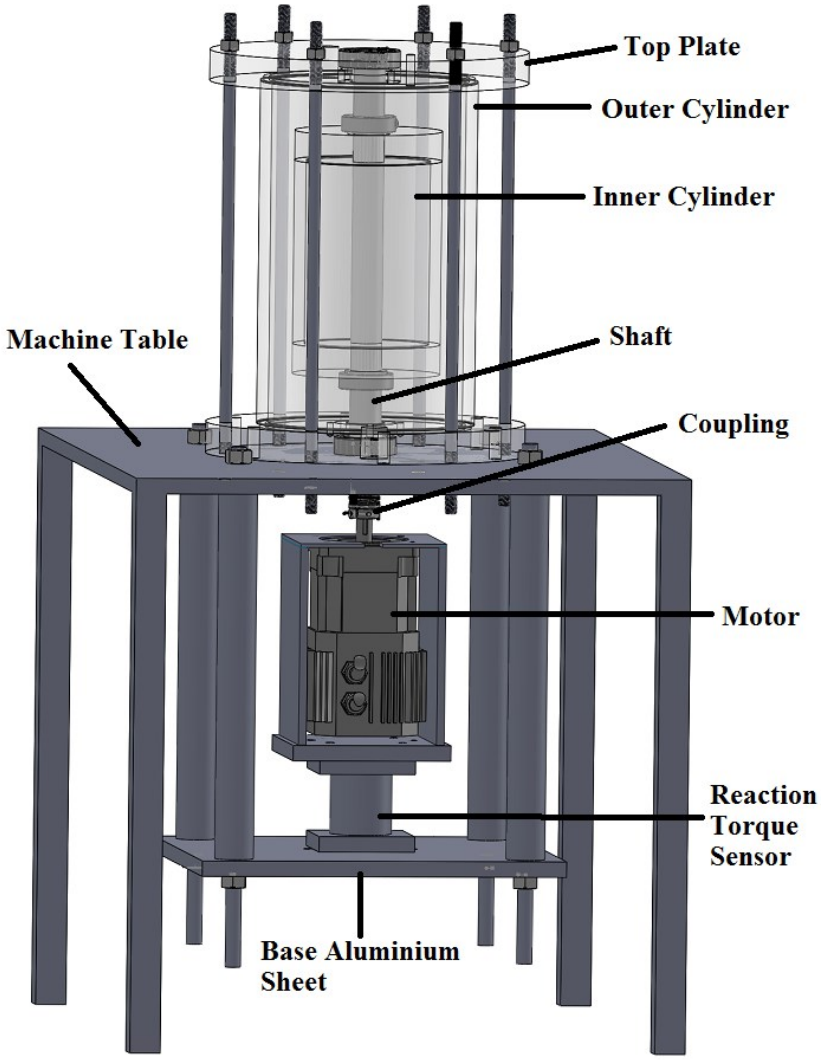

Figure 4-3: Complete assembly Taylor Couette Setup.

The torque sensor utilized in this study has a capacity of 7 N-m with torsional stiffness of 501 N-m/rad. It provides a rated output (RO) of 2mV/V. The hysteresis of the torque sensor was less than +/- 0.2% of the RO and the system was calibrated by Futek Advanced Sensor Technology, Inc. at 5 different points between 0-7 N-m for both the clockwise and the anti-clockwise direction. A maximum system error was found to be 0.02% of RO in the clockwise direction, and -0.03% of rated output in the anti-clockwise direction.

A USB220 (*Futek Advanced Sensor Technology, Inc)* kit was used to digitize the analog output voltage of the sensor and had a sampling rate of up to 4800 Hz at a resolution of 13.5

(Noise free bits). SENSIT Test and Measurement software was used for recording the torque while testing.

A type K, 316 stainless steel air/immersion thermocouple probe was installed on the top plate to monitor the temperature of the fluid in the annular gap. A slotted wheel tachometer was installed on the shaft, which measures the angular velocity of the inner cylinder. The tachometer consisted of a slotted disk mounted on the shaft and recorded the frequency of pulses, thereby providing the speed of the shaft.

The detailed procedure of operating this setup is mentioned in Appendix A.2 and A.3.

In summary, a new platform for testing drag reduction was designed and explored in this study. The Taylor-Couette flow, because of its closed geometry offers several advantages over other fluid flow systems such as pipe/channel flow, and requires significantly less fluid for testing purposes.

This chapter has been published as "Bhambri, P., & Fleck, B. (2016). Drag Reduction using high molecular weight polymers in Taylor-Couette Flow. International Journal of Mechanical and Production Engineering Research and Development, 6(1), 59–72."

5. DRAG REDUCTION USING HIGH MOLECULAR WEIGHT POLYMERS

Turbulent drag reduction with high molecular weight polymers is examined experimentally using Taylor-Couette (TC) flow set-up. The set-up consisted of a rotating inner cylinder and a static outer cylinder with radius ratio (η) =0.76 and aspect ratio (Γ) =10.57. A reaction torque sensor was used to measure the torque acting on the inner cylinder. Initially, experiments were conducted using water as a working fluid, on a wide range of Reynolds numbers varying from 5×10^4 *to* 2.8×10^4 *and the dimensionless torque (G) was used to scale the torque which compared well with the previous TC studies. For drag reduction, four different concentrations i.e. 80, 120, 160 & 200 PPM of polyacrylamide/Drag Reducing Agent (DRA) solutions were used. The skin friction coefficient (c_f) was used to infer the drag reduction in the experiments. The effect of concentration and Re on Drag Reduction was investigated. A maximum drag reduction of 63% was observed for 160 PPM solution. The TC set up is a suitable configuration for drag reduction testing and is more convenient than channel flow set up. The results were found to scale well with the turbulent drag in wall bounded shear flows (such as pipe/channel flow).*

5.1 Introduction

Significant amount of power is depleted in pumping the fluids to overcome the pressure drop in pipelines. Substantial research has been intensively carried out to decrease this loss by either modifying the pipe inner surface or using some additives in the fluid. Reductions in pressure drop, or in other words drag reduction using high molecular weight polymers (known as Drag Reducing Agents (DRA)), is well recognized because simply by the addition of small concentration of DRAs, drag can be significantly reduced (up to 70%) leading to substantial energy savings (Ptasinski et al. 2001). After it was revealed by Toms (1949), this phenomenon has gathered enormous attention because of its practical application in pipelines.

Virk et al. (1967, 1969) studied the onset of polymer drag reduction and demonstrated that there is a critical value of Reynolds number required (i.e. 12000) for drag reduction to occur. Drag reduction doesn't take place in laminar flow and the polymer helps in reducing the drag only after a certain value of wall shear stress (which is equal to 7 Pa for Polyethylene oxide).

Since turbulent flow is easily achievable in pipe flow, the majority of the experimental investigations in this area are conducted in either channel or pipe flow (Hershey & Zakin 1967; Lumley 1969; White et al. 2004). Further, drag reduction in such a setup can be easily inferred from pressure drop at a constant flowrate. However, a significant amount of drag reducing agents are required for conducting tests at lab scale; making it an expensive process. In order to overcome this limitation, a Taylor Couette (TC) Flow setup has been utilized in this study to examine the commercially available polymers for drag reduction and to prove that turbulent Taylor-Couette testing is a convenient and cost effective analogue for pipe flow drag reduction. In addition, high Reynolds number and high wall shear stress can be easily accomplished in this setup.

Taylor-Couette flow is instability in fluid flow arising in between two differentially rotating concentric cylinders. Because of its convenient geometry, it is widely used to study the instability and pattern formulation in turbulence at a small scale (Cole 1976; Davey 1962; Lewis & Swinney 1999). It is a closed system and possesses a simple geometry permitting a well-defined energy balance. A TC setup can be of three types: a) rotating inner cylinder, b) rotating outer cylinder and c) rotating both inner and outer cylinder.

The following parameters describe a Taylor Couette System: r_i is inner cylinder radius, r_0 is the outer cylinder radius, Ω_i is inner cylinder angular velocity, Ω_o is outer cylinder angular velocity, L is the length of inner cylinder, ν is fluid kinematic viscosity and ρ is the fluid density.

$$\eta = r_i / r_o \tag{5.1}$$

$$Re = (\Omega_i r_i (r_0 - r_i))/\nu \tag{5.2}$$

$$Re_o = (\Omega_o r_0 (r_0 - r_i))/\nu \tag{5.3}$$

$$d = r_0 - r_i \tag{5.4}$$

$\Gamma = L/d$ (5.5)

where η is the radius ratio, *Re* is the inner cylinder Reynolds number, Re_o is the outer cylinder Reynolds number, d is the annular gap and Γ is the aspect ratio.

The described set-up was first utilized by Couette (1890) to measure viscosity and consisted of a rotating outer cylinder and a static inner cylinder. Two different regimes i.e. laminar and turbulent were studied. A later study was done by Taylor (1923) who examined flow in concentric cylinders (inner rotating cylinder) experimentally as well as numerically. Critical Reynolds number required to obtain the instability in fluid flow in this system was experimentally observed and numerically proven through his work. Wendt (1933) for the first time provided an extra dimension to this setup by studying TC flow with two independently rotating cylinders which easily enables the set up to reach highly turbulent regime. Torque was measured at different Reynolds number at several radius ratio of the setup.

Centrifugal instability is the reason for the development of taylor vortices at low *Re* in this setup (Di Prima and Swinney, 1985). With increasing *Re*, classical regime is obtained in which boundary layers are of laminar type however turbulence is developed in the bulk at length scales between the Kolmogorov and the integral scale. Further increasing the *Re*, leads to development of the ultimate turbulent regime in the system which consists of turbulent boundary layers (Huisman et al. 2013). Lathrop et al. (1992) observed that behavior of torque in TC flow, at such a large *Re*, is consistent with the turbulent drag in wall bounded shear flows such as turbulent channel/pipe flow. It was postulated that turbulent TC flow wall turbulence is similar to Boundary layer wall turbulence.

Lathrop et al. (1992) considered the core region as an extension of turbulent boundary layers and assumed logarithmic boundary layer at the wall. Whereas, Panton (1992) supposed constant angular momentum in the core. Both the authors arrived at a similar analytical solution using *G* and *Re*. Lathrop et al. (1992) equated Prandtl expression for turbulent shear stress with *T/(rA)* where *T* is the Torque and *A* is the area of cylindrical fluid element at radius *r*. The final expression obtained was

$$\frac{Re}{\sqrt{G}} = N log_{10}\sqrt{G} + M \quad (5.6)$$

$$\text{Where } N = \frac{(1-\eta^2)ln10}{\eta\kappa\sqrt{2\pi}} \tag{5.7}$$

$$M = N\left[ln\left\{\left(\frac{1-\eta}{1+\eta}\right)\frac{1}{y_0^+\sqrt{2\pi}}\right\} + \kappa y_0^+\right] \tag{5.8}$$

Here κ is the *von- Kármán constant* and $y_0^+$is the dimensionless distance from the wall stated in Law of the wall. Skin friction coefficient (c_f) is given by Equation 5.9, where τ_w is wall shear stress.

$$c_f = {G}/{Re^2} = {2\pi r_o^2\tau_w}/{\rho\nu^2 Re^2} \tag{5.9}$$

The final expression is obtained as

$$\frac{1}{\sqrt{c_f}} = Nlog_{10}(Re\sqrt{c_f}) + M \tag{5.10}$$

Following this, intensive research has been carried out in this region and several areas such as rise of instabilities with changing Reynolds number, pattern formation using flow visualization; end wall effects have been explored both experimentally as well as numerically (Merbold & Egbers 2012; Poncet et al 2013; Abshagen 1997). Experiments in the area of torque scaling at reasonably high Reynolds number have been demonstrated recently where dimensionless torque ($G= T/ (L\rho\nu^2)$) is used for scaling the torque (Lathrop 1992; Van Gils et al. 2011).

The TC system has been studied in the past for drag reduction using additives and surface modification. Yi and Kim (1997) experimentally studied the stability of TC flow with drag reducing solutions to investigate the effect of polymers on high molecular weight polymers. Increase in critical Reynolds number with addition of polymer was observed, however, drag reduction was not quantified in this study. Kalashnikov (1998) investigated drag reduction using high molecular weight polyethylene oxide as a DRA in rotating outer cylinder geometry and dimensionless representation of friction coefficient was achieved. However, the annular gap in the setup was significantly small which leads to high shear stress and subsequent shear degradation of polymer in the fluid. Further, the gap between the end plates of outer and inner cylinder was similar to annular gap between cylinders, indicating that there was significant

contribution of the torque coming from end effects or this gap (between the end plates of outer and inner cylinder) which is not relevant for the study. In the present study, moderately high annular gap was used, to minimize the shear stress acting on polymer chains. In addition, larger gap (> annular gap) between the end plates was provided to make sure that only annular gap generated the torque.

Koeltzsch et al. (2003) studied drag reduction using surfactants in a TC setup with a rotating outer cylinder rheometer and for the first time the effect of changing viscosity with varying shear stress was taken into account. However, the highest *Re* achieved was 3 x 10^4 in this study, which doesn't provide much insight on DR which demonstrates significant results at higher *Re*. Dutcher & Muller (2009) explored the effect of drag reducing agents on flow states in TC system at a wide range of Re_0 and Re_i. Eskin (2014) numerically verified the applicability of the TC setup for drag reduction characterization and recommended a radius ratio to be less than 0.5 for this purpose.

The current study utilizes different parameters (η= 0.76 and Γ = 10.57) for examining drag reduction which to the best of our knowledge have not been tested before. Initial validation tests were conducted with water for dimensionless torque and Reynolds number similar to pre-existing studies. Drag reduction at four different DRA concentrations was then explored and compared with literature.

5.2 Method

A TC set-up (Figure 5-1) with a static outer cylinder and a rotating inner cylinder was designed with the following parameters: r_i= 6.0325 cm, r_0= 7.9375 cm, L= 20.08 cm, η= 0.76, Γ= 10.57, d= 1.9 cm. There were three major components of this system: i) TC Chamber ii) DC Motor and iii) Torque Sensor.

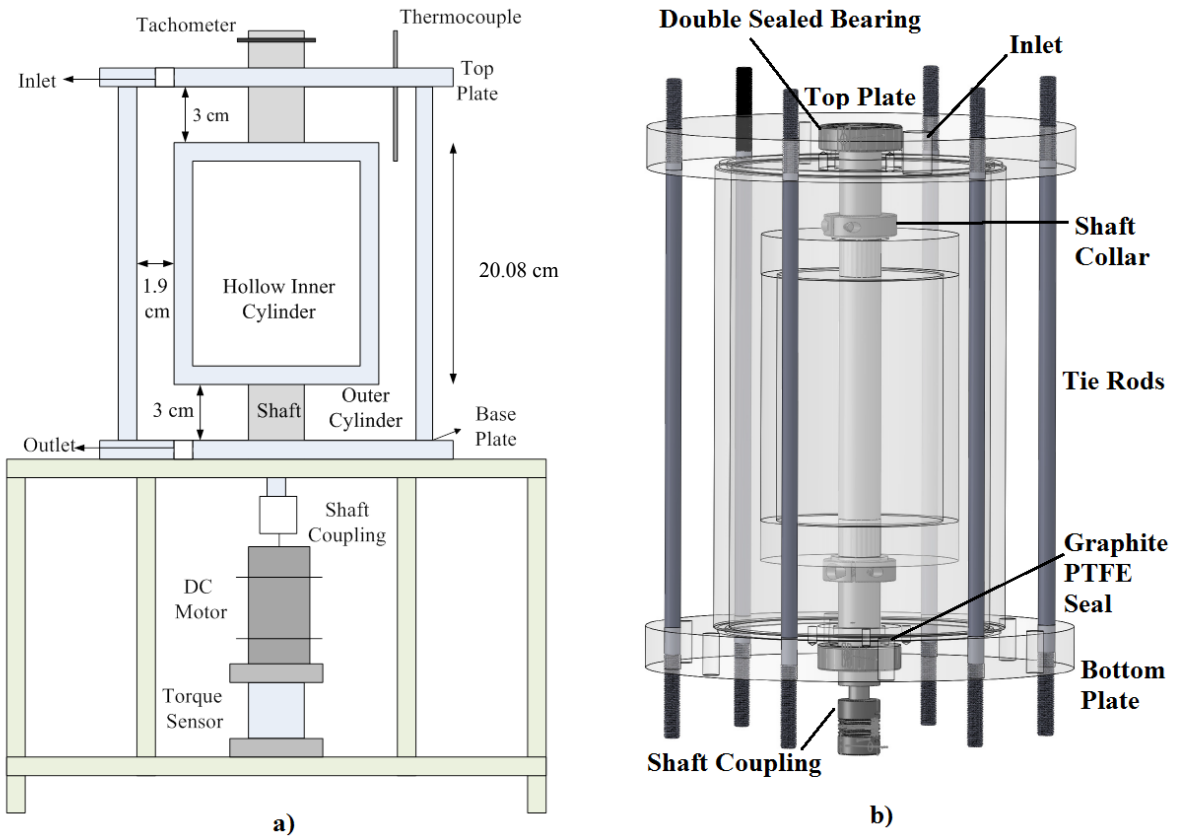

Figure 5-1: a) Schematics of the Taylor-Couette Setup used in the current study, and b) Solidwork model of the concentric cylinders of the setup connected using tie rod.

The main TC Chamber consisted of two concentric cylinders which were fabricated using acrylic thereby allowing flow visualization in the annular gap. A 3 cm gap between the end plates of two cylinders was deliberately provided in order to minimize the end effects. In case of smaller aspect ratio (< 10), significant end effect can be observed due to Ekman circulation (Burin et al., 2006). It arises due to no slip boundary condition at the ends because of which pressure forces are not centrifugally balanced leading to fluid movement in the radial direction. Some setups utilize intermediary rotating end rings in order to overcome this limitation (Hollerbach & Fournier 2005; Altmeyer et al. 2010). In the present setup, a gap (> annular gap) was provided between the end plates of inner and outer cylinder (Figure 5-1) to overpower the end effects. Further, smaller *d* ensured that effectively annular gap generated all the torque. Double sealed stainless steel bearings were used at the top and bottom plate of the outer cylinders. Graphite PTFE seals were selected due to their lower coefficient of

friction and good wear resistance. A hollow Inner cylinder was fixed to an aluminium shaft and the upper portion (Figure 5-1 b) of the set-up was connected using tie rods.

A 120V AC, NEMA 34, 1/3 hp speed control DC Motor (*Amatek Inc.*) was utilized with a speed range from 300-3450 RPM. In the current study, a maximum speed of 2100 RPM was used which created a corresponding Reynolds number of 283,157.

A reaction Torque Sensor (TFF425, *Futek Advanced Sensor Technology, Inc*.) was used for measuring the torque which was connected to the base of motor as shown in Figure 1. The torque sensor had a capacity of 7 N-m with torsional stiffness of 501 N-m/rad. It provided a rated output of 2mV/V. The hysteresis of the torque sensor was less than +/- 0.2% of the rated output and the system was calibrated by Futek Advanced Sensor Technology, Inc. at 5 different points between 0-7 N-m for both the clockwise and the anti-clockwise direction. A maximum system error was found to be 0.02% of rated output in the clockwise direction whereas -0.03% of rated output in the anti-clockwise direction. A USB220 kit was used to digitize the analog output voltage of the sensor and had a sampling rate of up to 4800 Hz. SENSIT Test and Measurement software was used for recording the torque while testing. A thermocouple was installed at the top plate for tracking the temperature changes and an optical tachometer was set up on the shaft for recording the angular velocity.

Initial experiments were conducted with water at eleven different angular velocities ranging from 600 RPM to 2100 RPM for a Reynolds number span of 8.1×10^4 to 2.83×10^5. Torque was measured in the chamber with air only to account for friction due to bearings. This measurement was done before and after each test which was found to be constant and was subtracted from the final readings taken with liquid. Polyacrylamide (Magnafloc 5250, *BASF*) was used in the experiments as a drag reducing agent (DRA). It is a high molecular weight (10-25 million Dalton) polyacrylamide flocculant supplied as a free flowing granular powder. Four different concentrations 80, 120, 160 and 200 PPM were employed in this study. DRA solution was prepared by dissolving the polymer in water for 2 hours at 200 rpm using magnetic stirrer and a separate solution was used for each measurement. The viscosity of the polymeric (DRA) solutions was measured using a Rheometer (Anton Paar, *RheolabQC*). In order to verify the effect of shear degradation of the polymer (due to stirring) on drag reduction, 120 ppm DRA solution was stirred for eight different time periods. Degradation of

polyacrylamide due to high shear stress has also been reported in the literature (Abdel-Alim et al. 1973) and hence a small study was conducted in which solution was examined in the TC chamber for 80 minutes and torque was measured at different time periods. Temperature was monitored before and after every reading. Even for the highest speed, significant increase in the temperature was not detected and temperature variation was found to be less than +/- 1°C.

5.3 Results and Discussion

5.3.1 Torque Scaling

Dimensionless Torque ($G= T/ (L\rho\nu^2)$) was used to scale the torque and was compared with the previous literature (Fig. 2). Experimental setup utilized in Lewis & Swinney (1999) had a η= 0.724 whereas the current study has a η= 0.76 justifying the slight deviation of G. We obtained $G = 0.4592*Re^{1.8568}$ for the present experimental results. Lathrop et al. (1992) did the similar scaling ($G \sim Re^{\alpha}$) and concluded that the exponent increases from 1.66 to 1.87 beyond Re of 1.3 x 10^4 validating our results.

Comparing to work of Wendt (1933) who employed four different radius ratio η (0.5, 0.68, 0.85 and 0.935); an insight on effect of radius ratio on G was shown. G was interpolated for η=0.76 and was compared vs. Re in Figure 5-2. G observed in the present setup is in well accordance with the past findings validating the torque measurements of the system. Figure 5-3 compares the non-dimensional torque at Re=1x10^5 for several values of η (includes data from other studies as well). The Dashed line indicates the theoretical value of G (Wendt 1933) obtained using

$$G= 0.23\frac{\eta^{3/2}}{(1-\eta)^{7/4}}Re^{1.7} \tag{5.11}$$

where Re= 1x10^5. G values observed in this study falls in line with the theoretical value (Equation 5.11) and with the previous studies conducted on other radius ratios.

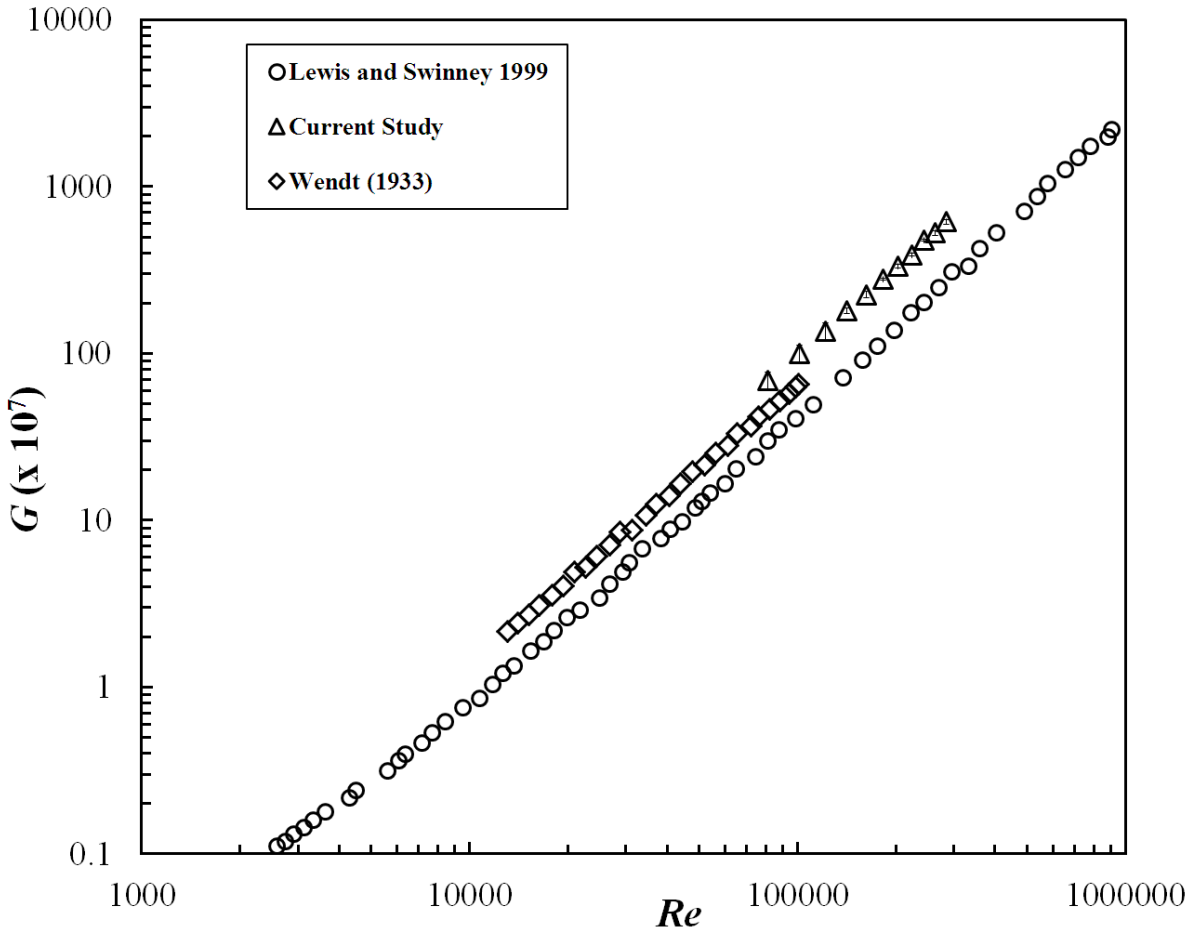

Figure 5-2: Experimental values of Dimensionless Torque (*G*) vs. Reynolds number (*Re*) obtained in the present study in comparison to previous literature.

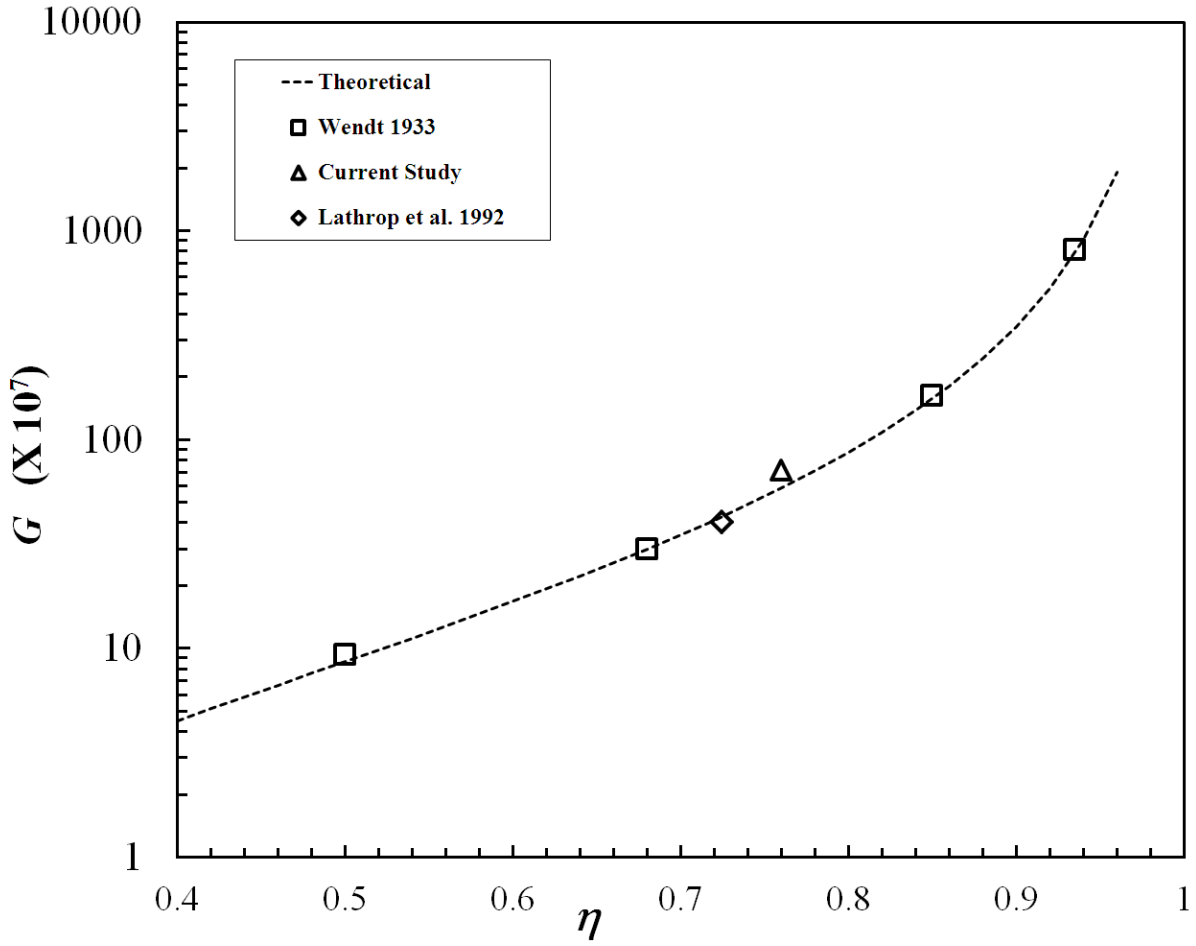

Figure 5-3: Comparison of Dimensionless Torque (G) for various radius ratios (η) at Re=1x10^5.

5.3.2 Comparison with *Prandtl-von Kármán* Law

As discussed in Introduction, Lathrop et al. (1992) found a similar expression (Equation 5.10) to *Prandtl von Kármán* Law by considering logarithmic velocity profile in the core of turbulent TC flow. Figure 5-4 compares the c_f obtained in the current experiments with $Re\sqrt{c_f}$ and a good fit is obtained which is consistent with the above mentioned theory. A linear expression is found with N=1.1045 and M= -1.7141 (Equation 5.10). This value of N in the Equation 5.7 yields a value of *von Kármán* constant κ = 0.46 which is in reasonable agreement with the accepted value of κ = 0.40.

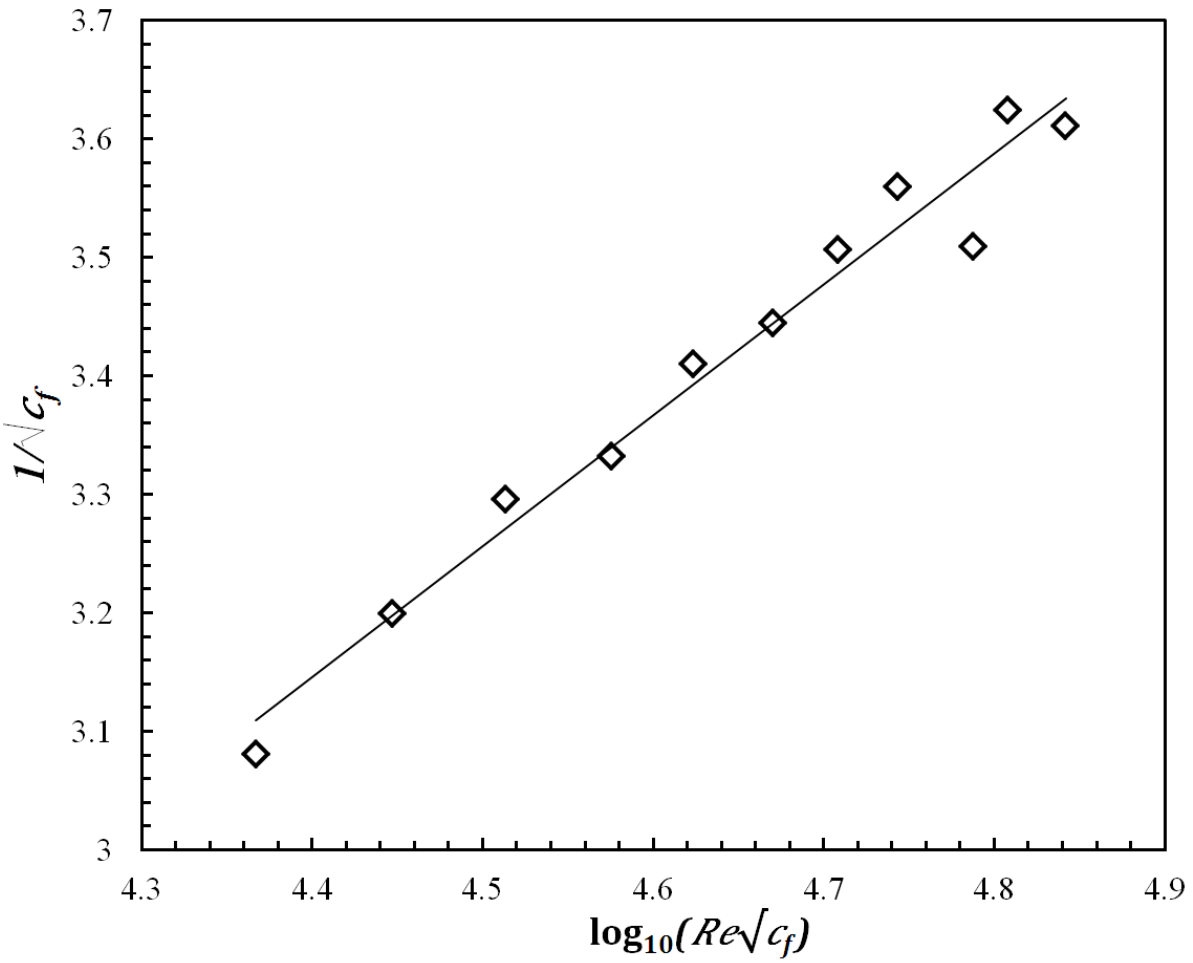

Figure 5-4: Comparison of *Prandtl von-Kármán* type skin friction law with the current experimental data.

5.3.3 Rheological properties of the polymer solution

Shear stress of the DRA solution was measured at different strain rate varying from 1-1000 s^{-1} and Power law model ($\tau = K \frac{du}{dy}^n$)was used for correlation. Here τ is the shear stress, $\frac{du}{dy}$ is the strain rate, K is a constant and $K \frac{du}{dy}^{n-1}$ is the effective viscosity (μ) of the solution. For Newtonian fluid n=1 i.e. viscosity remains constant for various strain rate and for Non Newtonian fluid such as pseudo plastics n<1 i.e. viscosity decreases with increasing strain rate. Following are the relations observed for different solution:

80 PPM $\tau=0.0016 \frac{du}{dy}$ (Newtonian Behavior)

120 PPM $\tau = 0.0046(\frac{du}{dy}^{0.781})$ (Pseudoplastic-Non Newtonian behavior)

160 PPM $\tau = 0.0061(\frac{du}{dy}^{0.7748})$ (Pseudoplastic-Non Newtonian behavior)

200 PPM $\tau = 0.0108(\frac{du}{dy}^{0.707})$ (Pseudoplastic-Non Newtonian behavior)

Since the shear rate is variable in the annular gap, viscosity of 120 PPM, 160 PPM and 200 PPM solution is not constant due to non-Newtonian behavior. Hence effect of varying viscosity needs to be taken into account and the following method employed by Koeltzsch et al. (2003) is used. Shear rate for the laminar flow in current geometry is given by (u_φ is the azimuthal velocity):

$$\frac{du}{dy} = r\frac{\partial}{\partial r}\left(\frac{u_\varphi}{r}\right) = -\frac{2\Omega_i r_i^2 r_o^2}{r^2(r_o^2 - r_i^2)} \tag{5.12}$$

Shear rate is highest at the inner cylinder hence further calculation are done at $r=r_i$. Equating μ_{pseudo} and μ_{actual} in case of non-Newtonian at inner cylinder

$$\mu_{actual}\{r\frac{\partial}{\partial r}\left(\frac{u_\varphi}{r}\right)\}_{in} = -\mu_{pseudo}\frac{2\Omega_i r_o^2}{(r_o^2 - r_i^2)} \tag{5.13}$$

$$\frac{\mu_{actual}}{\mu_{pseudo}} = -\frac{\frac{2\Omega_i r_o^2}{(r_o^2 - r_i^2)}}{\{r\frac{\partial}{\partial r}\left(\frac{u_\varphi}{r}\right)\}_{in}} \tag{5.14}$$

Using power law model for non-Newtonian viscosity, the following relation is obtained (as described in Koeltzsch et al. 2003)

$$\{r\frac{\partial}{\partial r}\left(\frac{u_\varphi}{r}\right)\}_{in} = \{\frac{1-\eta^2}{n(1-\eta^{2/n})}\}\frac{2\Omega_i r_o^2}{(r_o^2 - r_i^2)} \tag{5.15}$$

$$\frac{\mu_{actual}}{\mu_{pseudo}} = \frac{n(1-\eta^{2/n})}{1-\eta^2} \tag{5.16}$$

For 120 PPM $\mu_{actual} = 0.933\,\mu_{pseudo}$, for 160 PPM $\mu_{actual} = 0.931\,\mu_{pseudo}$ and whereas for 200 PPM $\mu_{actual} = 0.904\,\mu_{pseudo}$. Since viscosity is used in calculating the *Re*, corrected *Re* near the inner cylinder will be 6.7% higher.

A second rheology test was conducted by varying strain rate from 1-1000 s^{-1}. Constant viscosity (known as μ_{inf} according to Carreau Model) was obtained after a strain rate of 800 s^{-1}. Since in our study the strain rate is much higher than 800 s^{-1}, μ_{inf} will be used to calculate the *Re*. Table 5-1 lists μ_{inf} and ρ for various DRA solutions used in this study.

Table 5-1: Density and dynamic viscosity of DRA solutions used in the study.

DRA concentration	Density ρ (kg/m^3)	Dynamic Viscosity μ_{inf} (Pa.s)
80 PPM	984.66	1.28 X 10^{-3}
120 PPM	977	1.34 X 10^{-3}
160 PPM	962.66	1.94 X 10^{-3}
200 PPM	958.66	2.16 X 10^{-3}

5.3.4 Drag reduction using Polymers

Figure 5-5 shows the skin friction coefficient (c_f) vs. *Re* for water (as a reference case) and drag reducing solutions at several polymeric concentrations. Only the turbulent regime is shown in the plots where skin friction coefficient of water is found to scale well with $c_f \propto Re^{-1/4}$. Virk et al. (1967) witnessed the onset of drag reduction and observed that there is a critical value of *Re* required to realize the DR. When this condition is met, the polymer chains are elongated and demonstrate enhanced elongational viscosity (Lumley 1973). This substantial increase in viscosity, combined with the interaction of these stretched chains with vortices dampens the turbulence. This onset was observed for 80 PPM DRA solution and critical value of *Re* for this solution was found here to be $7x10^4$. With increasing DRA concentration, there is a decrease in this critical value of *Re*, and since the experiments were not conducted below $Re=5x10^4$ (due to setup limitation), this onset wasn't observed for other DRA solutions. Furthermore it can be observed from the plot, that all the DRA solutions show a smaller value of skin friction coefficient in comparison to water. Similar observations were reported by Koeltzsch et al. (2003), for drag reduction using surfactant and by Kalashnikov (1998), for

drag reduction using high molecular weight polyethylene oxide (2-100 PPM) in a TC Set up. Kalashnikov (1998), similar to the present study, observed a threshold value of *Re* for DR and found it to be related to a transition from inertial to inertial-elastic turbulence. It was postulated in their study that a critical value of Weissenberg number (ratio of viscous forces to elastic forces) is required for this transition, which occurs at a threshold wall shear stress (which scales with threshold *Re*). Once the critical value of Weissenberg number is achieved, coil-stretch transition of the polymer chains occurs, which facilitates in dampening the turbulent structures (Sreenivasan & White, 2000). Turbulent drag reduction has been observed as a boundary layer effect with an increase in the buffer layer thickness, which has been noticed after the drag reduction. Hence, an increase in the slope (c_f vs *Re*) after the addition of DRA was observed in the current study, and is in good agreement with the literature (Kalashnikov 1998; Sreenivasan & White, 2000; White et al., 2004).

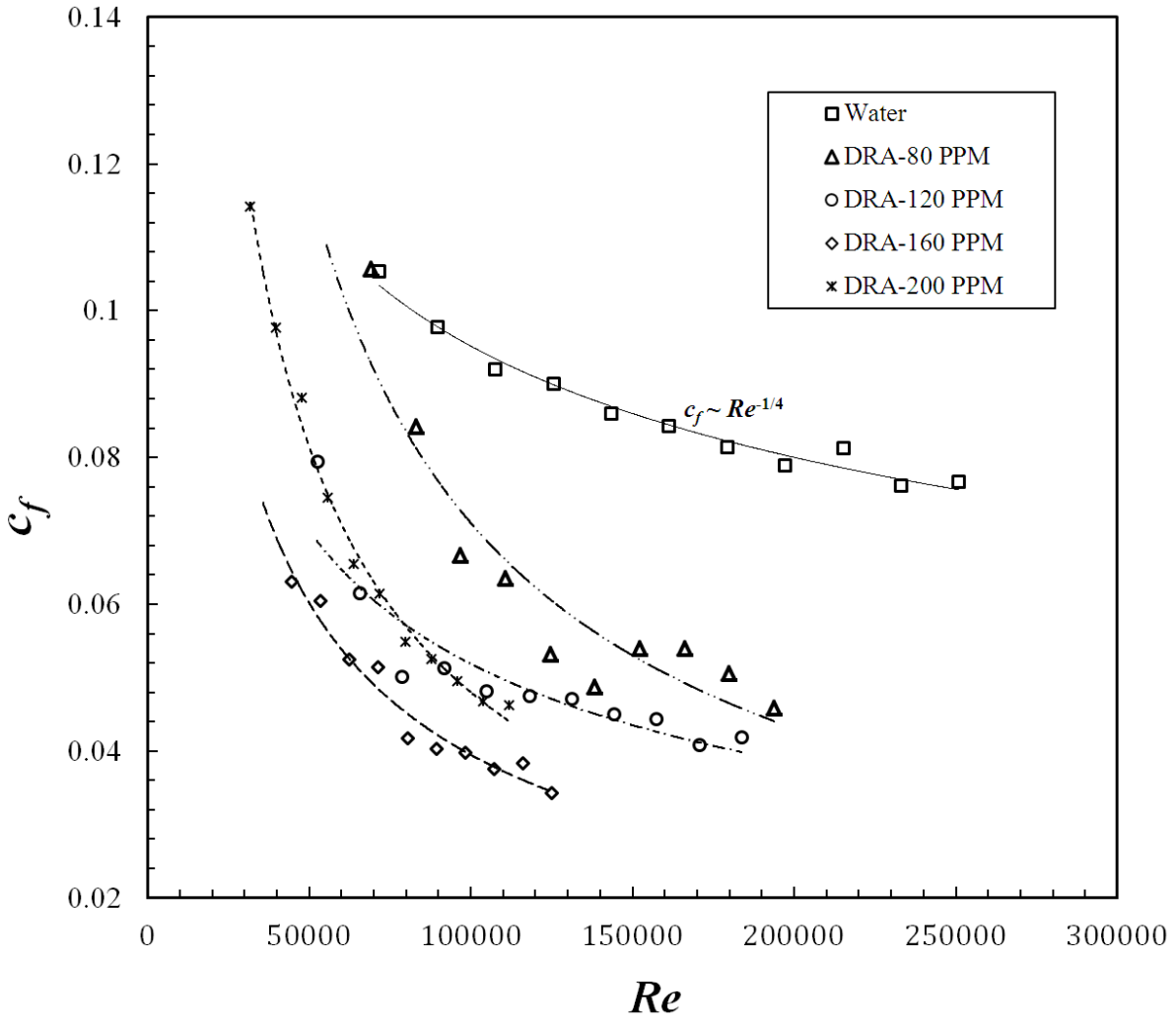

Figure 5-5: Skin friction coefficient (c_f) vs Reynolds number (Re) for water and drag reducing solution at various polymeric concentrations.

In order to understand the drag reduction, a different plot (Figure 5-6) is chosen in which Drag Reduction ($DR\%$) is expressed by Equation 5.17, where $c_{f,w}$ is the skin friction coefficient of water and $c_{f,s}$ is the skin friction coefficient of DRA solution.

$$DR\% = \frac{c_{f,w} - c_{f,s}}{c_{f,w}} \text{x } 100 \qquad (5.17)$$

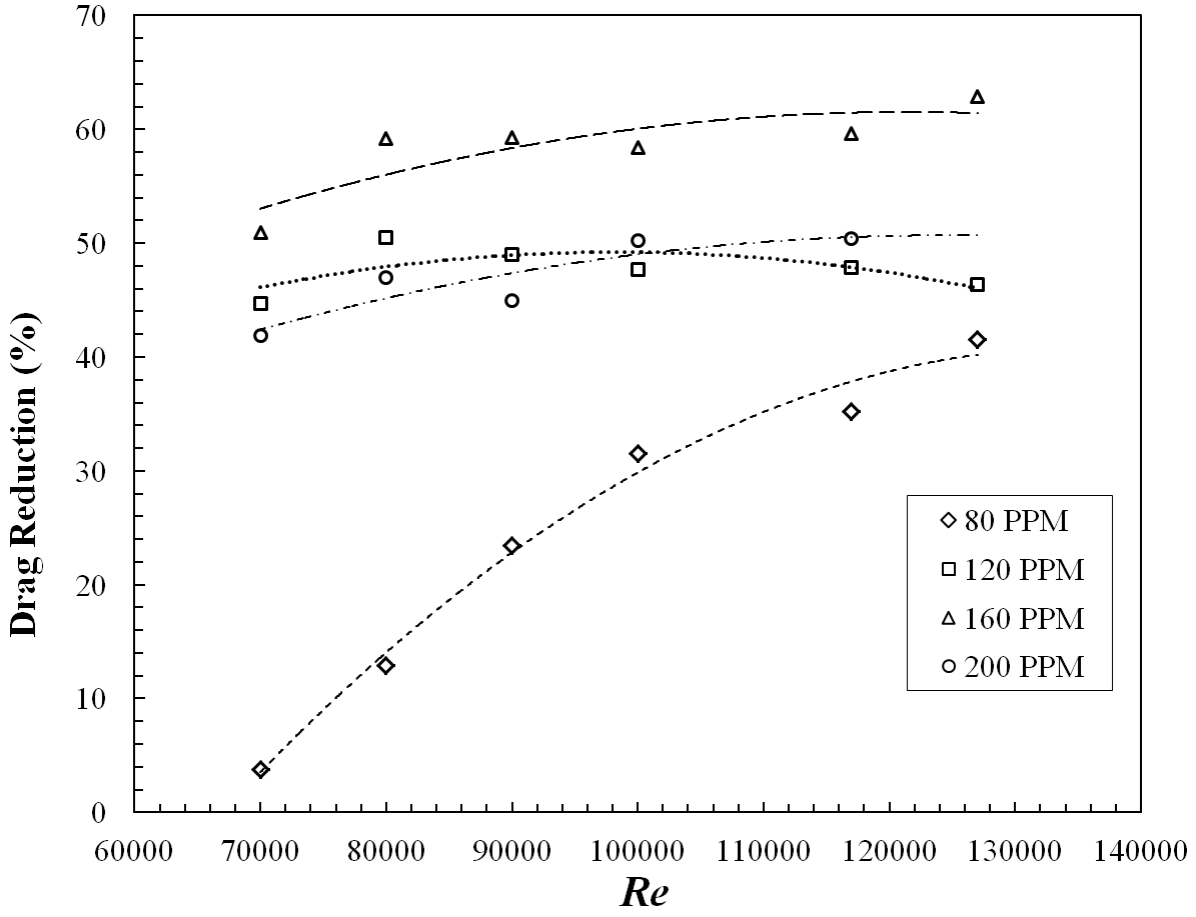

Figure 5-6: Drag reduction (%) vs *Re* for different concentrations of DRA solution.

Results from Figure 5-5 were used to obtain the plots in Figure 5-6. For the 80 PPM DRA solution, it is evident that there is an increase in *DR%* with increasing *Re*. It is in good agreement with the results reported by Virk et al.(1967). With an increase in *Re*, there is an increase in wall shear stress which improves the stretching of polymer chains, resulting in higher DR. Further it can be observed that with an increase in concentration, there is an increase in DR% up to 160 PPM, beyond which there is a decrease in drag reduction. This increase in DR with the increase in concentration is due to increased interaction of polymers with turbulent structures and is in accordance with the observations of Bewersdorff (1982) and, Sa Pereira & Pinho (1994) in pipe flow. A decrease in DR beyond 160 PPM could be attributed to increased entanglements of polymer chains amongst themselves, leading to reduced mobility of the polymer chains and is in agreement with the observations made by Fernandes et al. (2009). Further, DR% increases slightly with *Re* for 160 PPM solution

however it was found to be constant for 120 PPM and 200 PPM solution. These solutions (120PPM, 160 PPM and 200 PPM) demonstrate the asymptotic value of DR i.e. 47%, 63% and 50% respectively. This is similar to the findings of Virk et al. (1967) who also observed a Maximum Drag Reduction (MDR)Asymptote, which was independent of pipe size and type of polymer used (Virk & Merrill, 1969). In summary, all the observations made in this study were in agreement with the previous studies on pipe and channel flow validating that the TC setup is an excellent tool for drag reduction testing.

Some experiments were conducted for 120 PPM DRA solution at Re=1.8 X 10^5 for a longer time (80 min) period in order to see if the shear rate deteriorated the polymer chains and in turn could affect the DR, however, torque (similarly DR) was found to be unchanged with time.

Since the DRA solution was prepared by mixing the polymer in water using a magnetic stirrer, a brief study was conducted to examine the effect of the stirring time of the polymer in water on DR% (for 120 PPM DRA solution) at Re=1.8 X 10^5. Stirring time was found to have significant effect on DR%. Shorter stirring time (1000s) and longer stirring time (1x10^5 s) lead to decrease in DR%. 1000s was observed to be insufficient for the polymer to completely dissolve in water, whereas 100000s is considerably long for the polymer chains to dissolve leading to deterioration of the polymer chains.

5.4 Conclusion

Drag reduction in turbulent pipe flow using high molecular weight polymer as additives, known as drag reducing agents (DRA), is a well-recognized field and has been an area of extensive research. However, a significant amount of polymer is utilized to test the polymers for drag reduction at lab scale, using pipe flow or a channel flow setup. In the current study, a Taylor Couette flow apparatus was designed and tested for drag reduction using high molecular weight polymers. The setup consisted of a stationary outer cylinder and rotating inner cylinder, where drag (skin friction coefficient) was inferred from torque acting on inner cylinder. Initial experiments were conducted with water in which torque was scaled using dimensionless torque (G) and Reynolds number (Re). The results obtained were compared

with the previous literature and were found to be in good agreement. The effect of the changing molecular viscosity of the polymeric solution with varying shear rate was discussed. It can cause a difference of 6.7% in the measurement of *Re* across the inner and outer wall. However, beyond particular strain rate, a constant viscosity (μ_{inf}) of the polymeric solution is obtained. In the present study, Re was deliberately chosen to be high enough that it surpassed the strain rate to achieve μ_{inf} and $\mu_{inf}$was used to calculate *Re*. Further, drag reduction was measured for four different concentrations of polymeric/DRA solution. An increase in DR% was observed for increase in concentration and *Re*. An onset of drag reduction was observed for 80 PPM DRA solution at *Re*=7 x 10^4 and Maximum Drag Reduction (MDR) or the Virk asymptote of 63% DR was observed for 160 PPM DRA solution. The effect of stirring time of the polymer solution was found to have a profound effect on DR and longer stirring time was found to decrease the DR% (attributed to polymer chain breakage).

In summary, the TC setup is a powerful tool to assess the drag reduction with an important advantage being its small geometry. In addition, it is quick to use and requires smaller solution volumes. This provides an excellent platform for evaluating a wider range of DRA solutions.

This chapter has been submitted in Journal of Rheology as "Bhambri, P., Narain, R. & Fleck, B. (2016). Drag Reduction using Polysaccharides in Taylor-Couette Flow."

6. DRAG REDUCTION USING POLYSACCHARIDES IN A TAYLOR-COUETTE FLOW

Three different polysaccharides: aloe vera, tamarind powder and pineapple fibers are utilized as drag reducing agents in a turbulent flow. Using a Taylor-Couette setup, consisting of a rotating inner cylinder, for measuring the drag reduction; a range of Reynolds numbers from 4×10^4 *-* 3×10^5 *has been explored in this study. The results are in good agreement with previous studies on polysaccharides conducted in a pipe/channel flow and a maximum drag reduction of 35% has been observed. Further, novel additives such as Cellulose Nano Crystals (CNC), surfactants and CNC grafted with surfactants are also examined in this study for drag reduction. CNC due to its rigid rod structure reduced the drag by 30%. Surfactant, due to its unique micelle formation showed maximum drag reduction of 80% at low Re. Further, surfactant was grafted on CNC and was examined for drag reduction. However, drag reduction property of surfactant was observed to be significantly reduced after grafting on CNC. The effect of Reynolds number on drag reduction is studied for all the additives investigated in this study.*

6.1 Introduction

The pressure drop in closed conduits is significant in turbulent flow and a considerable amount of energy is depleted in pumping the fluids to overcome this pressure drop, particularly in rough walled geometries. Reduction in this drag leads to substantial amount of cost and energy savings, so it is not surprising that it has been an area of extensive research in the past few decades.

Drag can be either reduced by modifying the surface of pipe/channel or by adding some additives such as polymers, surfactants, fibers, bubbles etc. Drag Reduction (DR) using high molecular weight polymers as additives is well documented and after it was first discovered during the Second World War (Bismarck et al. 2004); an enormous amount of work has been

carried out in this field. Additive concentration in the order of parts per million of these dissolved polymers has been shown to diminish the drag by 60-70% (Ptasinski et al. 2001). However, due to their high molecular weight (1-25 million Da), these materials have the disadvantage of being susceptible to mechanical degradation i.e. chains get broken at higher strain rates (Shin 1965). The phenomenon of drag reduction has not been clearly understood in spite of several attempts made by various researchers. Virk (1967, 1971) and Lumley (1969) have contributed significantly in understanding the DR mechanism. Virk (1969, 1989) observed the onset of drag reduction and concluded that turbulence is required for drag reduction to occur. Lumley (1973) provided a time criterion hypothesis to explain the mechanism of drag reduction and postulated that a coil stretch transition of the polymer chains is the reason behind DR. Polymer chains are significantly stretched in this transition state, which increases the elongational viscosity by ten thousand fold. This increase in elongational viscosity, which is prominent near the wall regions, dampens the turbulent structures thereby decreasing the drag.

Surfactants such as hexadecyltrimethylammonium bromide (CTAB) have also been studied widely for reducing drag (Zakin and Chiang 1972; Zakin et al. 1996). Micelle formation (microscopic units assembled from the molecules of surfactants) of the surfactants above the critical micelle concentration exhibit viscoelastic properties similar to polymers which remarkably diminishes the drag. Surfactants have an advantage over polymers due to their tendency to self-repair i.e. if the micelle structure is broken by strain; they can automatically reorganize once the shear stress is lower, thereby restoring the drag reduction effect (Hoyt 1989). Similarly, fibers have also been reported as drag reducing additives. This mechanism is referred to as solid suspension drag reduction. Turbulence suppression by fibers weakens the transverse momentum transport, which subsequently reduces turbulent dissipation (Patterson et al. 1969).

Currently, synthetic polymers such as polyacrylamides, polyethylene oxide, polyisobutylene etc. are widely utilized as drag reducing agents in industry. However, due to environmental impact caused by slower degradation of these high molecular weight polymers, attention has been shifted to biopolymers. Plant polysaccharides such as xylan, guar gum etc. have been identified as a natural substitute to synthetic DRA and these have the advantage of being

biodegradable (Hong et al. 2010; Abdulbari et al. 2013). Singh & Rao (1995) observed 70% drag reduction using guar gum at 500 PPM concentration, whereas Abdulbari et al. (2010) used 400 PPM okra mucilage to achieve 60% DR. In addition, aloe vera has demonstrated 62 % DR at *Re* of 10,000 in a pipe flow with 400 PPM concentration.

In the present study, three different polysaccharides: aloe vera; tamarind powder and pineapple fibers are studied for DR. Aloe vera is composed of mucilaginous polysaccharides and contains different proportions of mannose, glucose and galactose. Pineapple fibers consist of a cellulose, hemicellulose and lignin; and possess good mechanical properties. Tamarind seed powder is a high molecular weight branched polysaccharide consisting of a cellulose-like backbone that carries xylose and galactoxylose substituents.

Along with polysaccharides, pure cellulose nano crystals (CNC) and surfactant grafted cellulose nano crystals are also employed as DRA in this study. Cellulose nanocrystals are rods like cellulose crystals, which possess hydroxyl groups and negative charge on the surface. Due to their favorable mechanical properties and high surface to volume ratio, these are widely studied as a composite material. Further, due to functional groups available on the surface, their surface can be easily modified (Peng et al. 2011). Here, hexadecyltrimethylammonium (CTAB) bromide, a cationic surfactant, is used to graft to the surface of CNC and then further utilized for DR. CNC and surfactant grafted CNC has not been previously studied for DR.

Instead of commonly used pipe/channel flow, a Taylor-Couette setup is used for measuring the Drag reduction in this work as it has several advantages. It is a fluid motion between two coaxial cylinders with one or both the cylinders co-rotating/ counter-rotating and possesses similar characteristics of a turbulent boundary layer (Greidanus et al. 2011). The TC setup has been proven as a convenient and reliable testing platform for drag reduction using both additives and super hydrophobic coatings (Bhambri & Fleck, 2016; Koeltzsch et al. 2003; Srinivasan et al. 2015). Specifically it allows for good control of the fixed batch of fluid and detailed monitoring of DRA degradation as a function of time as well as energy dissipation. Torque measured on either inner or outer cylinder of this setup has been found to scale well using dimensionless torque ($G= T/(\rho v^2 L)$) (Lathrop et al. 1992); where T is the torque, ρ is the

density of fluid, v is the kinematic viscosity and L is the length of inner cylinder. Skin friction coefficient (c_f) is then calculated from dimensionless torque by

$$c_f = \frac{G}{Re^2} \tag{6.1}$$

Drag reduction can be computed using Equation 6.2; where $c_{f,w}$ is the skin friction coefficient of water and $c_{f,s}$ is the skin friction coefficient solution with drag reducing additives.

$$DR\% = \frac{c_{f,w} - c_{f,s}}{c_{f,w}} \times 100 \tag{6.2}$$

6.2 Method

The employed Taylor-Couette system has a rotating inner cylinder and a stationary outer cylinder, both of them manufactured using acrylic, and has been previously used (Bhambri & Fleck, 2016) successfully (Fig. 6-1). The system is closed at both the ends with static end plates. The radius of the inner cylinder (r_i) is 6.03 cm whereas, the radius of the outer cylinder (r_o) is 7.94 cm which provides a radius ratio ($\eta = r_i / r_o$) of 0.76. The inner cylinder has a length (L) of 20.08 cm which leads to an aspect ratio [$\Gamma = L/(r_o - r_i)$] of 10.56. A 120V AC, NEMA 34, 1/3 hp speed control DC Motor (*Amatek Inc*.) with a range from 300-3450 RPM, is connected to an anodized aluminum shaft. This shaft is fixed to the hollow inner cylinder using O-rings and shaft collar. Tie rods are used to connect the cylinders to end plates. A reaction torque sensor (TFF425, *Futek Advanced Sensor Technology, Inc.*), with a capacity of 7 N-m and 2mV/V of rated output, is mounted at the base of motor which measures the reaction torque acting on the inner cylinder. The sensor was calibrated by *Futek Advanced Sensor Technology, Inc* and had an error of 0.02% of rated output in the clockwise direction and -0.03% of rated output in the anti-clockwise direction. An optical tachometer was utilized to measure the angular velocity of the inner cylinder and a type K thermocouple was used to monitor the temperature of the fluid in the annular gap. The temperature difference before and after every reading was found to be less than 0.2 ºC. The Reynolds number (*Re*) was calculated by Equation 6.3, where Ω_i is the angular velocity of the inner cylinder and ν is the fluid kinematic viscosity.

$$Re = \frac{\Omega_i r_i (r_0 - r_i)}{\nu} \tag{6.3}$$

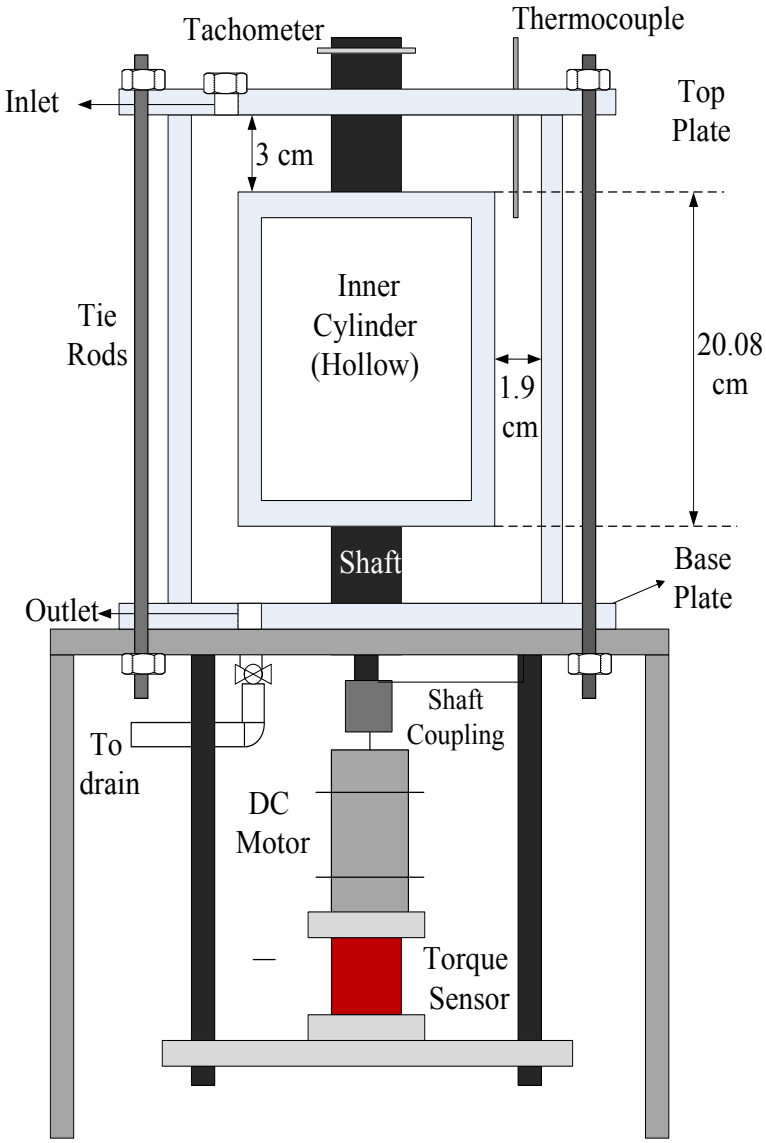

Figure 6-1: Schematics of Taylor-Couette Setup used in this study.

6.2.1 Preparation of polysaccharide solution

Aloe vera, pineapple fibers and tamarind powder obtained from Chulalongkorn University, were used in the study. The same technique was used to prepare all the polysaccharide samples. A concentrated solution (2.4% wt. /v) was first prepared by sonicating the

polysaccharides in water for 30 minutes, followed by stirring for 1 hour. Solutions were then diluted and the final concentration of 600 PPM was utilized in the study for DR measurement.

6.2.2 Preparation of CNC, Surfactant and CNC-Surfactant solution

Cellulose nano-crystals supplied by Alberta Innovates Tech Futures, with a particle length of 100-200 nm and a diameter 5-15 nm were used. For pure CNC solution, a concentrated (2 wt.%) solution was first prepared by sonicating CNC in water for 30 minutes followed by overnight stirring. Final concentration of 600 PPM was then utilized.

For preparing the CNC-Surfactant (50/50) solution, the method provided by Kaboorani and Riedl (2015) was used. Briefly, 2.4 wt% of CNC solution was obtained using 30 minute of sonication, followed by 3 hours of stirring. 2.4 wt% of CTAB (*Sigma Aldrich*) solution was prepared by magnetic stirring for 4 hours. Both the solutions were then mixed and stirred for overnight. CNC has negative charge on the surface whereas CTAB is a cationic surfactant which leads to grafting of surfactant on CNC during mixing. Mixture was then centrifuged for 12 minutes at 15,000 RPM to remove the excess surfactants. CNC suspension was finally freeze dried for 2 days. A 600 PPM concentrated solution was prepared in water by magnetic stirring for 4 hours. A 600 PPM solution of surfactant was also separately prepared and tested as a control.

6.2.3 Characterization of Additives

In order to calculate the *Re*, the viscosity of the solutions was measured using a rheometer (*Anton Paar, RheolabQC*) by varying shear rate from 1-1000 s^{-1} at 21°C. The molecular weight of the aloe vera was determined by gel permeation chromatography (GPC) at room temperature and a Viscotek model 250 dual detector (refractometer/viscometer in aqueous eluents (0.5 M sodium acetate and 0.5 M acetic acid)) with a flow rate of 0.5 mL/min. Dynamic light scattering (DLS) was used to measure the effective diameter of pineapple fibers, tamarind powder, CNC, Surfactant and CNC-Surfactant in the solution. Dynamic light scattering (*Brookhaven*) was performed at a fixed angle y = 90° with an incident light of wavelength λ = 658 nm. Polysaccharide samples were also analyzed under scanning electron microscope (SEM, *Philips/FEI XL30*). The Samples for SEM were coated with gold-palladium prior to imaging. Thermogravimetric analysis (TGA) was carried out using a

SDTQ600 (*TA Instruments*) analyzer between 10°C and 700°C in air at a heating rate of 10°C min^{-1}.

6.3 Results and Discussion

6.3.1 Characterization of Additives

Figure 6-2 and Figure 6-3 shows shear stress (τ) vs. strain rate (γ) for polysaccharides and CNC respectively, measured using rheometer. In the case of polysaccharides, aloe vera shows Newtonian behavior, whereas pineapple fibers and tamarind powder demonstrate non-Newtonian behavior. Both CNC and CNC-Surfactant exhibited Newtonian behavior. Power law model $\tau = K\frac{\partial u}{\partial y}^{n}$ was used to fit the curves; where $\frac{\partial u}{\partial y}$ is strain rate (γ) and $K\frac{\partial u}{\partial y}^{n-1}$ represents viscosity (μ) (Table 6-1).

Table 6-1: Power law model expression for different polysaccharides.

Aloe Vera	$\tau = 0.0011\ \gamma$
Tamarind Powder	$\tau = 0.0016\ \gamma^{0.9649}$
Pineapple fiber	$\tau = 0.0037\ \gamma^{0.8307}$
CNC	$\tau = 0.0013\ \gamma$
CNC-Surfactant	$\tau = 0.0011\ \gamma$
Surfactant	$\tau = 0.001\ \gamma$

Viscosity obtained from the above mentioned expressions was used to calculate the *Re.* In the case of the non-Newtonian fluid, average viscosity was considered.

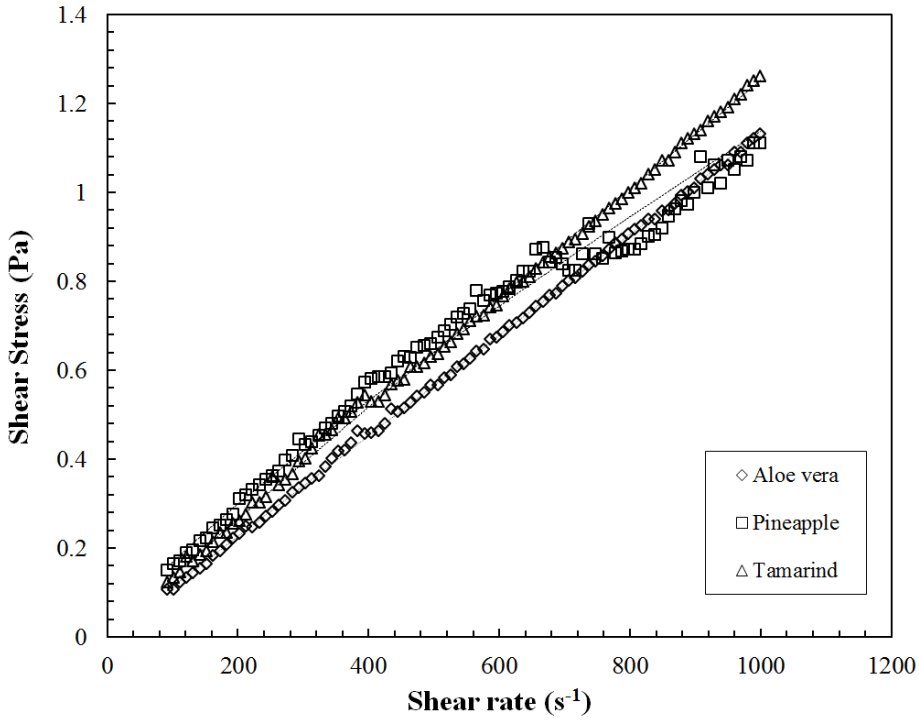

(a)

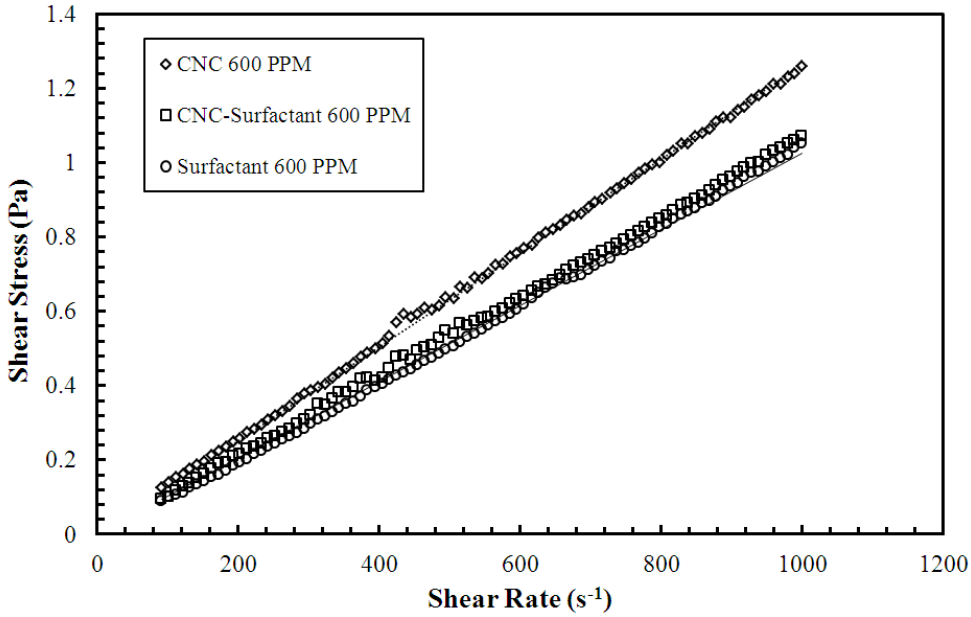

(b)

Figure 6-2: Shear Stress vs. Strain Rate for a) Polysaccharides and b) for CNC and CNC-Surfactant at 600 PPM.

The molecular weight (M_w) of aloe vera was measured to be 2.8 x 10^4 Da indicating a sufficiently high molecular weight for drag reduction. Effective diameter of additives measured using DLS is shown in Table 6-2. The size of CNC-Surfactant is more than CNC alone, thereby confirming the grafting of CTAB on CNC. Figure 6-3 shows the TGA curves for CNC and CNC surfactant, demonstrating early decomposition of CNC Surfactant as compared to CNC. The surfactant begins to decompose at 230°C whereas CNC will degrade at 300°C. From these observations, the rough composition of CNC in CNC Surfactant is estimated to be 55%. Figure 6-4 shows the SEM images of polysaccharides. Pineapple fibers consist of flakes and rigid rod type structure with approx. length of 20 μm and diameter of 1-2 μm with a huge variation in size. On the other hand Tamarind powder consists of spherical particles with diameter of 2.5 μm. In the dried form particles were agglomerated as seen in the Figure 6-4 (b). Aloe Vera was used in a dissolved state; however SEM images were taken to visualize the shape of Aloe Vera particles in the dried form. Spherical particles with huge polydispersity can be seen in Figure 6-4(c) and 6-4(d).

Table 6-2: Size of the additives measured using DLS.

Additive	Effective Diameter (nm)	Standard Deviation (nm)
Tamarind	2466	414.4
CNC	736	24
CNC-Surfactant	1877	300
Surfactant	214	45

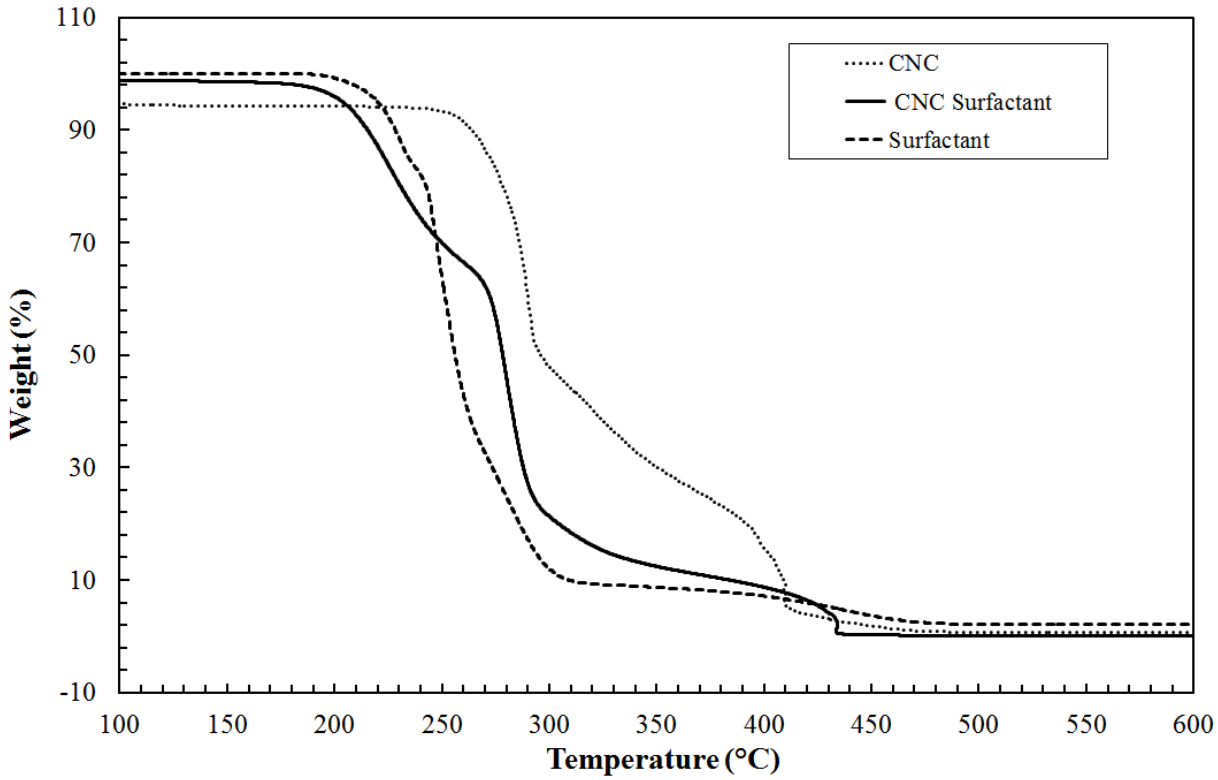

Figure 6-3: Thermogravimetric analysis of CNC and CNC Surfactant.

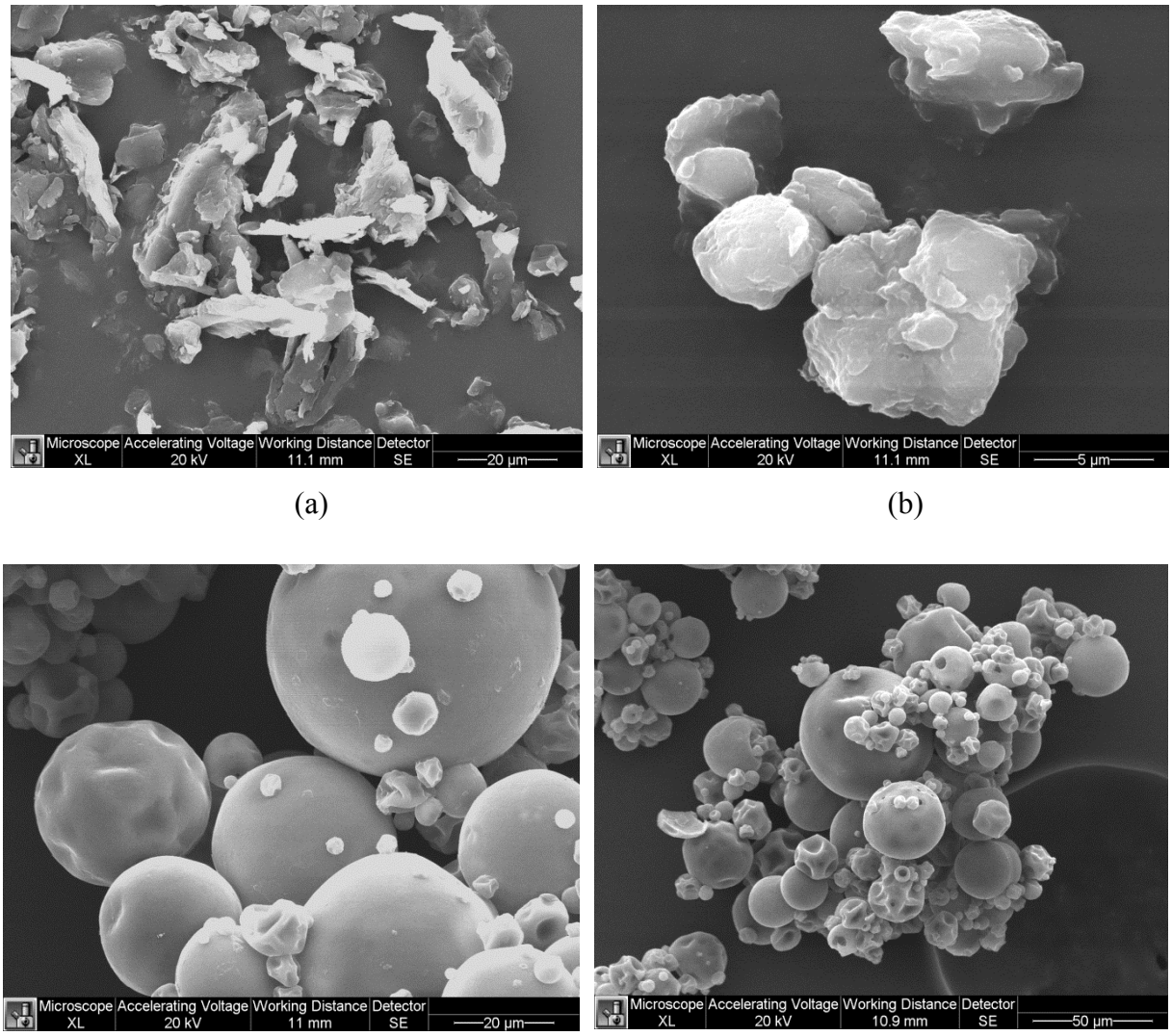

Figure 6-4: SEM images of a) Pineapple fibers b) Tamarind Powder and c) & d) Aloe Vera.

6.3.2 Drag Reduction using Polysaccharides

Figure 6-5 shows dimensional torque (G) at various inner cylinder angular velocities (Ω_i) for polysaccharides. Each point represents the average of three repeat measurements, while error bars indicates the data variability in the measurements. With increasing angular velocity, the difference between the dimensionless torque for the water and for the polysaccharide solutions is observed to increase with this phenomenon being most pronounced for pineapple fibers. This is in good agreement with the observations made by Campolo et al. (2015) for xanthan gum in pipe flow.

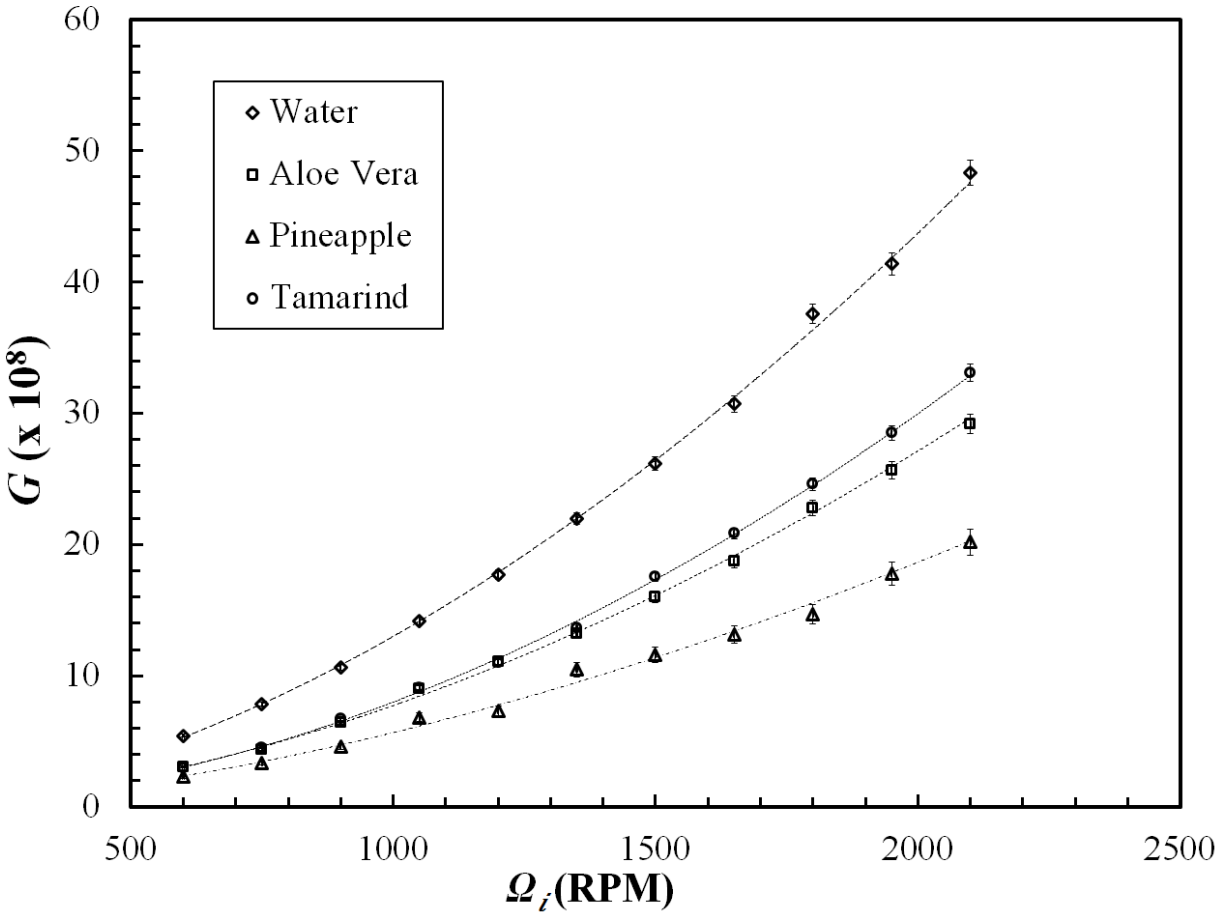

Figure 6-5: Dimensionless torque vs. angular velocity for polysaccharides.

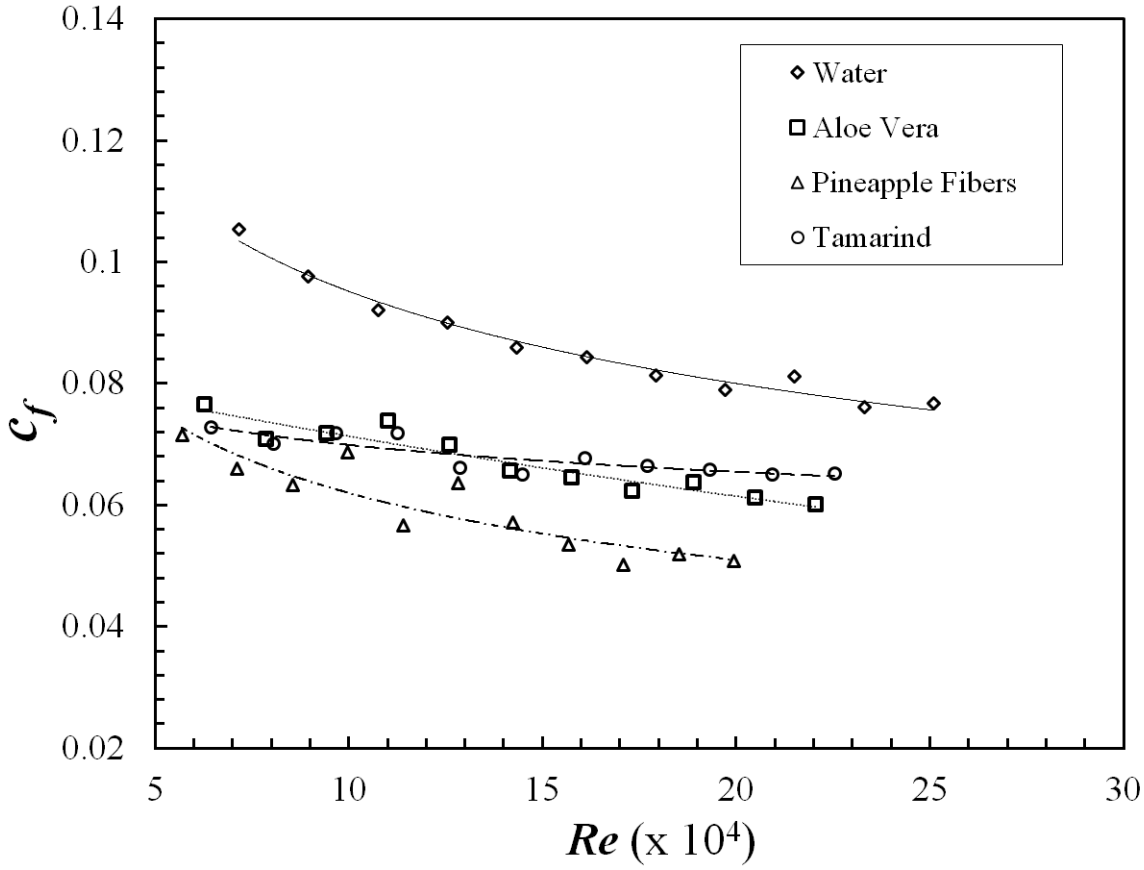

Figure 6-6: Skin friction coefficient vs. Reynolds number for polysaccharides.

Figure 6-6 indicates skin friction coefficient vs. *Re* for the polysaccharides and Figure 6-7 shows Drag reduction (%) which is interpreted from skin friction coefficient (Equation 6-2). Pineapple exhibited similar behavior to xanthan gum (Campolo et al. 2015), and a slight increase in DR% with increasing *Re* can be seen. On the contrary, aloe vera and tamarind showed decreasing DR% with increasing *Re*. This is in agreement with the observations made by AbdulBari et al. (2011) & (2010) for aloe vera and okra mucilage respectively. On the other hand, synthetic polymers such as polyacrylamide and polyethylene oxide exhibit increased DR up to a critical *Re* and then a constant DR% beyond this critical *Re* (Virk et al. 1967; Hoyt 1972). This could be attributed to poor shear stability of polysaccharides in comparison to synthetic polymers. Contrarily, Fibers have good stability at high shear stress (Vaseleski & Metzner 1974), which can be also observed in the case of Pineapple fibers in the currents study. It can be concluded that amongst the polysaccharides considered in this study, Pineapple fibers and Tamarind had the best and worst resistance to shear degradation

respectively. A comparison was also conducted at lower concentration of 200 PPM and 400 PPM. Tamarind showed similar DR at both the lower concentration; however Aloe Vera and Pineapple demonstrated negligible DR at these concentrations. Hence in order to make an appropriate comparison; 600 PPM concentration was utilized.

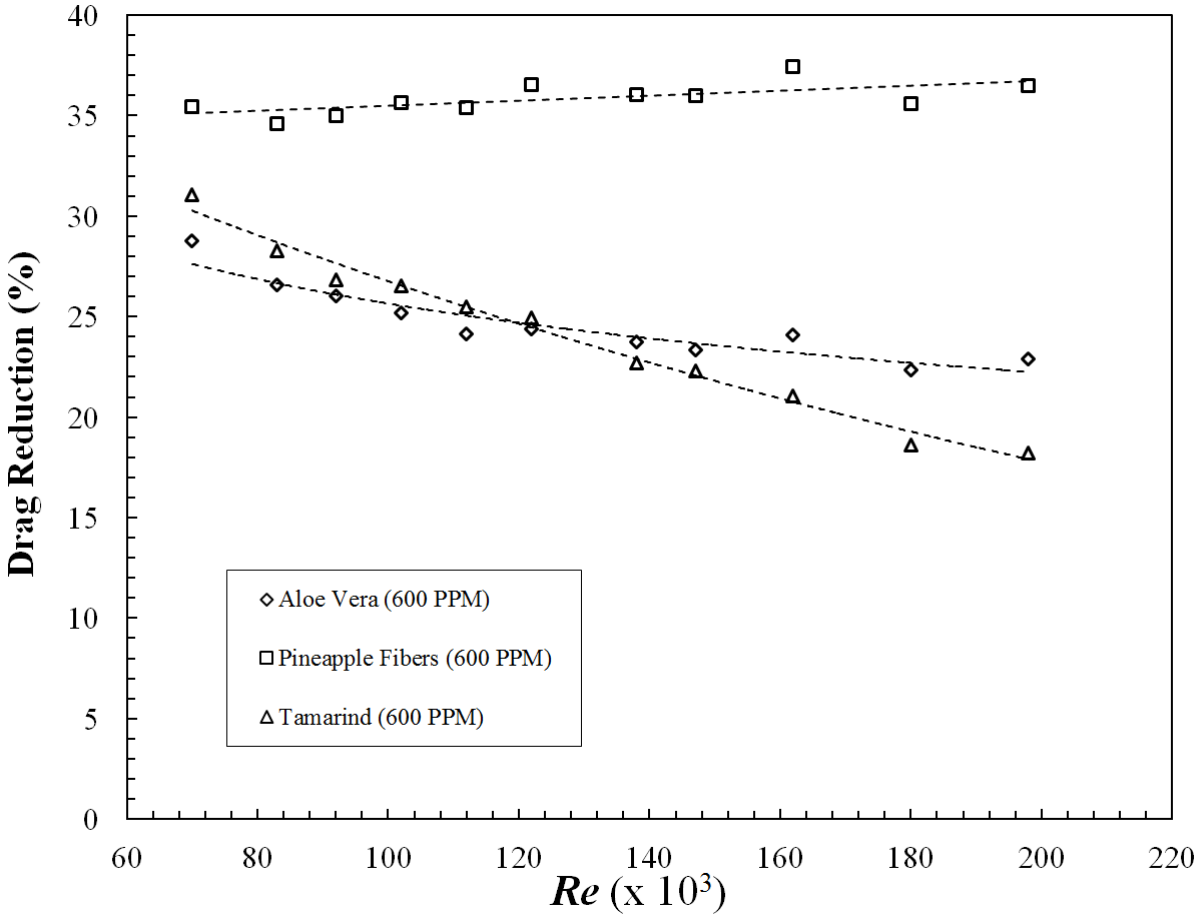

Figure 6-7: Drag reduction of polysaccharides with increasing Reynolds number.

6.3.3 Drag Reduction using CNC, Surfactant and CNC-Surfactant

Figure 6-8 and Figure 6-9 shows skin friction coefficient and drag reduction respectively, for Surfactant, CNC and CNC-Surfactant. Drag reduction with surfactants can be observed to sharply decrease with increasing *Re*. The formation of micelle structures is the reason behind the DR in case of surfactants, however these thread-like structures easily break up at higher shear stress or *Re;* making them ineffective at large *Re*. These results agree well with the observations made by Zhang et al. (2005). On the other hand, due to the rigid rod structure of

CNC, it exhibits only 30% DR which varies slightly with the *Re*. Due to their non-deformable structure, the size and shape of CNC doesn't vary much with strain rate which leads to nearly constant DR with increasing DR. This is consistent with the drag reduction shown by colloidal crystals of milling yellow dye having an aspect ratio of 5.7. However, grafting of surfactant on CNC reduced the DR to 10%, indicating the obtained structure doesn't exhibit viscoelastic properties similar to micelles in the case of pure surfactants. It could be either due to poor grafting density of surfactants on CNC or the rigid structure of CNC which is at the core of surfactants in this structure. Due to weak bonding between CNC and surfactant, DR can be observed to decrease with increasing *Re*. Similar to polysaccharides, DR for these samples were also tested at lower concentrations of 200 PPM and 400 PPM. CNC-Surfactant and CNC demonstrated similar DR at these lower concentrations; however the surfactant showed negligible DR at lower concentrations. The surfactant required a critical concentration beyond which the micellar structure is formed, which possesses the viscoelastic properties required to demonstrate DR. Since 600 PPM concentration was observed to the appropriate concentration for surfactant, the same concentration was chosen for CNC and CNC Surfactant for comparison.

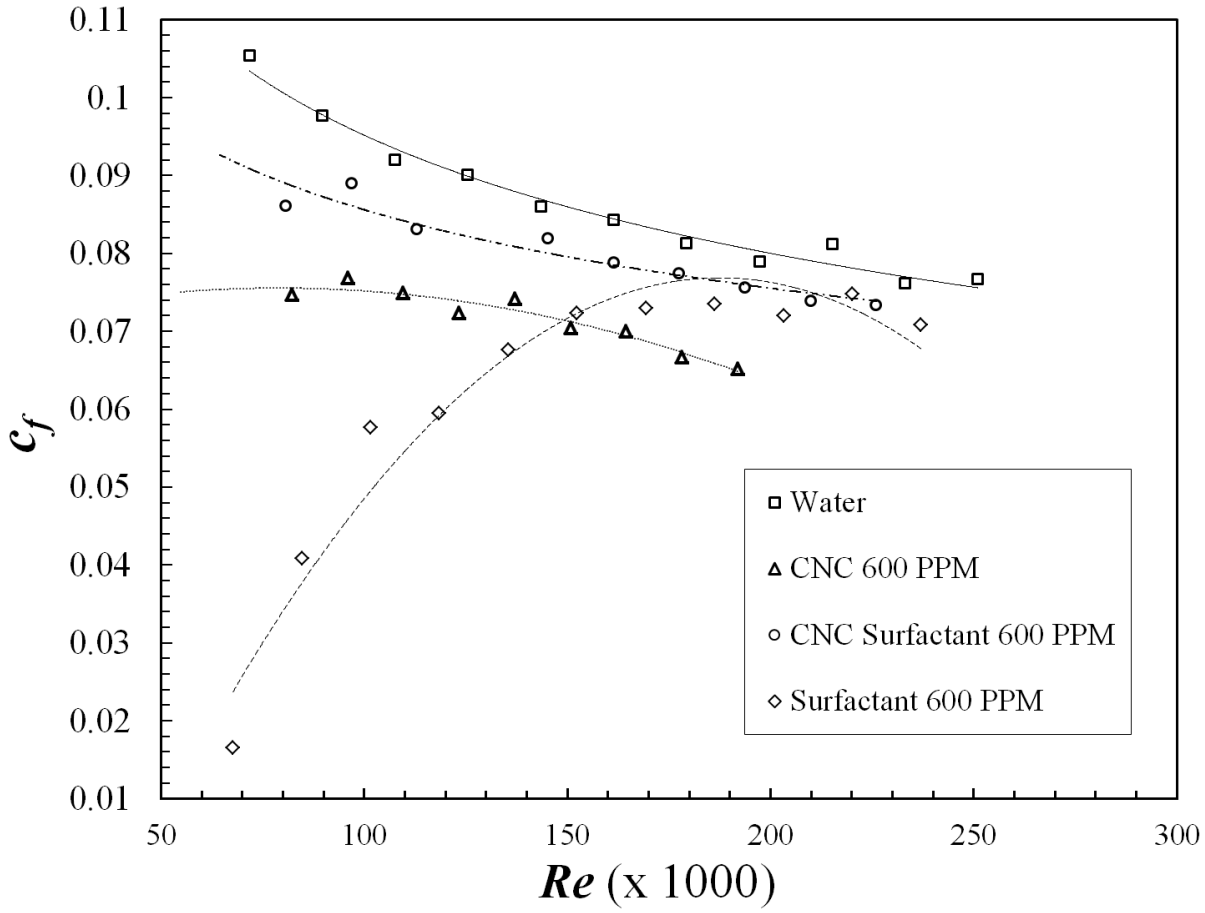

Figure 6-8: Skin friction Coefficient vs. Reynolds number for CNC, Surfactant and CNC-Surfactant.

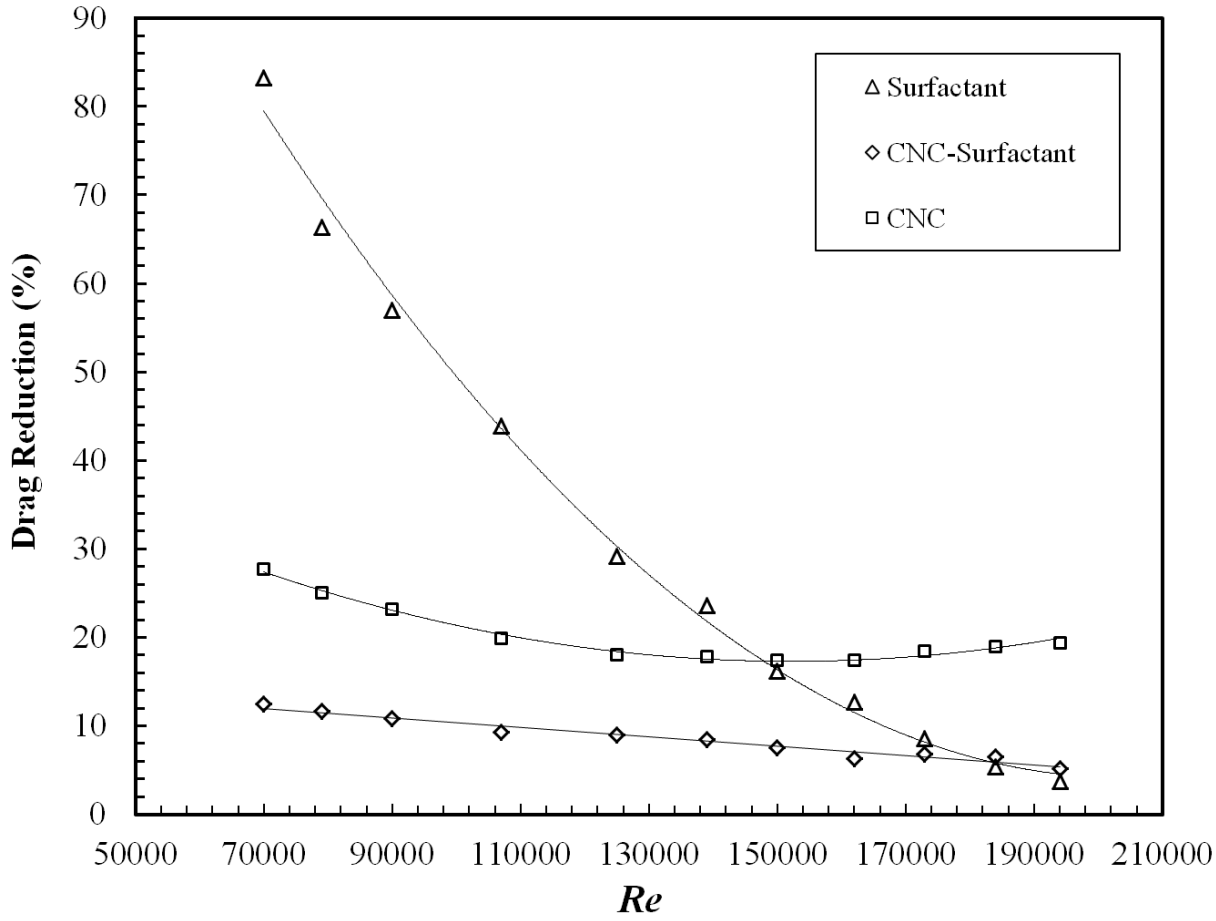

Figure 6-9: Drag reduction with increasing Reynolds number for CNC, Surfactant and CNC-Surfactant.

6.4 Conclusion

Additives such as aloe vera, pineapple fibers and tamarind powder are explored as drag reducing agents using a Taylor-Couette flow setup. These polysaccharides exhibit 35% of DR at fairly low concentration of 600 PPM and have an advantage of being biodegradable as compared to Synthetic polymers. However, these have drawback of being more susceptible to mechanical degradation and show decreased DR with an increase in *Re*. The current study also investigates cellulose nano crystals, both rigid rod and biodegradable cellulose crystals with aspect ratio varying from 10-20, for DR. Due to their non-deformable structure, CNC demonstrated roughly constant DR with an increase in strain rate or *Re*. Further, a cationic surfactant (CTAB) was grafted to the CNC and was then subsequently investigated as drag

reducing additives. The surfactant was also investigated separately for DR in order to make a comparison and showed 80% DR at low *Re* which significantly dropped down with increase in *Re.* However, CNC-surfactant exhibited reduced DR as compared to CNC and surfactant separately, signifying that the grafted structure doesn't show similar viscoelastic properties as the micelle formation of the surfactant. In summary, CNC and other polysaccharides studied are identified as a potential biodegradable and environmentally friendly drag reducing additives.

This chapter has been submitted in Journal of Applied Polymer Science as "Bhambri, P., Narain, R. & Fleck, B. (2016). Thermo-Responsive polymers for Drag Reduction in Taylor-Couette Flow."

7. THERMO-RESPONSIVE POLYMERS FOR DRAG REDUCTION IN TAYLOR-COUETTE FLOW

The addition of a small amount of high–molecular weight polymer to a solvent can substantially decrease friction losses by approximately 80%. This phenomenon known as Drag Reduction (DR) is used extensively in oil recovery during hydraulic fracturing and in many other applications to reduce the pumping costs. However, due to long chain length, these polymers get adsorbed on the surface of reservoir, diminishing the effectiveness of fracking. In the current study, a thermo-responsive polymer i.e. Poly-N-isopropylacrylamide (PNIPAM) is investigated as a Drag Reducing Agent (DRA), which collapses reversibly above 33 °C known as Lower Critical Solution Temperature (LCST), thereby preventing it from getting adsorbed beyond this temperature. Free radical polymerization was used to synthesize the PNIPAM and a Taylor-Couette (TC) setup with a rotating inner cylinder was utilized for measuring the Drag Reduction. The effect of concentration, Reynolds number (Re) and temperature on DR were studied and a maximum of 50% DR was observed at 400 PPM concentration. PNIPAM demonstrated significant decrease in DR beyond LCST, validating its thermo-responsive nature which could be beneficial for DR in oil recovery, or in providing a control modality to DR technologies.

7.1 Introduction

Drag reduction in turbulent flow using high molecular weight polymers, known as DRA, has been a field of intensive research (Toms 1949; Warholic et al. 1998; Sreenivasan et al. 2000). Utilization of these long chain polymers at a very low concentration as additives can significantly reduce the pressure drop, leading to substantial cost and energy savings (Lumley 1969). Because of these benefits, DRA has gained wide attention in fluid transportation pipelines and has enhanced oil recovery such as in hydraulic fracturing (Amro 2008). Polyacryalmide (PAM) is the most commonly used DRA for this purpose and has been

studied extensively in the past (Kurenkov et al. 2002; Hoyt 1972). Pipe diameter (*d*), *Re (=ud/v;* where *u* is the fluid velocity and *v* is the fluid kinematic viscosity), DRA concentration and DRA molecular weight have been reported to be the significant parameters affecting DR in a pipe flow (Lumley 1973; Virk 1975; Bewersdorff 1982). Several theories have been postulated in the last few decades to explain the mechanism of DR by polymers (Hoyt 1972). All these theories revolve around a major idea that the long chain polymers are extended in high shear rate zones, leading to enhanced elongational viscosity in this extended state, which interacts with the micro vortices in turbulent flow and diminishes the energy required to grow (Lumley 1973; De Gennes 1986). Although the mechanism behind DR is not completely understood yet, it is well acknowledged that considerably high molecular weight or long chain length of the polymer is one of the key requirements for DR (Virk 1967; Bismarck et al. 2008).

Due to the low permeability of the shale gas reservoirs, hydraulic fracturing is a commonly used well-stimulation technique (to achieve improved recovery rate) in which a fracking fluid is injected at high pressure into wellbore (Gandossi 2014). This fracking liquid consists of sand, proppants and high molecular weight polymers as DRA. However, the conventional long chain polymers used as DRA in fracturing gets adsorbed on the surface, reducing the permeability of reservoirs and requires cleanup procedures with the help of oxidizers to break the adsorbed polymers (Hollander et al. 1981; Kot et al. 2011). Using a polymer which gets degraded into a short chain length with some trigger could be a potential solution to decrease the adsorbance of these polymers.

Kot et al. (2011) introduced some weak links in the polymer chain which degrades with increase in temperature, narrowing the chain length. However, the degradation was irreversible, making the polymer cost ineffective. Responsive polymers which could collapse reversibly with a trigger such as pH or temperature could be a potential solution to overcome this limitation. Thermo-responsive polymers exhibit reversible shrinkage of polymer chains with change in temperature. These polymers drastically transits from its hydrophilic nature to hydrophobic nature at a temperature, known as Lower Critical Solution Temperature (LCST). Poly (N-isopropylacrylamide) (PNIPAM) is a widely known thermo-responsive polymer with an LCST of 32ºC (Heskins & Guillet 1992).

7.1.1 Poly-N-isopropylacryamide

Poly-N-isopropylacryamide (PNIPAM), is the most commonly used thermo-responsive polymer and was first synthesized in 1950's. It demonstrates a Lower Critical Solution Temperature (LCST) in aqueous media. Due its reasonable LCST of around 33°C and its biocompatibility, it has found a huge application in the field of biomedical for controlled drug delivery. The thermo-responsive nature in PNIPAM arises from the balance between entropy and enthalpy term in Gibbs free energy. The polar groups in PNIPAM form hydrogen bonding with the water molecules, which leads to negative ΔH (enthalpy) in free energy (ΔG).

$$\Delta G = \Delta H - T\Delta S \tag{7.1}$$

This requires reorientation of PNIPAM molecules, thereby decreasing the entropy of mixing (ΔS) making the second term positive. For the polymer to be soluble, Gibbs free energy in equation 7.1 needs to be negative. Below LCST, due to small temperature, the first term dominates and due to negative ΔG, the polymer is soluble in water. However, with an increase in temperature, the second term starts dominating, leading to positive ΔG above the LCST, and in turn precipitation of the polymer (Schild 1992). Further, this change in polymer solubility is reversible i.e. cooling the solution back below 32°C will lead to solubility of PNIPAM in water again.

LCST of PNIPAM doesn't depend on the molecular weight or concentration of the solution; however, it can be modified by introducing hydrophilic or hydrophobic groups in the polymeric chain. Introduction or copolymerization of PNIPAM with hydrophobic molecules/copolymer increases the LCST whereas copolymerization with hydrophilic monomers decreases the LCST. Hence, the desired LCST of the polymer can be easily accomplished by copolymerizing it with another suitable polymer. PNIPAM is widely used in macroscopic gels, microgels, latexes, coatings, membranes, sensors, tissue engineering and drug delivery (Schild 1992).

Since high chain length ($n > 1 \times 10^5$) is an important criteria for a polymer to show DR, PNIPAM can be easily synthesized using free radical polymerization to achieve longer chain length, qualifying them as a potential DR candidate (Ye & Narain 2009).

7.1.2 Free Radical polymerization

This section provides a brief insight about Free radical polymerization, the technique utilized to synthesize Poly-n-isopropylacrylamide. It is the most common form of addition polymerization. A free radical is a molecule with an unpaired electron and is highly reactive due to its affinity to gain an extra electron from other molecules. There are three major steps in this polymerization: initiation, propagation and termination. Briefly, the initiator radical attacks one monomer, and the electron is transferred to another part of the molecule. The new free radical attacks another monomer and the procedure is repeated.

Initiation

Propagation

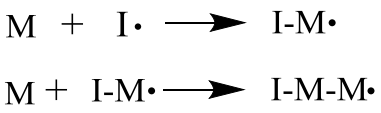

Termination

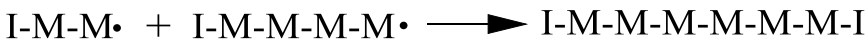

Figure 7-1: Free radical polymerization mechanism.

The mechanism of polymerization is briefly shown in Figure 7-1. In the first step, the initiator (Ammonium per sulfate in this study) is decomposed into free radicals either by heating (thermal decomposition) or by the use of an accelerator (redox initiation; TEMED in this study). TEMED reduces the initiator and accelerates the formation of free radical which in turn catalyzes the polymerization reaction. After the reaction has been initiated, the propagation reaction is started. In this stage, the initiator attacks the monomer which transfers the free radical from initiator to monomer. In the consequent steps, a new monomer is added to the chain due to the attack of these free radicals and polymerization reaction is propagated. This step takes place rapisly and thousands of monomers are added to the chain in this short span of time. In the final step, known as termination, two free radical chains combine to form an inactive polymer chain, thereby stopping the further reaction. Oxygen acts as the inhibitor in free radical polymerization since it can trap the free radicals which can terminate the

reaction (and prevent the polymerization). Hence, removal or degassing of oxygen from the polymerization flask is an important step to achieve polymerization (Narain, R. 2015).

PNIPAM can be synthesized with the help of free radical polymerization or redox polymerization using Ammonium persulfate or Potassium persulfate as an initiator in aqueous media. A high molecular weight polymers can be easily achieved in these polymerization techniques, however the polydispersity is comparatively high (>1.5). The polydispersity index is a method to measure the distribution of molecular mass in a given polymer sample. A sample with polydispersity of unity has all the polymer chains of equal length and the value of polydispersity increases with the increase in dispersity of polymer chains. Low polydispersity (<1.5) can be accomplished by using a controlled polymerization technique such as Atom transfer radical polymerization (ATRP) or Reversible addition−fragmentation chain-transfer (RAFT) polymerization, however the molecular weight achieved at atmospheric pressure is reasonably low in these techniques. Hence, a reactor operating at reasonably high pressure is required to synthesize high molecular weight polymers, which is difficult to design at lab scale with appropriate safety measures (Narain, R. 2015). Further, polydispersity is not a major issue for drag reduction applications; hence, in the present study free radical polymerization with a redox pair of Ammonium persulfate (APS) and Tetramethylethylenediamine (TEMED) was utilized to synthesize the PNIPAM.

Murnick et al. (1994) studied PNIPAM in a laminar flow and reported maximum DR of 30%. However, this study was not extended to a turbulent regime.

Pipe/Channel flow is the commonly used platform for testing the drag reducing additives (Hoyt & Sellin 1988). However, synthesizing polymers at a lab scale is challenging as a large amount of polymer is required to test for drag reduction properties in a channel flow. Taylor Couette Flow (TC) set-up can overcome this constraint due to its requirement of less fluid volume and has been identified as a reliable platform for measuring drag reduction (Koeltzsch et al. 2003; Dutcher & Muller 2009). Hence, in the present investigation, a TC setup consisting of two concentric cylinders was utilized to measure the drag reduction. High *Re* TC flow is a turbulent fluid motion in an annular gap due to rotation of either one or both of the concentric cylinders. Considerably high *Re* ($\sim 4 \times 10^5$) can be easily achieved by simply rotating either of the cylinders at high speed (Lathrop et al. 1992). Drag can be inferred from

the torque acting on either inner or outer cylinder using a torque sensor or load cells. Torque in this setup can be non-dimensionalized using the Equation 7.2 (Lewis & Swinney 1999):

$$G = \frac{T}{\rho \nu^2 L} \tag{7.2}$$

where G is the non-dimensional torque, ρ is the fluid density, ν is the kinematic viscosity and L is the length of inner cylinder. Drag reduction (*DR%*) is then calculated from the difference between skin friction coefficient (c_f) of pure solvent and DRA solution by equation (7.3) and (7.4).

$$c_f = \frac{G}{Re^2} \tag{7.3}$$

$$DR\% = \frac{c_{f,w} - c_{f,s}}{c_{f,w}} \times 100 \tag{7.4}$$

Here, $c_{f,w}$ is the skin friction coefficient of water and $c_{f,s}$ is the skin friction coefficient of DRA solution.

Although significant research has been conducted on DR in past 60 years, thermo-responsive polymers have not been looked into as a DRA in turbulent flow. Employment of responsive polymer as a DRA leads to tailored drag reduction, which could be easily controlled by an external stimulus, such as temperature. The current investigation studies the effect of PNIPAM on DR in a turbulent Taylor Couette Flow. The effect of *Re*, temperature and polymer concentration is investigated. Further, the reversible nature of these responsive polymers on DR is also verified.

7.2 Method

7.2.1 Materials

All the chemicals were purchased from *Sigma-Aldrich Chemicals* (Oakville, ON, Canada). N-isopropylacrylamide (NIPAM) was purified in benzene and recrystallized in hexane prior to

use. Ammonium per sulphate (APS) and Tetramethylethylenediamine (TEMED) were used as such.

7.2.2 Polymer Synthesis and Characterization

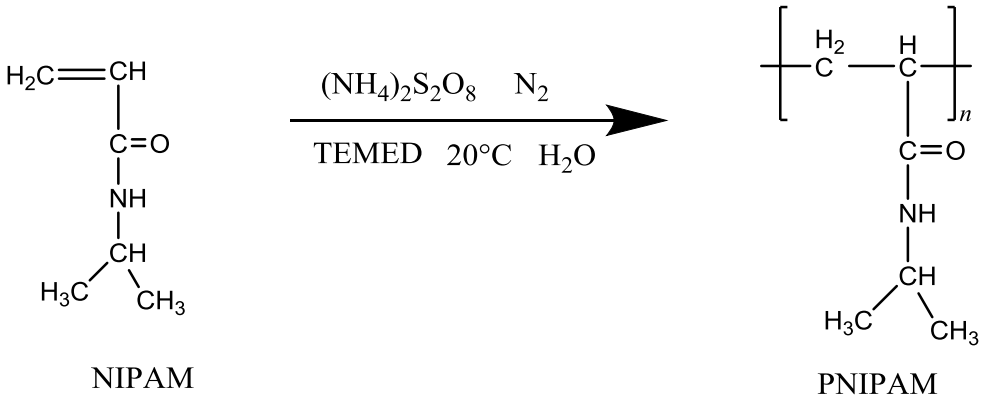

NIPAM PNIPAM

Figure 7-2: Synthesis of PNIPAM using free radical polymerization.

Conventional free-radical polymerization using redox initiation was used to synthesize the Poly-N-isopropylacrylamide (PNIPAM) in an aqueous media in an inert environment at 20°C (Figure 7-2). APS ($(NH_4)_2S_2O_8$) was used as an initiator whereas TEMED was used as an accelerator. In a round bottom flask, 0.45M solution of NIPAM in DI water was prepared by stirring for 10 minutes. 0.2 mole% (% of NIPAM) APS was separately dissolved in 2 ml of DI water and then added to the monomer solution. In the final step, 10-15 µl of TEMED was added, followed by immediate sealing of the flask. After degassing the flask by purging with N_2 for 30 minutes, the solution polymerization reaction was maintained by stirring it for 24 hours. The polymer solution was then purified by dialysis, using membrane tubing with a molecular weight cutoff of 6,000 to 8,000 g/mol to remove the unreacted monomers and initiator. After 48 hours of dialysis, the solution was then freeze dried for 3 days.

Gel Permeation chromatography was used to determine the molecular weight of PNIPAM. LCST of the PNIPAM was determined using a UV-vis spectrometer by measuring transmittance of 400 PPM aqueous solution of PNIPAM at 500 nm. Transmittance was continuously recorded by the spectrometer at a heating rate of 0.5 °C/min with temperature range from 20 to 40°C. The viscosity of PNIPAM solution at desired concentrations was

measured using a Rheometer (*Anton Paar, RheolabQC*) by varying the shear rate from 1-1000 s^{-1} at different studied temperatures.

7.2.3 Measurement of Drag Reduction

Drag reduction was measured using a Taylor-Couette setup with a stationary outer cylinder and a rotating inner cylinder, both the cylinders fabricated from acrylic (Figure 7-3). The following parameters describe the system utilized in this study:

$$\text{Annular gap } (d=r_o-r_i) = 1.9 \text{ cm}$$

$$\text{Radius ratio } (\eta=r_i/r_o) = 0.76$$

$$\text{Inner Cylinder Length } (L) = 20.08 \text{ cm}$$

$$\text{Aspect ratio } (\Gamma=L/d) = 10.56$$

$$\text{Reynolds number } (Re) = \frac{\Omega_i r_i (r_o - r_i)}{\nu}$$

Here r_i is the inner cylinder radius, r_o is outer cylinder radius, $\Omega_i$is the angular velocity of the inner cylinder and ν is the fluid kinematic viscosity. The inner cylinder is mounted on a shaft (using shaft collar) which is then connected to a speed control motor using a shaft coupling. The motor is a 120V AC, NEMA 34, 1/3 hp DC Motor (*Amatek Inc*.) having a speed range of 300-3450 RPM. The torque acting on the inner cylinder is measured using a reaction torque sensor (TFF425, *Futek Advanced Sensor Technology, Inc*) which is mounted at the base of the motor. The torque sensor has a capacity of 7 N-m and provides 2mV/V of rated output (RO). It was pre-calibrated by *Futek Advanced Sensor Technology, Inc* and showed an error of 0.02% of RO in the clockwise direction and -0.03% of RO in the anti-clockwise direction. A USB 220 kit was used to digitize the output signals of the sensor which were then recorded using SENSIT Test and Measurement software. The inner cylinder angular velocity was measured using an optical tachometer. The temperature of the fluid in annular gap was assessed using a K-type thermocouple which was mounted at the top plate of TC set-up.

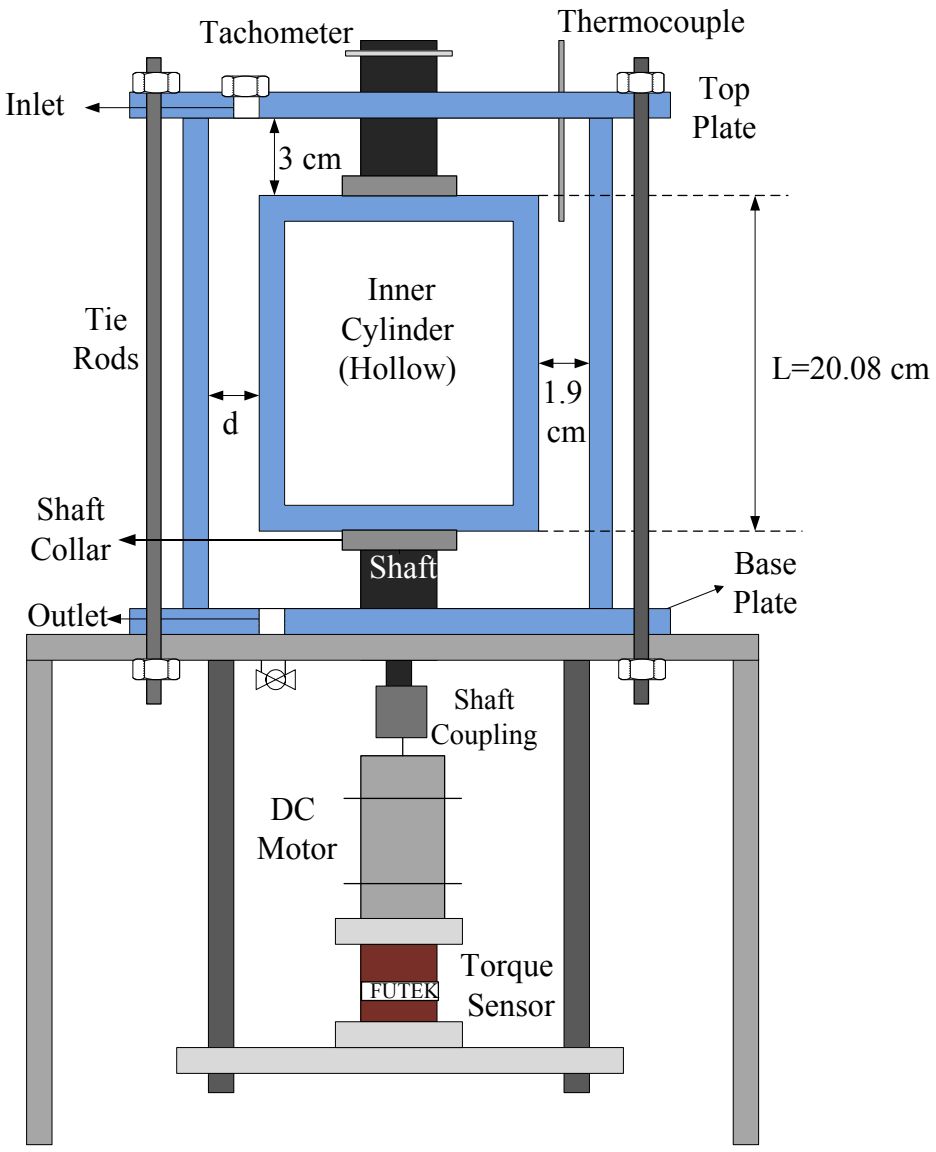

Figure 7-3: Schematics of Taylor Couette Setup used for measuring drag reduction.

DRA solution was prepared by stirring the desired amount of PNIPAM in water for 2 hours at 200 RPM on a magnetic stirrer. Six different concentrations ranging from 100-600 PPM were studied with *Re* varying from $4x10^4$-$2.5x10^5$. Drag reduction was measured at 20°C and 40°C in order to check the difference in DR below and above LCST. In order to verify the reversible nature of these polymers, the heated solution was cooled back again to 20°C and the corresponding DR was measured. For 500 PPM solution, DR was measured at 6 different

temperatures varying from 15°C - 40 °C in order to determine the effect of temperature (apart from LCST) on DR.

7.3 Results and Discussion

7.3.1 Polymer Synthesis and Characterization

Figure 7-4 shows the transmittance of 400 PPM aqueous PNIPAM solution at different temperatures varying from 20°C-40°C. Polymer is completely transparent in water below 33°C signifying good solubility. LCST of the polymer is observed at 33°C where transmittance is dropped from 99% to 0.15 % indicating precipitation of PNIPAM beyond 33°C. Insolubility of the polymer after 33°C verifies the thermos-responsive nature of the polymer.

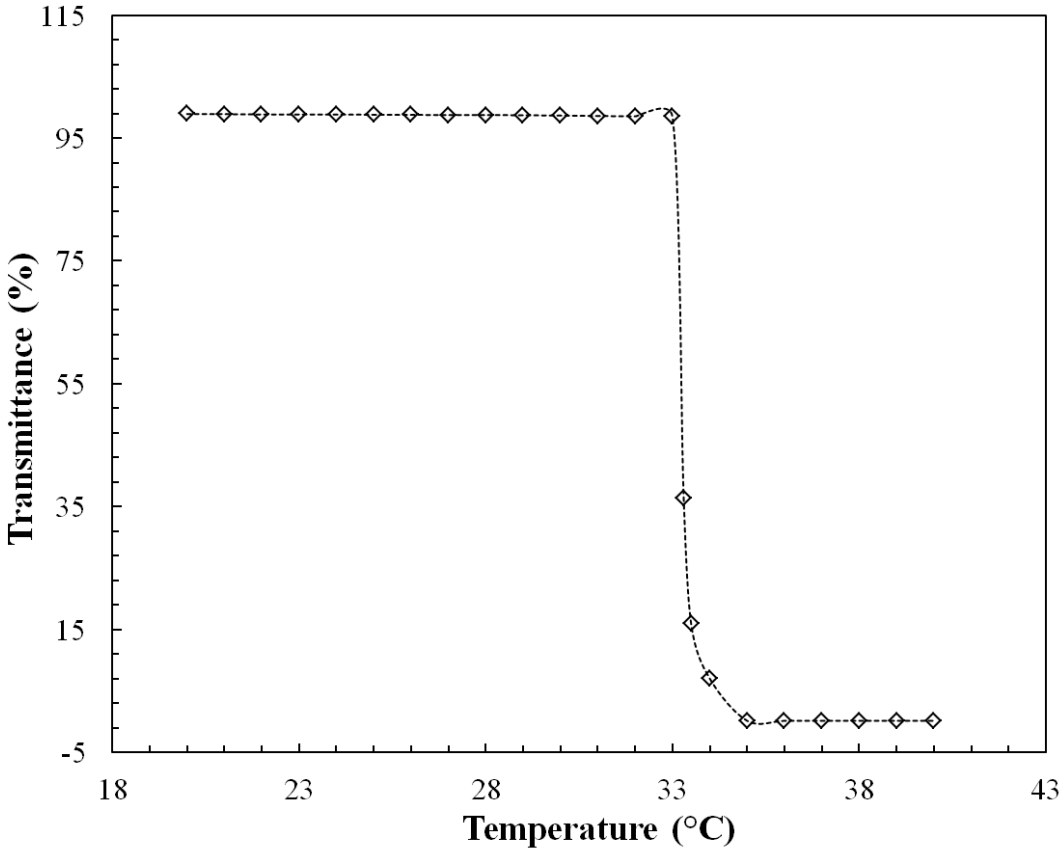

Figure 7-4: Transmittance of 400 PPM aqueous PNIPAM solution at different temperature.

Molecular weight of the polymer was observed to be 254,085 Da signifying a sufficiently long polymer chain length for DR. Rheological measurement provided stress vs. strain curves for the PNIPAM solutions and power law model was used to measure the solution viscosity. Due to very low concentration, all the solutions exhibited Newtonian behavior. Table 7-1 summarizes the viscosity of PNIPAM solutions at 20°C and 40°C. Table 7-2 provides viscosity of 500 PPM PNIPAM solution at different temperature ranging from 15°C to 40°C.

Table 7-1: Viscosity of PNIPAM solutions at 20°C and 40°C.

Concentration (PPM)	Viscosity at 20°C (Pa.s)	Viscosity at 40°C (Pa.s)
100	1.1×10^{-3}	0.9×10^{-3}
200	1.2×10^{-3}	0.9×10^{-3}
300	1.3×10^{-3}	0.9×10^{-3}
400	1.6×10^{-3}	0.9×10^{-3}
500	2.1×10^{-3}	0.9×10^{-3}
600	2.1×10^{-3}	0.9×10^{-3}

Table 7-2: Viscosity of 500 PPM PNIPAM solution at different temperature.

Temperature(°C)	Viscosity (Pa.s)
15	2.4×10^{-3}
20	2.1×10^{-3}
25	1.7×10^{-3}
30	1.4×10^{-3}
35	1.0×10^{-3}
40	0.9×10^{-3}

7.3.2 Drag Reduction

Figure 7-5 shows the Drag reduction vs. Re for different concentrations of PNIPAM ranging from 100-600 PPM at 20°C (Below LCST). Since all the measurements were conducted at fairly high Re, the effect of *Re* cannot be seen on DR. However, there is significant effect of PNIPAM concentration on DR indicating maxima at 400 PPM. As indicated in previous

studies on conventional DRA such as polyacrylamide (Virk 1975), there is a maximum concentration beyond which there is a decrease in DR with increasing concentration. This increase in DR with increase in concentration is due to higher interaction of polymer chains with turbulent micro-vortices leading to larger dissipation of turbulent energy (Sá Pereira & Pinho 1994). On the other hand, decrease in DR beyond 400 PPM could be attributed to enhanced entanglements of these long chain molecules amongst themselves, leading to reduced mobility of the polymer chains.

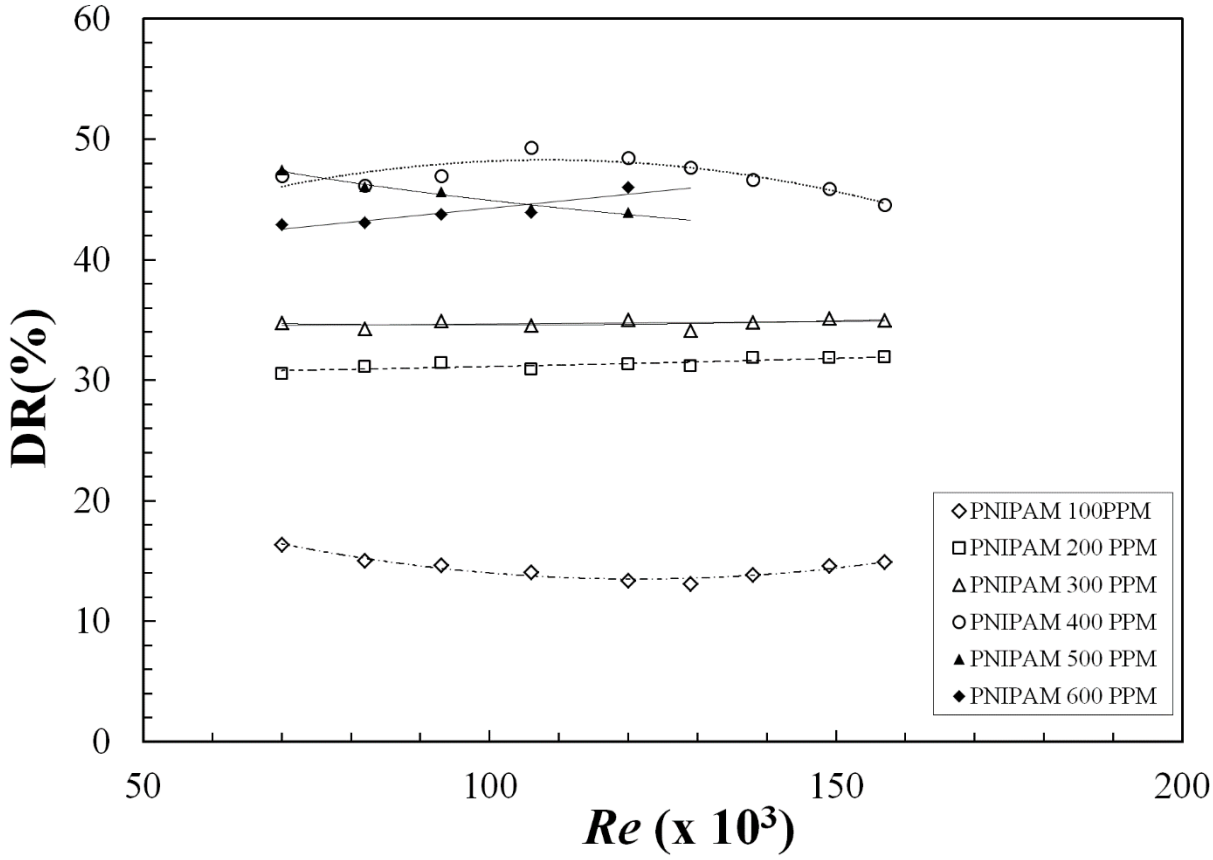

Figure 7-5: Drag reduction vs. Re for different concentrations of PNIPAM solution at 20°C.

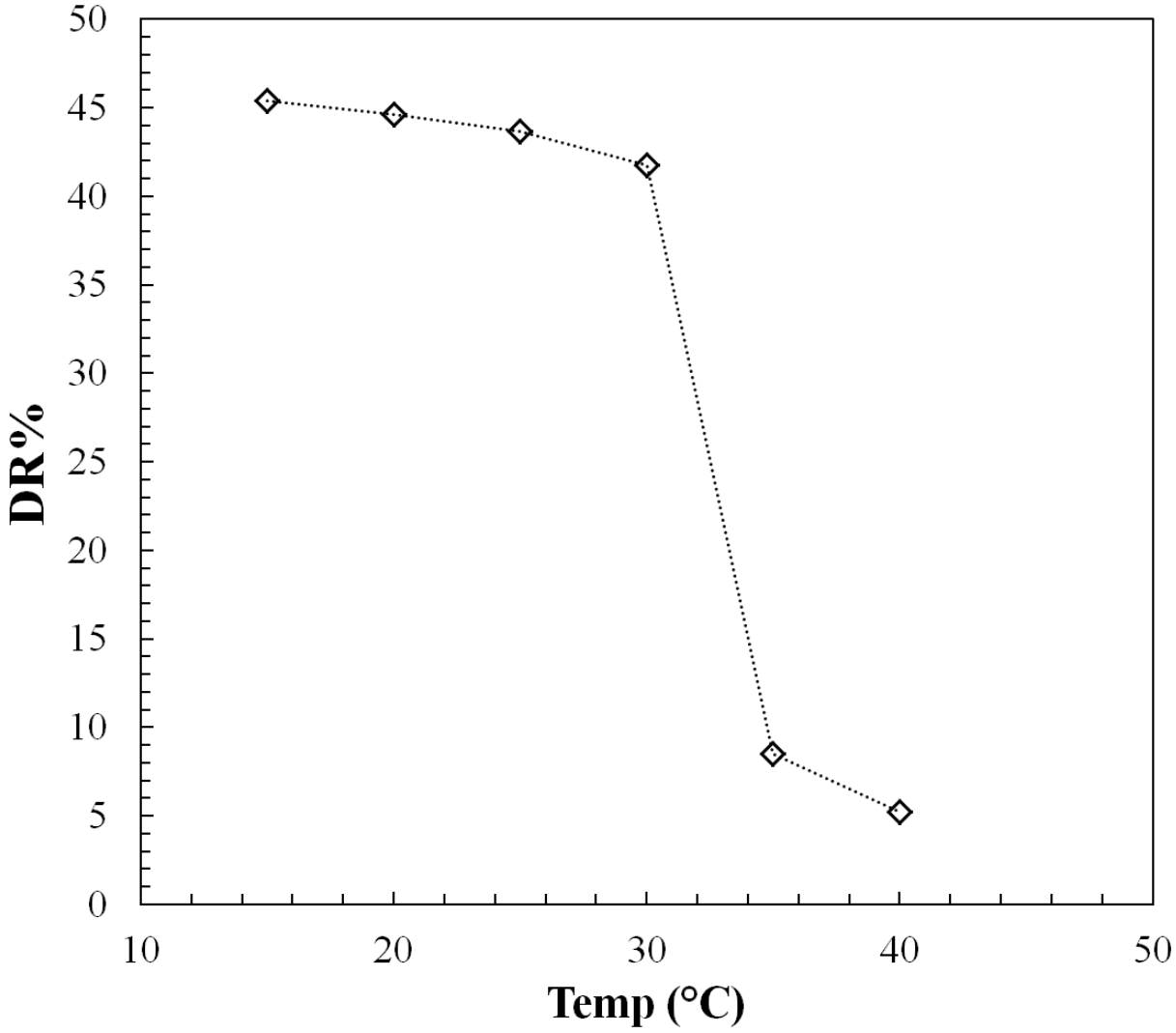

Figure 7-6: Drag Reduction vs. Temperature for 500 PPM solution at *Re* = $1x10^5$.

Figure 7-6 summarizes the effect of temperature on DR for 500 PPM concentration at Re=$1x10^5$. Temperature doesn't alter the DR below the LCST i.e. 33°C; however DR drastically reduces to 5% above the LCST. Above the LCST, the thermo-responsive polymers becomes hydrophobic in nature and act as collapsed particles which easily go along with the fluid flow without interacting with the turbulence and without getting adsorbed to the surface. This plot is similar to Figure 3 which shows transmittance of PNIPAM solution with a change in temperature.

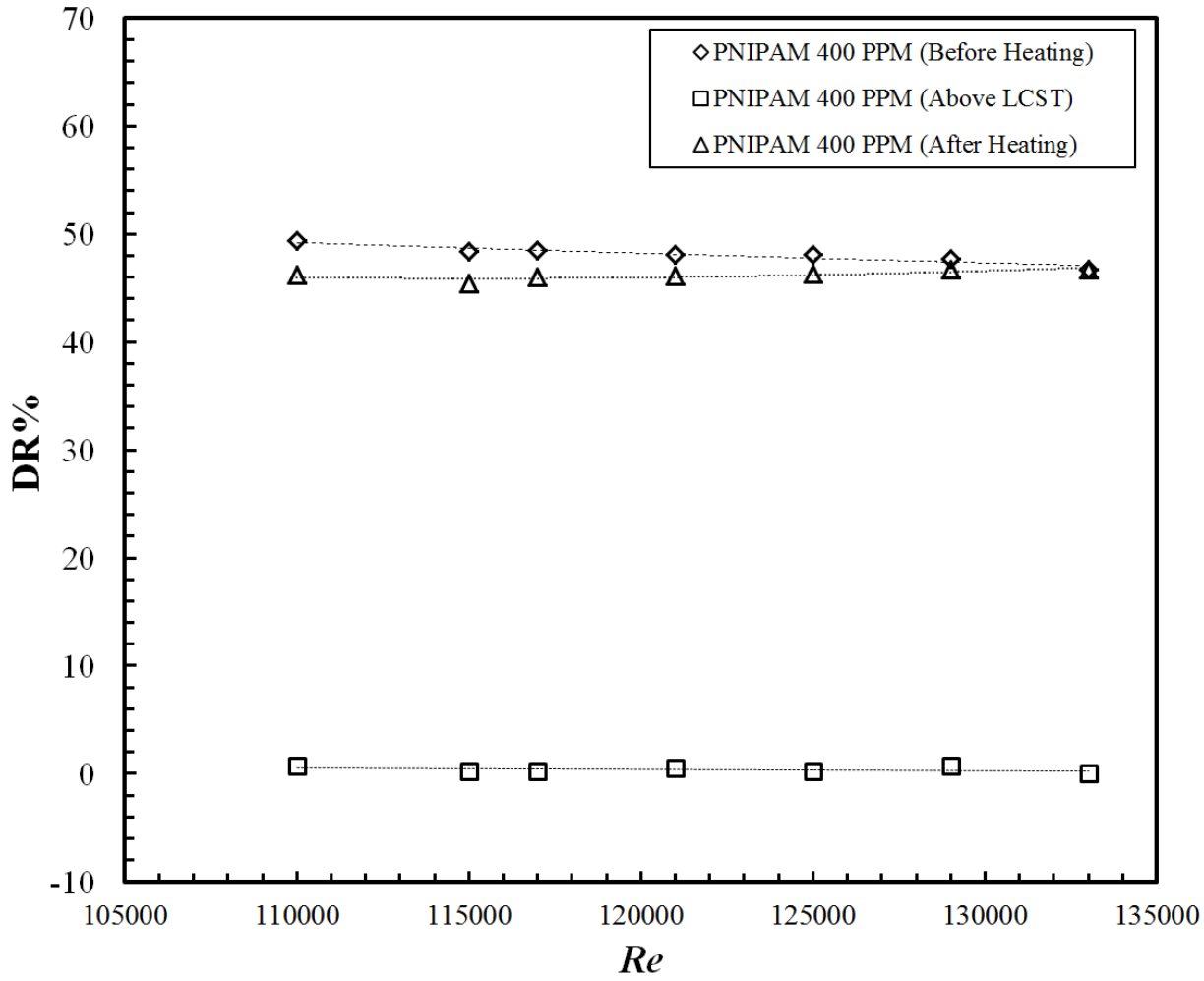

Figure 7-7: Drag Reduction vs. Re for 400 PPM solution below and above LCST.

Figure 7-7 compares the DR for 400 PPM at two different temperatures i.e. 20°C (Below LCST) and 40°C (Above LCST). The third plot with legend PNIPAM 400 PPM (after heating) indicates the DR of the solution at 20°C after it was cooled down from 40°C in order to verify the reversible nature of these polymers. PNIPAM, above its LCST at 40°C, shows negligible DR due to precipitation of molecules, validating its thermo-responsive nature. Further, after cooling back the solution to 20°C, drag reduction properties of the polymer are retrieved back, verifying the reversible nature of the polymer. Similar behavior was observed for other concentrations where polymer exhibited drastic decrease in DR above LCST and showed reversible DR after cooling back.

7.4 Conclusion

In the current study, a thermo-responsive polymer i.e. poly-N-isopropylacrylamide (PNIPAM) was investigated for the first time as a drag reducing agent in a turbulent Taylor Couette flow with water as solvent. Conventional free-radical polymerization using a redox pair i.e. ammonium persulfate and TEMED in an inert environment was used to synthesize the PNIPAM in aqueous solution. A high molecular weight of 254 kDa was confirmed using gel permeation chromatography. The effect of Reynolds number, concentration and temperature was studied on drag reduction, and maximum DR was observed to be 50% at 400 PPM concentration. The polymer exhibited a prominent responsive nature at its lower critical solution temperature (33°C), and precipitated in the solution at this temperature. It didn't exhibit any drag reduction beyond 33°C, making it a suitable candidate for DR in enhanced oil recovery, where temperature can be used as a trigger to prevent these polymers for getting adsorbed at reservoir surfaces. Further, on cooling back to 20°C, the drag reduction properties of the polymer could be retrieved back to their original value, making them cost effective additives for tailored and controlled DR in other applications. The study validates PNIPAM as a potential DRA, which won't affect the permeability of shale reservoirs and has a capability to be triggered for DR for other applications.

8. CONCLUSION & FUTURE WORK

8.1 Conclusion

Drag reduction using long polymer chains as additives has been extensively studied in the past using pipe or channel flow. However, due to the large amount of polymers required to quantify drag reduction in pipe/channel flow, it makes it an expensive and tedious procedure to develop new drag reducing agents for laboratory testing. As a solution, the current investigation develops a platform to test these additives for drag reduction requiring significantly small quantity for investigation purposes. A Taylor-Couette setup was designed with a stationary outer cylinder and rotating inner cylinder, in which drag (skin friction coefficient) can be inferred from torque acting on the inner cylinder. The detailed design considerations for TC apparatus are discussed in Chapter 4 of this thesis. Briefly, the TC setup has a radius ratio (η) of 0.76 and aspect ratio (Γ) of 10.57. The system can achieve a high Reynolds number (Re) of up to 2.9 x 10^5 with water as a working fluid. The torque acting on the inner cylinder is measured using a reaction torque sensor which was installed beneath the motor. The three main objectives of the study, discussed in Chapter 1, are studied separately in Chapter 5, 6 & 7 respectively. The following sections summarize the conclusions from each chapter.

8.1.1 Drag reduction using commercial polymer (Magnafloc 5250)

The first objective of this chapter was to validate the designed TC setup as a tool for drag reduction testing. Initial experiments were conducted with water as a working fluid by varying Re from 2 x 10^4 -2.8 x 10^5 and torque measured using a reaction torque sensor which was scaled using dimensionless torque (G) and Re. The results obtained were compared with the previous reported studies and were found to be in good agreement. In the next step, four different concentrations of commercial polyacrylamide; 80, 120, 160 and 200 PPM were examined for drag reduction (DR). All the solutions except 80 PPM, demonstrated non-Newtonian behaviour; however the solutions exhibited constant viscosity (μ_{inf}) beyond the strain rate of 800 s^{-1}. Hence, Re was purposefully chosen to be high enough so that it exceeded the strain rate to achieve μ_{inf} and this constant μ_{inf} was subsequently used to calculate Re. An

increase in DR% was observed with increase in concentration of polyacrylamide. Further, an onset of drag reduction was observed for 80 PPM DRA solution at *Re*=7x10^4 and Maximum Drag Reduction (MDR) asymptote of 63% DR was observed for 160 PPM DRA solution.

The TC setup was observed to be a convenient and powerful tool for assessing the drag reduction, with an important advantage being its small geometry. In addition, it is quick to use and requires smaller solution volumes. This provides an excellent platform for evaluating a wider range of DRA solutions.

8.1.2 Drag reduction using Polysaccharides

In this chapter, polysaccharides such as aloe vera, pineapple fibers, tamarind powder, cellulose nanocrystals (CNC) and modified structure of CNC were evaluated for drag reduction (DR). The effect of *Re* on DR of these polysaccharides was investigated. The results were found to be in good agreement with the previous studies on polysaccharides conducted in a pipe/channel flow. Pineapple fibers exhibited a maximum of 35% drag reduction amongst aloe vera, pineapple fibers and tamarind powder. These polysaccahrides have a unique advantage of being biodegradable as compared to synthetic polymers, making them environmentally friendly. However, these have a disadvantage of being more susceptible to mechanical degradation due to higher strain rate and exhibited decreased DR with increasing *Re*.

Cellulose Nanocrystals which are rigid rod crystals of biodegradable cellulose with an aspect ratio varying from 10-20 were also investigated for DR. Due to their non-deformable structure, CNC demonstrated roughly constant DR with increase in *Re*. As a next step, the surface of CNC was modified using a cationic surfactant i.e. CTAB, which was grafted on CNC and was then subsequently examined as drag reducing additives. The surfactant was also investigated separately for DR in order to make a comparison and showed 80% DR at comparatively low *Re* of 7 x 10^4. However, DR significantly dropped down with increase in *Re,* due to breakage of micellar structure in surfactants. It was observed that the drag reduction properties of surfactant were significantly reduced after grafting on CNC. CNC-surfactant exhibited reduced DR as compared to CNC and surfactant separately, indicating that the grafted structure doesn't possess similar viscoelastic properties as the micelle formation in

surfactant does. To sum-up, CNC and other polysaccharides studied were identified as prospective biodegradable and environmental friendly candidates for drag reduction.

8.1.3 Thermo-responsive polymers for drag reduction

Drag Reduction (DR) is extensively used in oil recovery during hydraulic fracturing and in many other applications to reduce the pumping costs. However, due to long chain length, these polymers get adsorbed on the surface of reservoir, diminishing the effectiveness of fracking. Thermo-responsive polymers could be a potential solution for this problem. PNIPAM, a thermo-responsive polymer collapses reversibly beyond its lower critical solution temperature (LCST) of 33°C, thereby preventing it from getting adsorbed beyond this temperature.

In this chapter, a thermoresponsive polymer i.e. Poly-(N-isopropylacrylamide) (PNIPAM) was synthesized and further, investigated for DR. Free radical polymerization was used to synthesize the polymer at high molecular weight of 254,000 Da. The polymer had a LCST of 33°C and precipitated in water beyond this temperature. Briefly, the polymer is hydrophilic below LCST and becomes hydrophobic above LCST. The effect of concentration of PNIPAM, *Re* and temperature was studied on drag reduction. A maximum DR was observed to be 50% at 400 PPM concentration. PNIPAM demonstrated negligible DR beyond its LCST of 33°C, validating its thermo-responsive nature which could be beneficial for DR in oil recovery, or in providing a control modality to DR technologies. Further, on cooling back to 20°C, the drag reduction properties of the polymer could be retrieved back to their original value, making them cost effective additives for tailored and controlled DR in other applications. The study validates PNIPAM as a potential DRA, which won't affect the permeability of shale reservoirs and has a capability to be triggered for DR for other applications.

8.2 Scope for Future Work

The following recommendations could be made for future work on this study.

- The current study investigates single radius and aspect ratio of the Taylor-Couette (TC) system. It would be interesting to test this instrument at varying radius and aspect ratio and to verify if these parameters have a significant effect on drag reduction. Change in radius and aspect ratio might lead to modification in dimensionless parameters such as dimensionless torque.
- Since the chamber of the TC system is optically clear, visualization techniques such as Laser Doppler Velocimetry (LDV) or Particle Image Velocimetry (PIV) could be utilized to study the fluid flow behaviour in this setup. The effect of drag reducing additives on turbulent structures of TC flow could be investigated in detail using these techniques.
- The thermoresponsive polymer studied in Chapter 7 could be modified with other monomers such acrylamide to alter the Lower critical solution temperature (LCST) of DRA. Poly-(N-isopropylacrylamide) (PNIPAM) could be copolymerized with polyacrylamide which would increase the LCST of the polymer. It would be interesting to investigate different monomer ratios of the copolymer for drag reduction, which would be beneficial in achieving desired LCST of the polyme

BIBLIOGRAPHY

Abdel-Alim, a. H., & Hamielec, a. E. (1973). Shear degradation of water-soluble polymers. I. Degradation of polyacrylamide in a high-shear couette viscometer. Journal of Applied Polymer Science, 17(12), 3769–3778. http://doi.org/10.1002/app.1973.070171218

AbdulBari, H. A., Letchmanan, K., & Yunus, R. M. (2011). Drag Reduction Characteristics Using Aloe Vera Natural Mucilage: An Experiment Study. *Journal of Applied Sciences*., 11:1039-1043.

Abdulbari, H. a., Shabirin, A., & Abdurrahman, H. N. (2013). Bio-polymers for improving liquid flow in pipelines-A review and future work opportunities. *Journal of Industrial and Engineering Chemistry*, *20*(4), 1157–1170. http://doi.org/10.1016/j.jiec.2013.07.050

Abdul-Bari, H.A., M.A. Ahmad and R.B.M. Yunus,, (2010). Formulation of okra-natural mucilage as drag reducing agent in different size of galvanized Iron pipes in turbulent water flowing system. *J. Applied Sci.,* 10: 3105-3110.

Abshagen, J., Schulz, A., & Pfister, G. (1997). The Couette-Taylor Flow : A Paradigmatic System for Instabilities , Patterm Formation and Routes to Chaos. Nonlinear Physics of Complex Systems, 476, 63–72.

Altmeyer, S., Hoffmann, C., Heise, M., Abshagen, J., Pinter, a., Lücke, M., & Pfister, G. (2010). End wall effects on the transitions between Taylor vortices and spiral vortices. Physical Review E - Statistical, Nonlinear, and Soft Matter Physics, 81(6), 1–9. http://doi.org/10.1103/PhysRevE.81.066313

Amro, M. M. (2008). Investigation of Polymer Adsorption on Rock Surface of High Saline Reservoirs. SPE Saudi Arabia Section Technical Symposium, 25(SPE 120807), 1–7. http://doi.org/10.2118/120807-MS

Ashrafi, N. (2011). Stability analysis of shear-thinning flow between rotating cylinders. Applied Mathematical Modelling, 35(9), 4407–4423. http://doi.org/10.1016/j.apm.2011.03.010

Barnes, H. A., & Walters, K. (1968). Dynamic Similarity and Drag Reduction in Flow of Elastic Liquids through Curved Pipes. Nature, 219(5149), 57–59. Retrieved from http://dx.doi.org/10.1038/219057a0

Benson, M., Tanaka, T., & Eaton, J. K. (2005). Effects of wall roughness on particle velocities in a turbulent channel flow. Journal of Fluids Engineering, 127, 250–256.

Bewersdorff, H. W. (1982). Progress and Trends in Rheology: Proceedings of the First Conference of European Rheologists Graz (Austria), April 14--16, 1982. In H. Giesekus, K. Kirschke, & J. Schurz (Eds.), (pp. 233–235). Heidelberg: Steinkopff. http://doi.org/10.1007/978-3-662-12809-1_61

Bewersdorff, H.W., (1982)Effect of Centrally Injected Polymer Thread on Drag in Pipe Flow, Rheol Acta., 21: 587-589.

Bhambri, P., & Fleck, B. (2016). Drag Reduction using high molecular weight polymers in Taylor-Couette Flow. International Journal of Mechanical and Production Engineering Research and Development, 6(1), 59–72.

Bismarck, A., Chen, L., Griffin, J. M., Hewitt, G. F., & Vassilicos, J. C. (2008). Polymer drag reduction. In Heat Exchanger Design Updates (Hewitt, G.). (Begell House, Inc., Redding, CT, USA).

Bismarck, A., Chen, L., Griffin, J. M., Hewitt, G. F., & Vassilicos, J. C. (2004). 2.14.1 Drag Reduction: Introduction. *Heat Exchanger Design Updates*, *11*(3), 1–5.

Bobkowicz, A. J. and Gauvin, W. H. (1965), The turbulent flow characteristics of model fibre suspensions. Can. J. Chem. Eng., 43: 87–91. doi: 10.1002/cjce.5450430210

Burin, M. J., Ji, H., Schartman, E., Cutler, R., Heitzenroeder, P., Liu, W., Raftopolous, S. (2006). Reduction of Ekman circulation within Taylor-Couette flow. Experiments in Fluids, 40(6), 962–966. http://doi.org/10.1007/s00348-006-0132-y

Cadot, O., Bonn, D., & Douady, S. (1998). Turbulent drag reduction in a closed flow system: Boundary layer versus bulk effects. Physics of Fluids, 10(2), 426–436. http://doi.org/10.1063/1.869532

Campolo, M., Simeoni, M., Lapasin, R., & Soldati, A. (2015). Turbulent Drag Reduction by Biopolymers in Large Scale Pipes. *Journal of Fluids Engineering*, *137*(4), 041102. http://doi.org/10.1115/1.4028799

Cengel, A., & Cimbala, J. (2006). Fluid mechanics: fundamentals and applications. International Edition, McGraw Hill Publication (1st edition). New York: The McGraw-Hill Companies, Inc.

Choi, U.S. and Kasza, K.E. (1981): "Long Term Degradation of Dilute Polyacrylamide Solutions In Turbulent Flow", Drag Reduction in Fluids Flows, Ellis Harwood Limited pp. 163-169.

Cole, J. a. (1976). Taylor-vortex instability and annulus-length effects. Journal of Fluid Mechanics, 75(01), 1. http://doi.org/10.1017/S0022112076000098

Couette, M. M. (1890). Études sur le frottement des liquids. Ann. Chim. Phys. 6, Ser. 21, 433-510, 1890.

Davey, a. (1962). The growth of Taylor vortices in flow between rotating cylinders. Journal of Fluid Mechanics, 14(03), 336. http://doi.org/10.1017/S0022112062001287

De Gennes, P. G. (1971). "Reptation of a Polymer Chain in the Presence of Fixed Obstacles". The Journal of Chemical Physics (American Institute of Physics) 55 (2): 572–571. Bibcode:1971JChPh..55..572D. doi:10.1063/1.1675789

De Gennes, P. G. (1986). Towards a scaling theory of drag reduction. Physicia, 140 A, 9–25. http://doi.org/10.1016/0378-4371 (86) 90200-1

Delfos, R., Hoving, J., & Boersma, B. (2011). Experiments on drag reduction by fibres in turbulent pipe flow Background. Euromech Meeting 513, 1–27.

Deshmukh, S. R., Sudhakar, K., & Singh, R. P. (1991). Drag-reduction efficiency, shear stability, and biodegradation resistance of carboxymethyl cellulose-based and starch-based graft copolymers. Journal of Applied Polymer Science, 43(6), 1091–1101. http://doi.org/10.1002/app.1991.070430609

Dezhong, W., Songping, W., Shan, S., & Yingzheng, L. (2005). Experimental investigation of turbulent boundary layer flow with surfactant additives using PIV and PDA. Heat Transfer-Asian Research, 34(2), 99–107. http://doi.org/10.1002/htj.20047

Donnelly, R. J., & Simon, N. J. (1960). An empirical torque relation for supercritical flow between rotating cylinders. Journal of Fluid Mechanics, 7, 401–418. http://doi.org/10.1017/S0022112060000177

Dutcher, C. S., & Muller, S. J. (2009). The effects of drag reducing polymers on flow stability : Insights from the Taylor-Couette problem. Korea-Australia Rheology Journal, 21(4), 223–233.

Ellis, H. D. (1970). Effects of Shear Treatment on Drag-reducing Polymer Solutions and Fibre Suspensions. Nature, 226(5243), 352–353. Retrieved from http://dx.doi.org/10.1038/226352a0

Eskin, D. (2014). Applicability of a Taylor–Couette device to characterization of turbulent drag reduction in a pipeline. Chemical Engineering Science, 116, 275–283. http://doi.org/10.1016/j.ces.2014.05.016

Fernandes, R. L. J., Fleck, B. a., Heidrick, T. R., Torres, L., & Rodriguez, M. G. (2009). Experimental Study of DRA for Vertical Two-Phase Annular Flow. Journal of Energy Resources Technology, 131(2), 023002. http://doi.org/10.1115/1.3120299

Forrest, F. and Grierson, G.A.H. (1931), “Friction losses in cast iron pipe carrying paper stock”, Paper Trade Journal. 92(22), 39-41.

Futek A. S. T.(2013, Dec 3) FUTEK Rotary Torque Sensor Webinar. Retrieved from https://www.youtube.com/watch?v=vHsl9e0ebrg

Gandossi, L. (2013). An overview of hydraulic fracturing and other formation stimulation technologies for shale gas production. European Commisison Joint Reserach Center Technical Reports. http://doi.org/10.2790/99937

Graham, M. D. (2004). Drag reduction in turbulent flow of polymer solutions. Rheology Reviews, 2004, 143–170.

Greidanus, a J., Delfos, R., & Westerweel, J. (2011). Drag reduction by surface treatment in turbulent Taylor-Couette flow. *Journal of Physics: Conference Series*, *318*(8), 082016. http://doi.org/10.1088/1742-6596/318/8/082016

Groisman, A., & Steinberg, V. (1996). Couette-Taylor Flow in a Dilute Polymer Solution. Physical Review Letters, 77(8), 1480–1483. http://doi.org/10.1103/PhysRevLett.77.1480

Hamilton, J. M., Kim, J., & Waleffe, F. (1995). Regeneration mechanisms of near-wall turbulence structures. Journal of Fluid Mechanics, 287, 317–348. http://doi.org/10.1017/S0022112095000978

Hershey, H. C., & Zakin, J. L. (1967). Existence of Two Types of Drag Reduction in Pipe Flow of Dilute Polymer Solutions. I&EC Fundamentals, 6(August), 381–387.

Heskins, M. & Guillet, J.E., 1992, "Solution Properties of Poly(N-isopropylacrylamide)", Journal of Macromolecular Science: Part A-Chemistry 2 (8):1441-1455.

Hof, B. (2005). IUTAM Symposium on Laminar-Turbulent Transition and Finite Amplitude Solutions. In T. Mullin & R. Kerswell (Eds.), (pp. 221–231). Dordrecht: Springer Netherlands. http://doi.org/10.1007/1-4020-4049-0_12

Hollander, A. F., Somasundaran, P., & Gryte, C. C. (1981). Adsorption Characteristics of Polyacrylamide and Sulfonate-Containing Polyacrylamide Copolymers on Sodium Kaolinite. Journal of Applied Polymer Science, 26, 2123–2138. http://doi.org/10.1002/app.1981.070260701

Hollerbach, R., & Fournier, A. (2004). End effects in rapidly rotating cylindrical Taylor Couette flow. AIP Conference Proceedings, 733, 114–121.

Hong, C. H., Zhang, K., Choi, H. J., & Yoon, S. M. (2010). Mechanical degradation of polysaccharide guar gum under turbulent flow. *Journal of Industrial and Engineering Chemistry*, *16*(2), 178–180. http://doi.org/http://dx.doi.org/10.1016/j.jiec.2009.09.073

Hou, Y. X., Somandepalli, V. S. R., & Mungal, M. G. (2008). Streamwise development of turbulent boundary-layer drag reduction with polymer injection. Journal of Fluid Mechanics, 597, 31–66. http://doi.org/10.1017/S0022112007009718

Hoyt, J. W. (1972). Effect of additives on fluid friction. J Basic Eng Trans ASME, 258–285.

Hoyt, J. W., & Sellin, R. H. J. (1988). Drag reduction by centrally-injected polymer "threads." Rheologica Acta, 27(5), 518–522. http://doi.org/10.1007/BF01329351

Huisman, S. G., Scharnowski, S., Cierpka, C., Kähler, C. J., Lohse, D., & Sun, C. (2013). Logarithmic Boundary Layers in Strong Taylor-Couette Turbulence. Physical Review Letters, 110(26), 264501.http://doi.org/10.1103/PhysRevLett.110.264501

Jones, W. M., & Marshall, D. E. (1969). Relaxation effects in Couette flow between rotating cylinders. British Journal of Applied Physics, 2(2), 809–814.

Kaboorani, A., & Riedl, B. (2015). Surface modification of cellulose nanocrystals (CNC) by a cationic surfactant. *Industrial Crops and Products*, 65, 45–55. http://doi.org/10.1016/j.indcrop.2014.11.027

Kageyama, A., Ji, H., Goodman, J., Chen, F., & Shoshan, E. (2004). Numerical and Experimental Investigation of Circulation in Short Cylinders. Journal of the Physical Society of Japan, 73(9), 2424–2437. http://doi.org/10.1143/JPSJ.73.2424

Kalashnikov, V. N. (1998). Dynamical similarity and dimensionless relations for turbulent drag reduction by polymer additives. Journal of Non-Newtonian Fluid Mechanics, 75(2-3), 209–230. http://doi.org/10.1016/S0377-0257(97)00093-1

Koeltzsch, K., Qi, Y., Brodkey, R. S., & Zakin, J. L. (2003). Drag reduction using surfactants in a rotating cylinder geometry. Experiments in Fluids, 34(4), 515–530. http://doi.org/10.1007/s00348-003-0590-4

Kot, E., Saini, R., Norman, L., & Bismarck, A. (2012). Novel Drag-Reducing Agents for Fracturing Treatments Based on Polyacrylamide Containing Weak Labile Links in the Polymer Backbone . *SPE Journal*, *17*(3):141257. http://doi.org/10.2118/141257-PA

Kundu, P. K., M., C. I., & Dowling, D. R. (2012). Fluid Mechanics (Fifth Edit). Boston: Elsevier. http://doi.org/http://dx.doi.org/10.1016/B978-0-12-382100-3.10012-5

Kurenkov, V. F., Hartan, H. G., & Lobanov, F. I. (2002). Degradation of polyacrylamide and its derivatives in aqueous solutions. Russian Journal of Applied Chemistry, 75(7), 1039–1050. http://doi.org/10.1023/A:1020747523268

Lathrop, D. P., Fineberg, J., & Swinney, H. L. (1992). Transition to shear-driven turbulence in Couette-Taylor flow. Physical Review A, 46(10), 6390–6405. Retrieved from http://link.aps.org/doi/10.1103/PhysRevA.46.6390

Lathrop, D. P., Fineberg, J., & Swinney, H. L. (1992). Turbulent-Flow between Concentric Rotating Cylinders at Large Reynolds-Number. *Physical Review Letters*, *68*(10), 1515–1518. http://doi.org/10.1103/PhysRevLett.68.1515

Lee PFW and G. G. Duffy, (1976). "An analysis of the drag reducing regime of pulp suspension flow," Tappi,59, 119-122

Lee, T. S. (1966). Turbulent Flow of Dilute Polymer Solutions: Studies in Couette Flow. M.I.T.; Department of Chemical Engineering. Retrieved from https://books.google.ca/books?id=waqNjgEACAAJ

Lewis, G. S., & Swinney, H. L. (1999). Velocity structure functions, scaling, and transitions in high-Reynolds-number Couette-Taylor flow. Physical Review. E, Statistical Physics, Plasmas, Fluids, and Related Interdisciplinary Topics, 59(5 Pt B), 5457–5467. http://doi.org/10.1103/PhysRevE.59.5457

Lumley, J. L. (1969). Drag Reduction by Additives. Annual Review of Fluid Mechanics. 1:367-384. http://doi.org/10.1146/annurev.fl.01.010169.002055

Lumley, J. L. (1973). Drag reduction in turbulent flow by polymer additives. Journal of Polymer Science: Macromolecular Reviews, 7(1969), 263–290. Retrieved from http://dynamicsystems.asmedigitalcollection.asme.org/article.aspx?articleid=1478256

McComb, W.D. and Rabie, L.H. (1982) Local Drag Reduction Due to Injection of Polymer Solutions into Turbulent Flow in a Pipe, AIChE J. 28:547-557.

McCormick, C. L., Hester, R. D., Morgan, S. E., & Safieddine, A. M. (1990). Water-Soluble Copolymers. 30. Effects of Molecular Structure on Drag Reduction Efficiency. Macromolecules, 23, 2124–2131. Retrieved from citeulike-article-id:592264

Merbold, S., & Egbers, C. (2012). Analysis of differentially rotating turbulent Taylor-Couette-flow using Laser Doppler Anemometry and comparison with torque measurements, 9–12.

Min, T., Choi, H., and Yoo, J.Y., (2003), Maximum Drag Reduction in a Turbulent channel flow by Polymer Additives, J. Fluid Mech., 492, pp. 91-100.

Morgan, S.E. and McCormick, C.L. (1990) Water-soluble polymers in enhanced oil recovery, Prog. Polym. Sci., vol. 15(1), pp.103-145.

Moussa, T and Tiu, C. (2001) "Factors affecting polymer degradation in turbulent pipe flow", Chemical Eng. Sci., 49, 10, pp 1681-1692.

Mumick, P. S., Hester, R. D., & McCormick, C. L. (1994). Water-Soluble Polymers. 55: N-isopropylacrylamide-co-Acrylamide Copolymers in Drag Reduction: Effect of Molecular Structure, Hydration, and Flow Geometry on Drag Reduction Performance. Polymer Engineering and Science, 34(18), 1429–1439.

Mumick, P. S., Welch, P. M., Salazar, L. C., & McCormick, C. L. (1994). Water-soluble copolymers. 56. Structure and solvation effects of polyampholytes in drag reduction. Macromolecules, 27(2), 323–331. http://doi.org/10.1021/ma00080a003

Myška, J., & Vocel, J. (1977). Experimental investigation of a micellar additive in suspension flow. Chemical Engineering Science, 32(6), 593–600. http://doi.org/http://dx.doi.org/10.1016/0009-2509(77)80224-8

Narain, Ravin. "Basic Concepts". Advance Chemical Engineering (Course). University of Alberta, Edmonton. January 26, 2015. Class Lecture.

Narain, Ravin. “Controlled Radical polymerizations”. Advance Chemical Engineering (Course). University of Alberta, Edmonton. February 2, 2015. Class Lecture.

Nsom, B. (1994). Computation of drag reduction in fiber suspensions. Fluid Dynamics Research, 14(5), 275–288. http://doi.org/10.1016/0169-5983(94)90036-1

Panton, R. L. (1992). Scaling laws for the angular momentum of a completely turbulent Couette flow. Comptes Rendus de l’Académie Des Sciences. Série 2, Mécanique, Physique, Chimie, Sciences de L'univers, Sciences de La Terre, 315(12), 1467–1473. Retrieved from http://cat.inist.fr/?aModele=afficheN&cpsidt=4446796

Patterson, G. K., Zakin, J. L., & Rodriguez, J. M. (1969). Drag reduction: polymer solutions, soap solutions and solid particle suspensions in pipe flow. Industrial And Engineering Chemistry, 61(1), 22–30.

Pazwash, H. (1984). Reduction of Friction Drag in Pipes by Polymers: A Review. Journal of Transportation Engineering, 110(2), 223–234. http://doi.org/10.1061/(ASCE)0733-947X(1984)110:2(223)

Peng, B. L., Dhar, N., Liu, H. L., & Tam, K. C. (2011). Chemistry and applications of nanocrystalline cellulose and its derivatives: A nanotechnology perspective. *The Canadian Journal of Chemical Engineering*, *89*(5), 1191–1206. http://doi.org/10.1002/cjce.20554

Pirih, R. J., & Swanson, W. M. (1972). Drag reduction and turbulence modification in rigid particle suspensions. *The Canadian Journal of Chemical Engineering*, *50*, 221–227.

Poncet, S., Da Soghe, R., Bianchini, C., Viazzo, S., & Aubert, A. (2013). Turbulent Couette-Taylor flows with endwall effects: A numerical benchmark. International Journal of Heat and Fluid Flow, 44, 229–238. http://doi.org/10.1016/j.ijheatfluidflow.2013.05.018

Prima, R. C. Di, & Swinney, H. L. (1965). Instabilities and Transition in Flow Between Concentric Rotating Cylinders. Hydrodynamic Instabilities and the Transition to Turbulence, 45, 139–180.

Ptasinski, P. K., Nieuwstadt, F. T. M., Van Den Brule, B. H. A. A., & Hulsen, M. A. (2001). Experiments in Turbulent Pipe Flow with Polymer Additives at Maximum Drag Reduction. *Flow, Turbulence and Combustion*, *66*(2), 159–182. http://doi.org/10.1023/A:1017985826227

Sá Pereira, A., & Pinho, F. T. (1994). Turbulent pipe flow characteristics of low molecular weight polymer solutions. Journal of Non-Newtonian Fluid Mechanics, 55(3), 321–344. http://doi.org/10.1016/0377-0257(94)80076-6

Saul, D., G.J.T. Tiddy, B.A. Wheeler, P.A. Wheeler, and E. Willis, (1974) Phase Structure and Rheological Properties of a Mix Zwitterionic/Anionic Surfactant System, J. Chem. Soc. Faraday Trans. I 70:163.

Savins, J. G. (1967). A stress-controlled drag-reduction phenomenon. Rheologica Acta, 6(4), 323–330. http://doi.org/10.1007/BF01984629

Schild, H. G. (1992). Poly (N-Isopropylacrylamide): Experiment , Theory And Application. Progress in Polymer Science, 17, 163–249.

Sellin, R.H.J., Hoyt, J.W. and Scrivener, O. (1982) The effect of drag-reducing additives on fluid flows and their industrial applications. Part I: Basic aspects, J.Hydr. Res., vol. 20(1), pp.29-68, 1982.

Shin, H. (1965). Reduction of Drag in Turbulence by Dilute Polymer Solutions. Massachusetts Institute of Technology. Doctoral thesis.

Singh, R., & Rao, S. N. (1995). Biological Control of Aphis gossypii Glover on Cucurbits by a Parasitic Wasp Trioxys indicus Subba Rao & Sharma. *Biological Agriculture & Horticulture*, *12*(3), 227–236. http://doi.org/10.1080/01448765.1995.9754743

Smith, G. P., & Townsend, a. a. (1982). Turbulent Couette flow between concentric cylinders at large Taylor numbers. Journal of Fluid Mechanics, 123, 187–217. http://doi.org/10.1017/S0022112082003024

Sreenivasan, K.R. and White, C.M.. (2000),The onset of drag reduction by dilute polymer additives, and the maximum drag reduction asymptote. J. Fluid Mech., vol. 409, pp. 149-164.

Srinivasan, S., Kleingartner, J. a., Gilbert, J. B., Cohen, R. E., Milne, A. J. B., & McKinley, G. H. (2015). Sustainable Drag Reduction in Turbulent Taylor-Couette Flows by Depositing Sprayable Superhydrophobic Surfaces. Physical Review Letters, 114(1), 014501. http://doi.org/10.1103/PhysRevLett.114.014501

Sugiyama, K., Calzavarini, E., & Lohse, D. (2008). Microbubbly drag reduction in Taylor–Couette flow in the wavy vortex regime. Journal of Fluid Mechanics, 608(2008). http://doi.org/10.1017/S0022112008001183

Sundstrom, D. W., & Kaufman, A. (1977). Pulsating Flow of Polymer Solutions. Industrial & Engineering Chemistry Process Design and Development, 16(3), 320–325. http://doi.org/10.1021/i260063a013

Taylor, G. I. (1923). Stability of a Viscous Liquid Contained between Two Rotating Cylinders. Philosophical Transactions of the Royal Society A: Mathematical, Physical and Engineering Sciences. http://doi.org/10.1098/rsta.1923.0008

Toms, B.A., (1949) Some observations on the flow of linear polymer solutions through straight tubes at large Reynolds numbers. In: Proceedings 1st International Congress on Rheology. North Holland, Amsterdam pp. 135–141.

Van Gils, D. P. M., Huisman, S. G., Bruggert, G. W., Sun, C., & Lohse, D. (2011). Torque scaling in turbulent Taylor-Couette flow with co- and counterrotating cylinders. Physical Review Letters, 106(2), 1–4. http://doi.org/10.1103/PhysRevLett.106.024502

Vaseleski, R. C., & Metzner, a B. (1974). Drag Reduction in the Turbulent Flow of Fiber Suspensions. *AIChE Journal*, *20*(2), 301–306..

Virk, P. S., & Merrill, E. W. (1969). The Onset of Dilute Polymer Solution Phenomena. In C. S. Wells (Ed.), *Viscous Drag Reduction SE - 5* (pp. 107–130). Springer US. http://doi.org/10.1007/978-1-4899-5579-1_5

Virk, P. S., & Wagger, D. L. (1990). Aspects of Mechanisms in Type B Drag Reduction. In A. Gyr (Ed.), *Structure of Turbulence and Drag Reduction SE - 17* (pp. 201–213). Springer Berlin Heidelberg. http://doi.org/10.1007/978-3-642-50971-1_17

Virk, P.S., (1971). Drag reduction in rough pipes. *Journal of Fluid Mechanics* 45 (2), 225-246.

Virk, P.S., (1975), "Drag reduction fundamentals", AIChE J. 21 625–656.

Virk, P.S., Merrill, E.W., Mickley, H.S., Smith, K.A., Mollo-Christensen, E.L., (1967). The Toms phenomenon: turbulent pipe flow of dilute polymer solutions. Journal of Fluid Mechanics 30, 305-328.

Virk, P.S., Wagger, D.L., (1989). Aspects of mechanisms in Type B drag reduction. In: Gyr, A. (Ed.), Structure of Turbulence and Drag Reduction. Springer-Verlag, Berlin, pp. 201-213.

Vleggaar, J., & Tels, M. (1973). Drag reduction by polymer threads. Chemical Engineering Science, 28(3), 965–NIL5. http://doi.org/http://dx.doi.org/10.1016/0009-2509(77)80031-6

Walsh, M. (1967) "Theory of Drag Reduction in Dilute High-Polymer Flows" Int Shipbuilding Prog 14:134-139

Wang, Y., Yu, B., Zakin, J. L., & Shi, H. (2011). Review on drag reduction and its heat transfer by additives. Advances in Mechanical Engineering, 2011. http://doi.org/10.1155/2011/478749

Warholic, M. D., Heist, D. K., Katcher, M., & Hanratty, T. J. (2001). A study with particle-image velocimetry of the influence of drag-reducing polymers on the structure of turbulence. Experiments in Fluids, 31(5), 474–483. http://doi.org/10.1007/s003480100288

Wells, C.S. and Spangler, J.G., (1967) Injection of a Drag Reducing Fluid into Turbulent Pipe Flow of a Newtonian Fluid. Phys Fluids. 10:1880-1890.

Wendt, F. (1933). Turbulente Strömungen zwischen zwei rotierenden konaxialen Zylindern. Ingenieur-Archiv, 4(6), 577–595. http://doi.org/10.1007/BF02084936

White, C. M., Somandepalli, V. S. R., & Mungal, M. G. (2004). The turbulence structure of drag-reduced boundary layer flow. Experiments in Fluids, 36(1), 62–69. http://doi.org/10.1007/s00348-003-0630-0

Ye, J. and Narain, R. 2009, "Water-Assisted Atom Transfer Radical Polymerization of N-Isopropylacrylamide: Nature of Solvent and Temperature", J. Phys. Chem. B 113, 676–681

Yi, M.-K., & Kim, C. (1997). Experimental studies on the Taylor instability of dilute polymer solutions. Journal of Non-Newtonian Fluid Mechanics, 72(2-3), 113–139.

Zakin, J. L., Myska, J. and Chara, (1996). Z. New limiting drag reduction and velocity profile asymptotes for nonpolymeric additives systems, *AIChE Journal* vol. 42(12), p.3544.

Zakin, J.L., and J.L. Chiang, (1972) Non-ionic Surfactants as Drag Re- ducing Additives, Nature Phys. Sci. 239:26.

Zhang, Y., Schmidt, J., Talmon, Y. and Zakin, J.L. (2005) Co-solvent effects on drag reduction, rheological properties and micelle microstructures of cationic surfactants, J.Collloid. Inter. Sci., vol. 286, pp.696-709.

APPENDIX

A.1 Taylor Couette Setup-Sketches

The following section consists of sketches of designed parts which were used to fabricate the Taylor-Couette setup. All the dimensions are in mm.

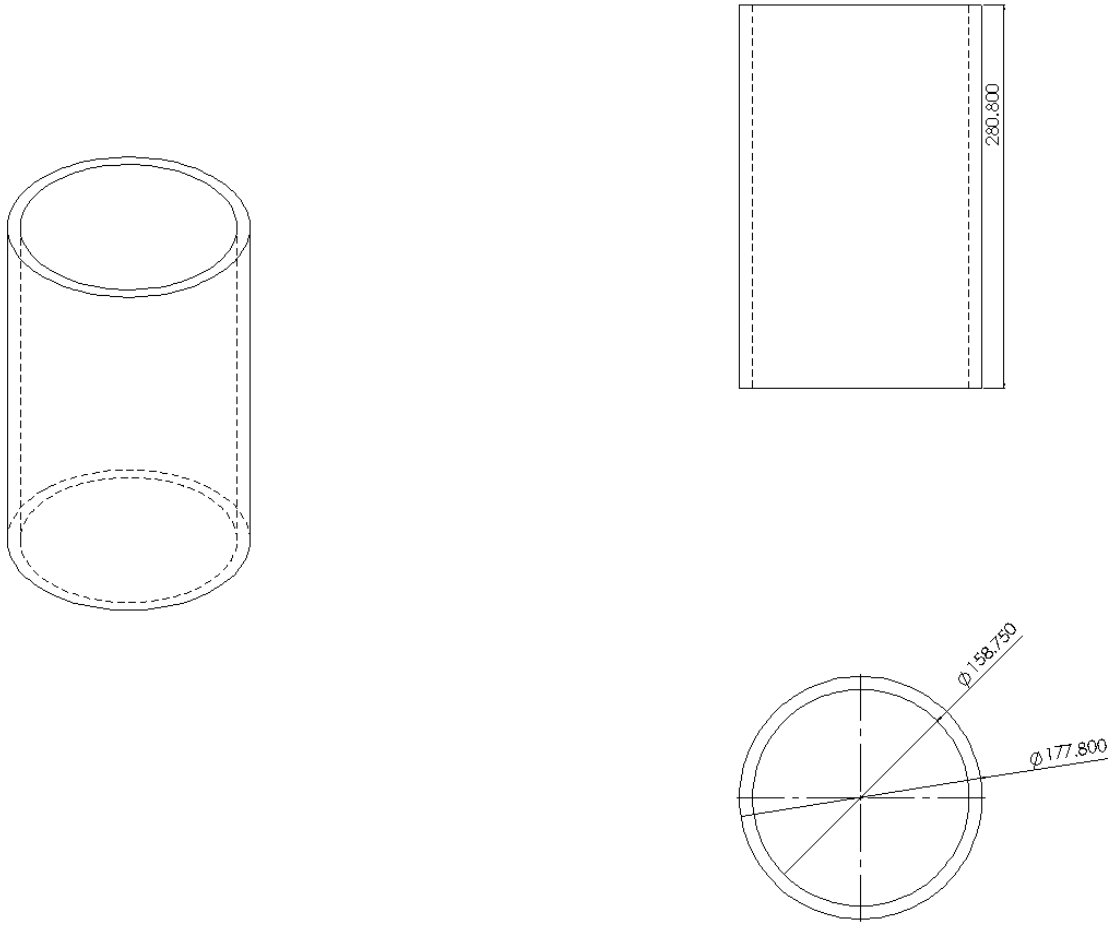

Figure A-1: Outer cylinder of TC Chamber.

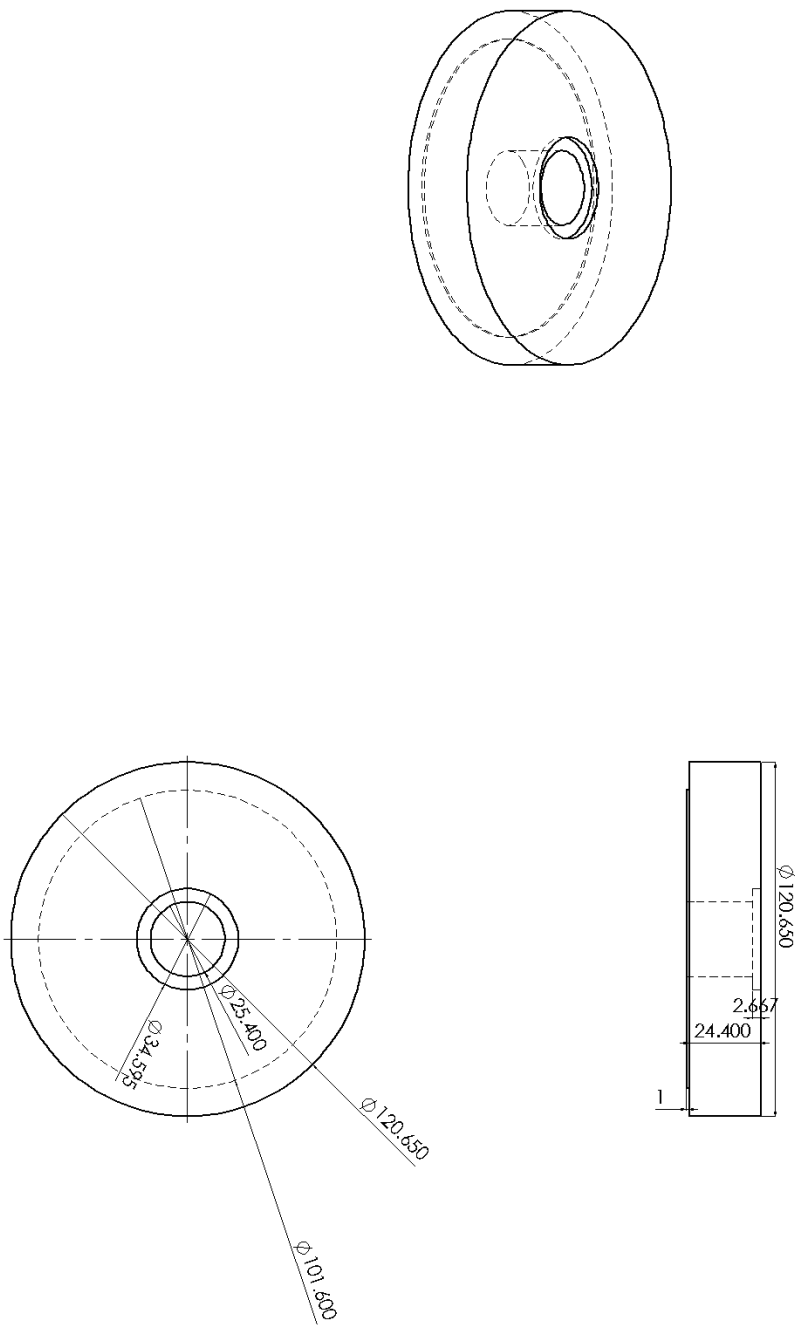

Figure A-2: Drawing for cover plate of inner cylinder.

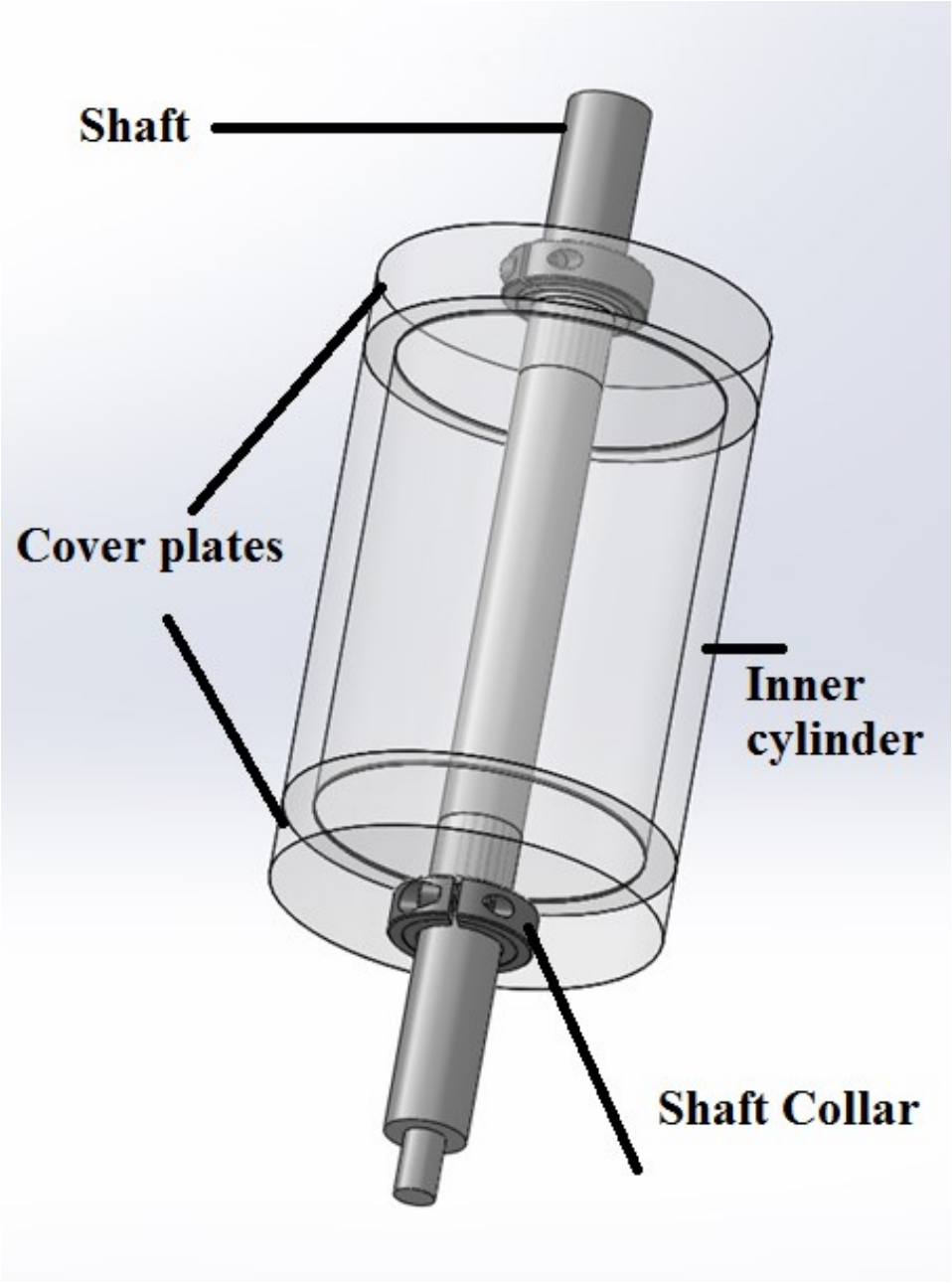

Figure A-3 Inner cylinder assembly.

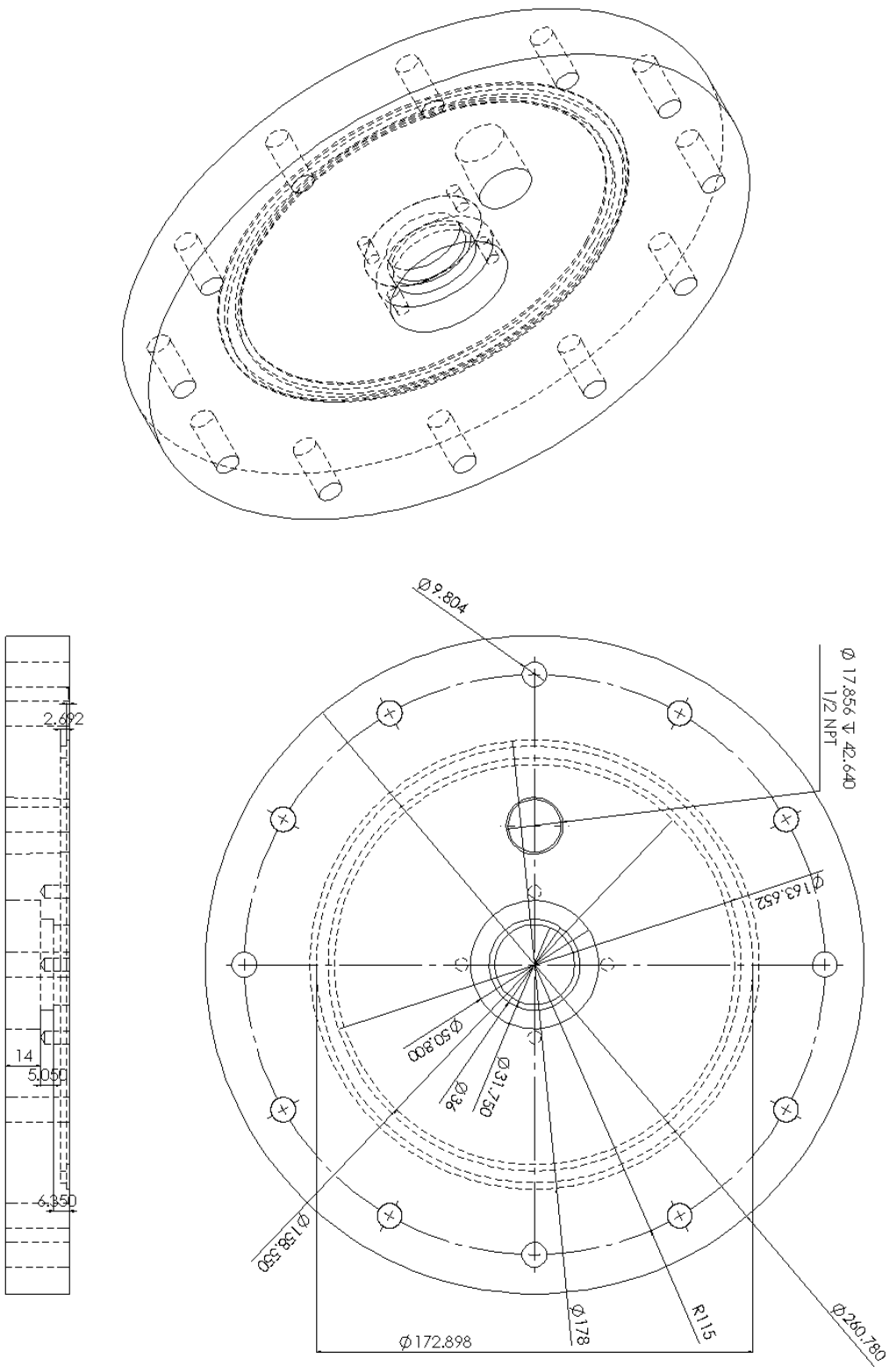

Figure A-4: Drawing for top plate of outer cylinder.

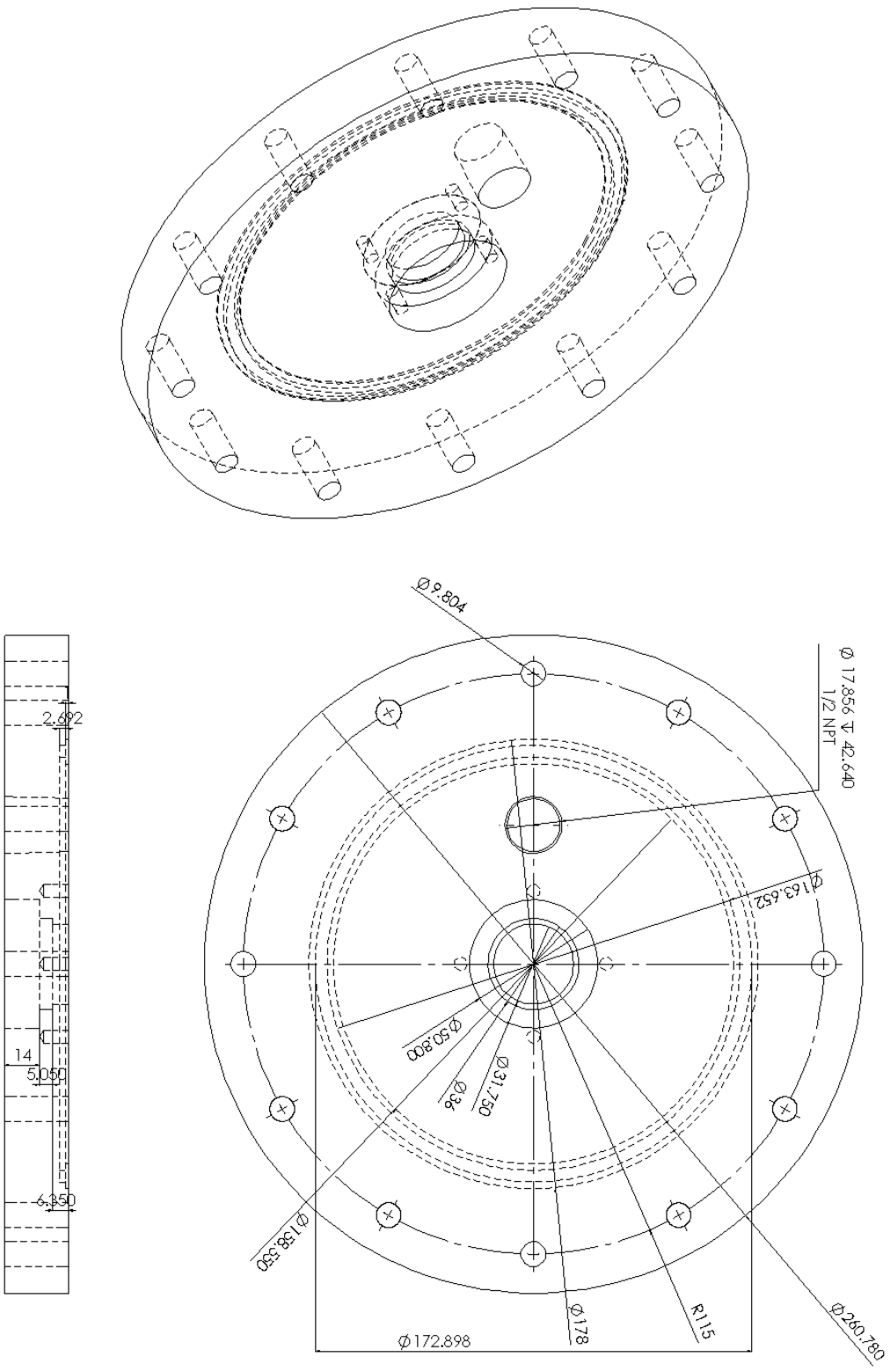

Figure A-5: Base plate for TC Chamber.

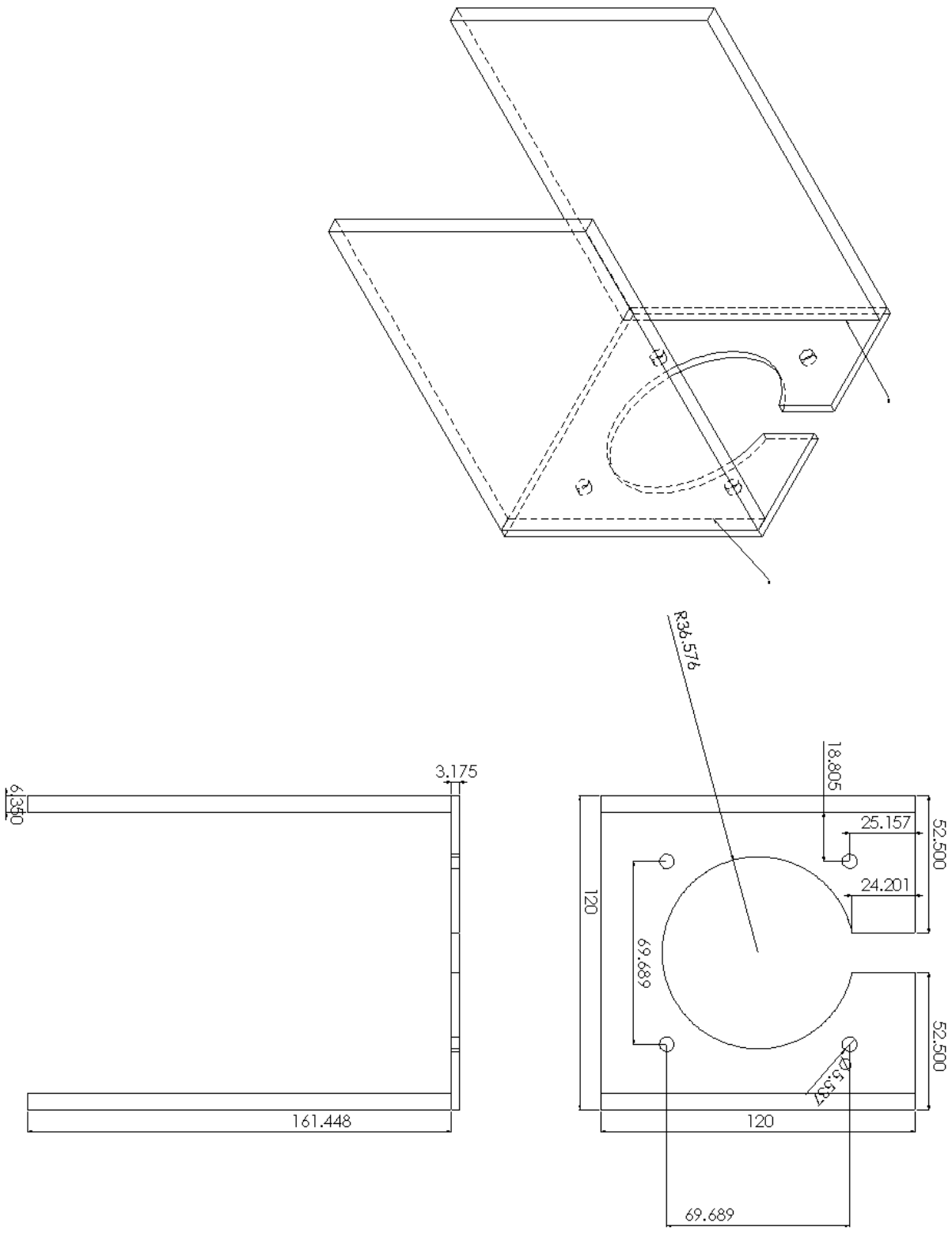

Figure A-6: Drawing for the frame used to hold the motor.

A.2 Procedure for conducting experiment with water as a working fluid

1. Switch ON the Torque sensor by plugging USB 220 into the computer. It should be started 15 minutes prior to start-up of the actual experiment.
2. Switch ON the Thermocouple.
3. Click on "SENSIT 2.3" on the computer Desktop. Select the serial number (630590) of Torque sensor used and Click on "Load". Tare the Torque sensor reading. Go to "Data Logging Mode" and click on settings. Select the "USB" and Enable the "630590". After setting the time duration, click "Apply". Select the File Path and Click "Start".
4. After 15 minutes, check if the TC chamber is empty and the inlet is closed.
5. Initial 5 measurements are taken with air, to account for contribution of bearing and seal friction losses. Monitor the temperature and if there is difference in temperature for more than +/-1°C, allow the system to cool.
6. After the system finishes each recording, the data is automatically saved in the excel sheet. Take an average of each recorded reading and save it.
7. To rotate the inner cylinder, Locate "Run" on the motor controller. Rotate the speed knob to desired RPM and verify it using tachometer.
8. Repeat this procedure for 5 times with air and take an average of these 5 readings.
9. Open the Inlet and fill it with water at desired temperature.
10. Repeat the same procedure to take 5 measurements with water and monitor the temperature. If there is difference in temperature for more than +/-1°C, allow the system to cool.
11. Open the outlet valve and remove the water and collect it in the bucket.
12. Take another 5 measurements with air to verify the reading is similar to the reading taken prior to water measurement. (Note: The readings observed were almost same with an error of +/-2.5%. It is just a check to make sure bearings are functioning properly).

13. Subtract the average of air measurements from the average of water measurements to get the net torque acting on inner cylinder. This step eliminates the torque due to bearings and seals.
14. The whole procedure was repeated 3 times for each working fluid in this study.

A.3 Procedure for conducting experiment with polymeric solution as a working fluid

1. The procedure is similar to take any measurement (as described in Section A.2). This section basically describes the preparation of solution.
2. Carefully measure the desired amount to prepare the polymer solution. While stirring with a rod, slowly adds the polymer to the water. Keep it for mixing on magnetic stirrer at 200 RPM.
3. For each reading, a separate solution was used in this study and time of stirring was carefully monitored.
4. If the concentration or polymer is changed for the next reading, clean the chamber by running the setup with water as a working fluid.

A.4 Plots for "Drag Reduction using Polysaccharides"

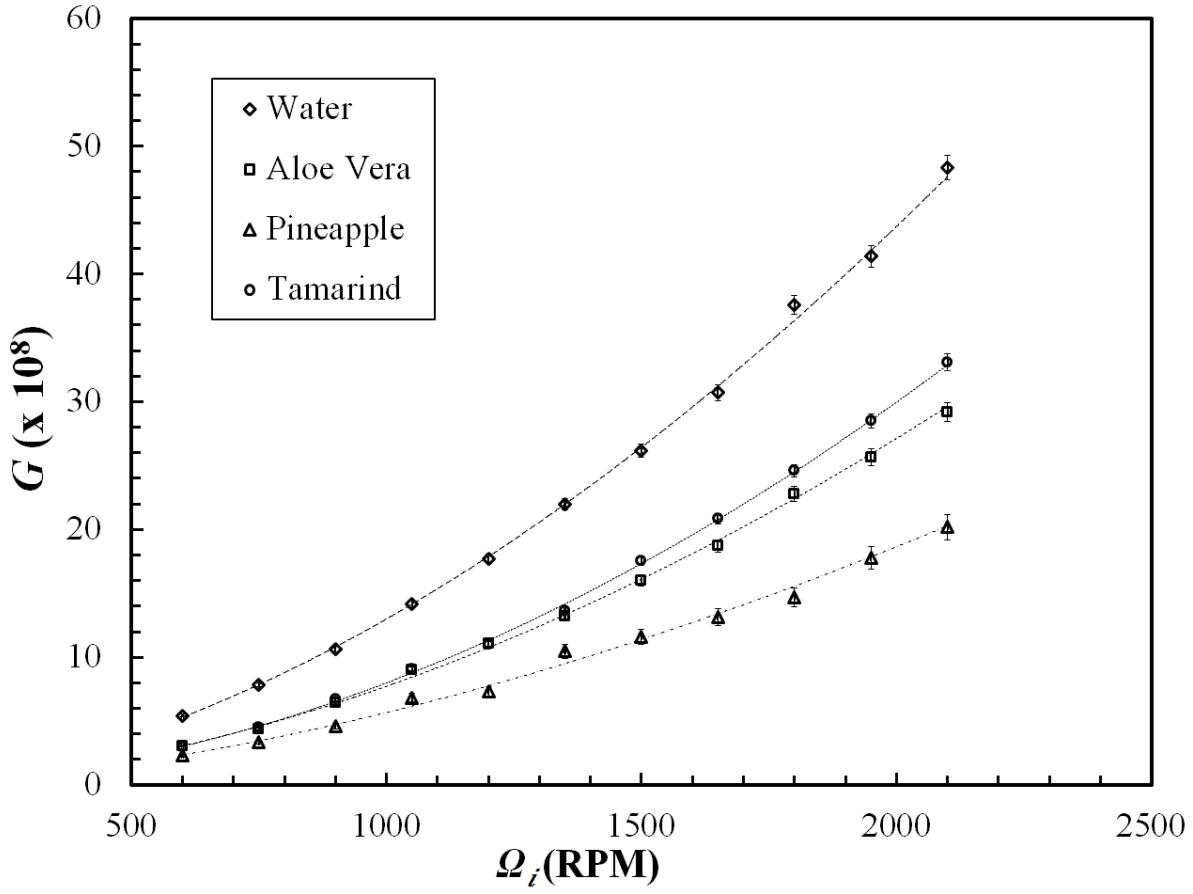

Figure A-7: Dimensionless torque vs. angular velocity for different Polysaccharides.

A.5 Plots for "Drag Reduction using Thermo-Responsive Polymers"

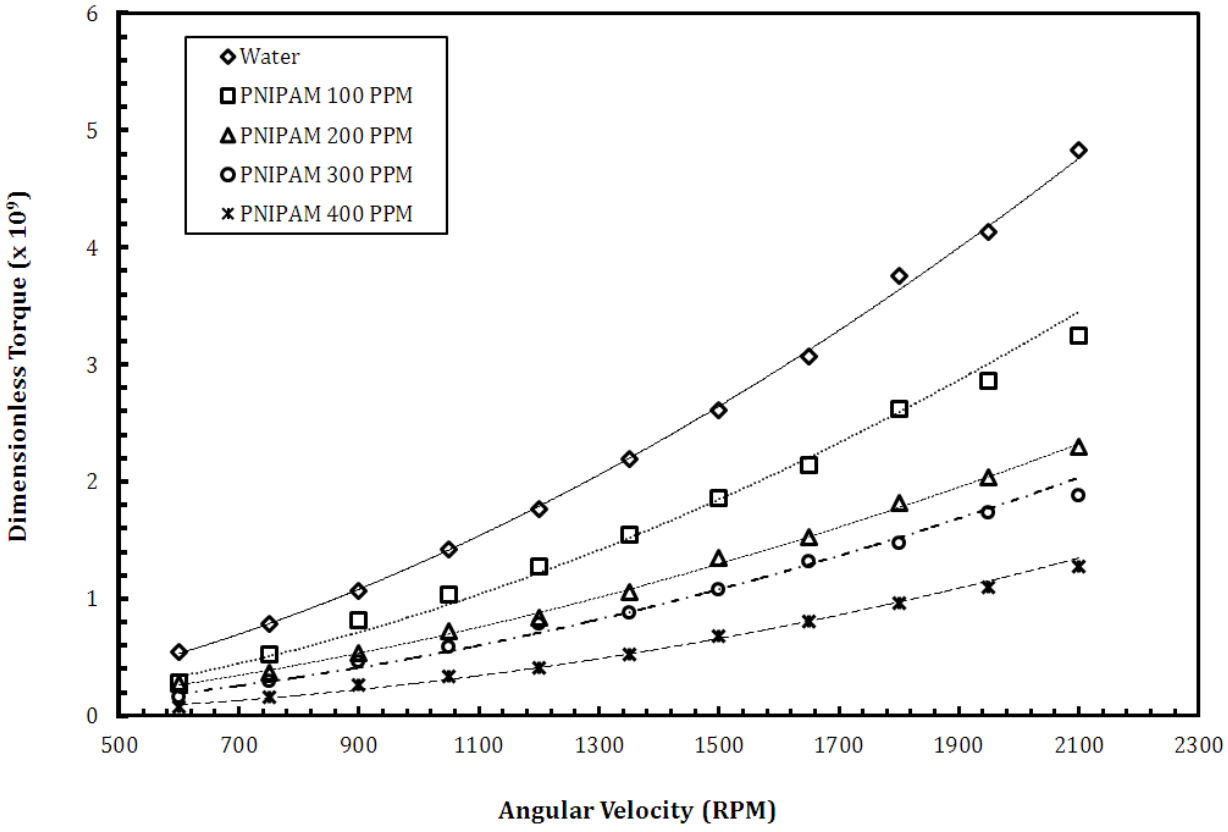

Figure A-8: Dimensionless Torque vs. Angular Velocity for difference concentrations of PNIPAM at 20°C.

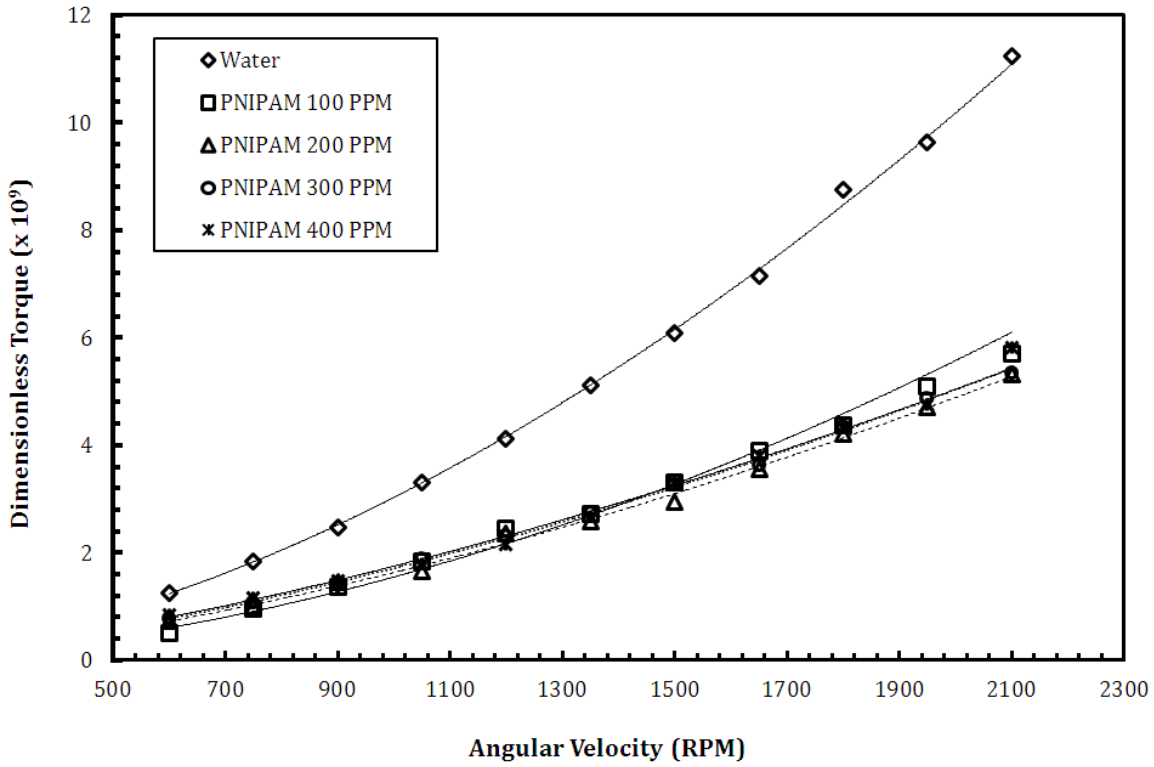

Figure A-9: Dimensionless Torque vs. Angular Velocity for difference concentrations of PNIPAM at 40°C.